Institut für Angewandte Photophysik

Fachrichtung Physik

Fakultät für Mathematik und Naturwissenschaften

Technische Universität Dresden

Influence of the Matrix Environment on the Optical Properties of Incorporated Dye Molecules

Dissertation

zur Erlangung des akademischen Grades

Doctor rerum naturalium

(Dr. rer. nat.)

vorgelegt von

Marieta Levichkova

geb. am 09.07.1970 in Dobrich, Bulgarien

Dresden 2007

Eingereicht am 11. September 2007

1. Gutachter: Prof. Dr. Karl Leo
2. Gutachter: Prof. Dr. Horst Hartmann
3. Gutachter: Prof. Dr. Wolfgang Brütting

Verteitigt am 30. Januar 2008

Abstract

The present thesis is concerned with solid solutions of organic dyes. The organic molecules are incorporated in both optically inert or active and in rigid or flexible matrices, respectively. Exclusively thin films prepared by physical vapor deposition are studied. The optical response of the systems, in dependence on their structure and on the matrix nature, is investigated by means of absorption and luminescence spectroscopy.

In the first part, perylene and 2,2-difluoro-1,3,2-dioxaborine derivatives, and Alq_3 (tris(8-hydroxyquinoline) aluminium) embedded in the optically inactive SiO_2 and polyimide hosts are studied. For the system dye molecules/SiO_2 matrix, two sample preparation approaches, co-deposition and layer-by-layer, are compared. It is demonstrated that the luminescence properties of the mixed layers are affected by dye distribution and thin film composition. The photoluminescence quantum efficiency is strongly influenced by dye aggregation and Förster transfer. Therefore, effective separation and isolation of dye molecules in the matrix results in increased PL efficiency. Furthermore, it is established that layer-by-layer growth mode assures more homogeneous dye distribution. The spectroscopic studies also show that, since dye and matrix condense successively in time, luminescence losses due to thermal degradation of molecules are reduced. Hence, the film structure can be optimized with regard to high absorption and luminescence quantum efficiency.

The experimental findings suggest that the luminescent properties of the embedded dyes are influenced by the nature of the host environment as well. In the rigid SiO_2 matrix, it is possible to observe isolated facial Alq_3 molecules with distinctive blue luminescence. In contrast, in the "soft" organic polyimide matrix Alq_3 exhibits ordinary green luminescence. Thus, the structural properties of the host, rigidity and density, are found to be crucial for preservation of the facial Alq_3 molecules. It is further demonstrated that the immobilization of molecules in the rigid SiO_2 matrix in combination with layer-by-layer growth results in improved photostability.

In polyimide matrix, the behavior of incorporated molecules is governed by the morphological changes of the host. These changes are defined by the curing procedure, needed for imidization, and give rise to a certain film structure.

In the second part, special attention is paid on the luminescence response of dispersed DCM (4- dicyanomethylene-2-methyl-6- (p-dimethylaminostyril)-4H-pyran) and rubrene (5,6,11,12-tetraphenyl-naphthacene) molecules in the optically active Alq_3 matrix. The observed enhancement of luminescence intensity and alteration of emitted color are favorable for application of the doped Alq_3 films as converter layers in combination with commercial blue light emitting diodes in luminescence conversion devices. It is demonstrated that by optimization of the conversion layer parameters white light generation can be achieved. The devices are characterized by high conversion efficiency and Lambertian distribution of the emitted light. However, they lack sufficient stability with regard to practical applications.

Contents

1 Introduction

In the last fifteen years, organic semiconductors have been intensely investigated and successfully introduced in various electronic and optoelectronic devices, since they offer many novel properties. The immense interest is caused by technological advantages such as low cost, easy synthesis and purification, as well as efficient processing on large areas. Additionally, quantum chemistry and the molecular design offer almost unlimited possibilities for synthesis of materials with desirable behavior, which allows tuning of energy levels, emission color, etc.

In comparison to inorganic semiconductors, organic semiconductors show unique physical properties as well. They have low refractive indices, thus the reflection losses at the interfaces are lower than for the III - V semiconductors. Many organic dyes have high selective absorption in the visible spectral range ($\sim$ 1x10^5 cm^{-1}), which allows to use very thin layers and accordingly thin devices, e.g. photovoltaic cells [1]. Also, some materials show large Stokes shift, hence self-absorption losses are avoided [2].

As photoreceptors in electrophotographic imaging and laser printing, organic photoconductive materials have already replaced inorganic semiconductors on a large scale. Most recently, substantial progress in the development and improvement of organic light emitting diodes (OLEDs) has enabled the commercial availability of flat panel displays based on organic semiconductors. In contrast to liquid crystal displays (LCD), they exhibit bright and saturated colors independent of the viewing angle [3]. Considerable efforts are also made in the development and optimization of organic thin-film transistors (OTFTs) [4] and photovoltaic cells [5, 6, 7] due to their low-cost and low-temperature fabrication process.

The immobilization of dye molecules in matrices is a basic technique in luminescence conversion systems [8], solid state dye lasers [9, 10], non-linear optics, etc. Here, the nature of the matrix governs nearly all characteristics of the dye: It causes a spectral shift in both absorption and emission, alters the distribution between processes which the excited state may undergo, e.g. intersystem crossing, and consequently the fluorescence lifetime, and influences the photostability [11]. In contrast to liquid systems, the solid solution of an organic dye represents a mechanical mixture. Thus, the structure of the solid system will affect the optical response of the embedded organic molecules as well.

In general, it is established that the separation in a rigid matrix leads to higher quantum efficiencies than in liquid solutions [12]. Furthermore, the maximum efficiency in solid systems is reached at concentrations which already cause the so-called concentration quenching in liquid systems [13]. In addition, the incorporation in rigid matrix leads to increased photostability of the dye molecules [14, 15, 16].

Commonly, sol-gel [17, 18] or polymer hosts [19, 20] are preferred. However, the

"wet" methods used for preparation of these systems have several disadvantages; thickness, uniformity of the films, and dye aggregation are difficult to control, and solvent is still present within the layers. Also, there are health and environmental problems due to the volatile solvents. An alternative method by which these drawbacks could be overcome is physical vapor deposition (PVD). It is compatible with the whole dry technology and hence is suitable for preparation of complete products. By means of co-evaporation of two or more materials, PVD enables the preparation of dye solutions at various concentrations in transparent matrices [21]. The choice of matrix is independent of the dye solubility. Furthermore, PVD offers controlled distribution of the incorporated dye in the whole film volume as well only in defined parts of it. The latter is particularly important for systems comprising two or more dyes (e.g. converter layers, doped layers for OLEDs). Therefore, the object of study of the present thesis are exclusively mixed thin films prepared by PVD.

Investigations on various dyes (e.g. merocyanine, Cu-phtalocyanine, etc.) embedded in oxide matrices (ZrO_2, SiO_2, TiO_2) and other inorganic materials (NaF, CaF) [22, 23] by PVD are reported in literature. Particular attention is paid to the structural and mechanical properties. For the optical properties, the emphasis is mostly laid on the dependence of the color coordinates on dye concentration. There are only few systematic studies on the photophysical properties of such systems [24, 25], which are restricted to layers obtained by simultaneous condensation (co-evaporation) of matrix and dye. In summary, the following effects are observed: (i) The solid state of the matrix (amorphous or crystalline) influences differently the distribution of incorporated dye molecules and thus the absorption and luminescence spectra (ii) Diluted solid solutions show predominant monomer emission and consequently enhanced luminescence quantum efficiency (iii) For polar dye molecules, dilution in the matrix results in pronounced solvent shifts of absorption and emission.

In general, the photophysical properties of vacuum deposited (VD) layers depend on their structure, which is defined by the preparation conditions. Therefore, this work is focused on investigation of the luminescent properties of composite dye/matrix VD films as function of their composition and structure, i.e. total dye concentration and especially dye distribution in the matrix. For this reason, we introduce a preparation approach which is not new but, to the best of our knowledge, unfamiliar in studies on dye/matrix VD systems. We refer to it as "layer-by-layer". In contrast to the classical co-evaporation, this approach enables separate condensation of matrix and dye during the deposition process and variety of film structures. Thus, we make a comparative study of solid solutions of organic dyes grown by simultaneous condensation and grown layer-by-layer. It is our aim to find a correlation between the structure of the mixed layers and their optical characteristics. Crucial parameters for the practical application of solid state organic systems in lighting applications are the quantum yield and the photostability. In this context, the subject of our interest is optimization of the film structure (dye distribution) for increased luminescence efficiency and photostability based on modification of the preparation technology.

As optically inert matrix materials we use SiO_2 and polyimide (PI). They exhibit high mechanical and photostability, along with chemical resistivity [26]. Both materials yield stable films with reproducible and well-controlled properties that have low absorbance in the visible spectral region. In addition, PI is easy evaporable at relatively low temperatures, close to those of the organic dyes to be embedded. The incorporation of proper dyes in these matrices could result in beneficial photophysical and mechanical properties.

The perylene and 2,2-difluoro-1,3,2-dioxaborine derivatives we investigate grow as crystalline structures. Therefore, they show rather different spectral response as isolated molecules and molecular crystals. Thus, using various deposition conditions (growth modes, evaporation rate, concentration ratio, etc.) we are able to influence dye aggregation in the layers. Another material of study is Alq_3, which is known to grow quasi-amorphous thin films [27]. Its optical properties in solution and in the solid state are rather similar. However, since Alq_3 has various polymorphs and two optical isomers [28, 29], it is possible to expect interesting optical properties in dependence on the grown mixed film structure. For this reason, we investigate how the nature of the matrix, rigid (SiO_2) or "plastic" (PI), affects the distribution of Alq_3 isomers in the solid solution.

A comparison of the photopysical response for different matrix nature can also provide valuable information about the feasibility of the hosts with respect to practical applications. We demonstrate that the structural properties of the SiO_2 matrix (density, rigidity) are a crucial factor not only for the luminescence behavior of the embedded organic dyes, but also for their photostability.

In addition, we study the optical behavior of dyes incorporated in Alq_3 as an example of optically active matrix. Optically active here denotes the ability of the material to absorb and fluoresce in the visible spectral range, thus energy transfer processes are to be expected. The latter are known to result in increased luminescence efficiency and alteration of luminescence color [36, 56]. Taking advantage of both effects, on the basis of doped Alq_3 films, we present the realization of efficient organic luminescence converter devices. We define the optimal combination of parameters such as thickness and dopant concentration for obtaining white light.

This work is organized as follows: In Chapter 2, the necessary theoretical background for describing the photophysical properties of solid solutions of organic dyes is introduced. After an overview of the basic materials, experimental details and methods used in the study (Chapter 3), the main experimental results are presented in Chapters 4 and 5. Chapter 4 is concerned with organic dyes distributed in the optically inactive matrices SiO_2 and PI. Chapter 5 addresses the luminescence behavior of doped with DCM and rubrene vacuum deposited Alq_3 thin films. Also, examples for application of the doped Alq_3 films as luminescence conversion (LUCO) layers in combination with blue light emitting diodes (LEDs) as excitation light sources are presented. In contrast to the preceding chapter, however, Chapter 5 deviates from the overall structure of the thesis. Before discussing the experimental results on the luminescence conversion devices, the theoretical basics about the LUCO principle, quantum efficiencies and chromaticity coordinates are

introduced. Conclusions and an outlook for further investigations are presented in Chapter 6.

2 Photophysical properties of organic molecules in solid films

The photophysical properties of solid organic films are readily traceable to the properties of the constituent organic molecules. Therefore, in this Chapter, we first address the basic concepts of optical excitation and subsequent relaxation of isolated molecules. Sections 2.2 to 2.4 consider the problem of interacting molecules by introducing the collective response of common molecular complexes and existing energy transfer mechanisms. Since solid solutions of organic dyes are subject of the thesis, in Section 2.5 we treat the effects of the physical environment on the molecular behavior. Next, we discuss the basic photobleaching reactions and parameters, influencing the photostability. Finally, in Section 2.7 we present a brief review of experimental results on the optical properties of various types multi-component solid systems.

2.1 Absorption and relaxation of isolated molecules

An isolated molecule (monomer) comprises nuclei and electrons which interact with each other. The nonrelativistic Hamilton operator is then given by:

$$H^{mol} = T_{el}(r_i) + V_{el-nuc}(r_i, R_A) + V_{el-el}(r_i) + T_{nuc}(R_A) + V_{nuc-nuc}(R_A), \quad (2.1)$$

where r_i, R_A are the electron and nuclei coordinates, respectively; T_{el} and T_{nuc} represent the kinetic energies of electron and nuclei [154]. Since both kinds of particles are charged, the Coulomb interaction potentials are V_{el-el} between electrons, $V_{nuc-nuc}$ between nuclei, and V_{el-nuc} between electrons and nuclei.

The stationary properties of the defined molecular system are contained in the solutions of the time-independent Schrödinger equation:

$$H^{mol}\Psi(r_i, R_A) = E\Psi(r_i, R_A). \quad (2.2)$$

The practical solution of (2.2) is based on the so-called Born-Oppenheimer approximation: due to the large mass difference, $m_{el} \ll M_{nuc}$, electrons respond instantaneously to any changes in the nuclear configuration. That is, the interaction between nuclei and electrons, V_{el-nuc}, is modified due to the motion of the nuclei only adiabatically and does not cause transition between different electronic states. Hence, the molecular wave function can be expressed as the product of electronic (ψ_n) and vibrational (ϕ_{nv}) wave functions:

$$\Psi(r_i, R_A) = \psi_n(r_i, \{R_A\})\phi_{nv}(R_A), \quad (2.3)$$

where n denotes the number of the electronic level and v of the vibronic levels. This leads to separation of the Hamiltonian into an electronic and a nuclear part.

The electronic part (neglecting the electron spin) is

$$H^{el}|\psi_n\rangle = E_n^{el}|\psi_n\rangle \tag{2.4}$$

with

$$H^{el} = T_{el}(r_i) + V_{el-el}(r_i) + V_{el-nuc}(r_i), \tag{2.5}$$

where $\psi_n(\mathrm{r}_i, \{R_A\})$ is the wave function for all electron coordinates r_i for a fixed nuclear configuration $\{R_A\}$. Correspondingly, $\phi_{nv}(\mathrm{R}_A)$ is the wave function of the v-th vibrational state of the electronic state n of energy $\mathrm{E}_n^{el}(\mathrm{R}_A)$:

$$H^{vib}|\phi_{nv}\rangle = E_{nv}^{vib}|\phi_{nv}\rangle, \tag{2.6}$$

with

$$H^{vib} = T_{nuc}(R_A) + V_{nuc-nuc} + E_n^{el}(R_A). \tag{2.7}$$

The total excitation energy relative to the ground state is thus a sum of electronic and vibrational part:

$$\Delta E_{nv} = (E_n^{el} + E_{nv}^{vib}) - E_0^{el}. \tag{2.8}$$

The adiabatic approximation implies that $\Delta\mathrm{E}^{vib} \ll \Delta\mathrm{E}^{el}$.

A molecule is promoted to an excited state by energy transfer, for example by absorption of a photon. This new energy state corresponds to electronic, vibrational, rotational and translational degrees of freedom. The subsequent process of returning to the ground state can occur via emission of a photon with lower energy (radiative transition) or can be radiationless (non-radiative transition). The prevailing energy transitions, illustrated in the Jablonski diagram in Fig. 2.1, are electronic in nature with energy spacing of a few eV (labelled as S_n or T_n). For each electronic level, a manifold of vibrational sublevels exists, which are represented in Fig. 2.1 by thin horizontal lines. The energy spacing between these levels is ~ 0.1 eV. To each vibrational sublevel, a number of rotational and translational molecular energies corresponds, with an energy difference between them of ~ 0.01 eV [30].

Each electronic state in the Jablonski diagram corresponds to a bonding or anti-bonding molecular orbital. A molecular orbital may be thought to originate from the coalescence of occupied atomic orbitals and its filling is governed by the Pauli exclusion principle. The orbitals associated with a carbon-carbon bond can be either σ or π type. In a σ bond, the electrons are localized between the carbon atoms, while the π-bond establishes delocalized electron density above and below the atomic plane. There are also valence-shell electrons that do not participate in formation of molecular bonds. Their molecular orbitals are designated as n. In addition, each molecule has associated with it a series of higher energy molecular orbitals that are unoccupied under ordinary conditions. These orbitals are called anti-bonding orbitals, and are designated σ^* and π^*.

Absorption of a photon can promote an electron from its σ, π, or n ground state to a σ^* or π^* excited state. In the ground state, the last orbital of an organic molecule is filled with two electrons with paired spins according to the

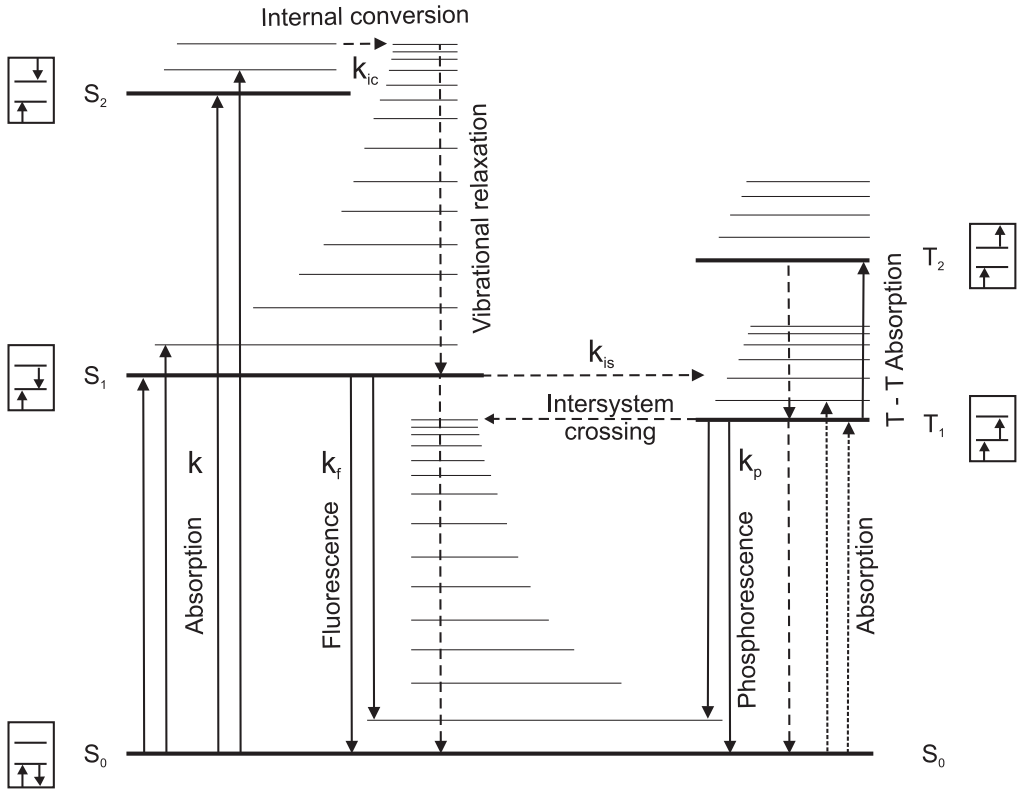

Figure 2.1: Jablonski diagram of an organic molecule presenting energy levels and photophysical processes. The solid and dotted upward and downward lines indicate the radiative processes, while the non-radiative transitions are depicted by dashed lines. All processes can be completed from one of the other sublevels of the corresponding energy level, depicted by thin horizontal lines. The variables k, k_f, k_p, k_{ic}, and k_{is} are the absorption rate constant, the radiative decay constants to the ground state for fluorescence and phosphorescence, the non-radiative decay rate to the ground state, and the intersystem crossing rate to the triplet state respectively (adapted from [31]).

Pauli principle, i.e. forming a singlet. In the excited state, one of the electrons is promoted to occupy a dissimilar orbital, therefore it is no longer required the electron spins to be paired. The resulted singlet (S_n) or triplet (T_n, unpaired spins) state has a net spin equal to 0 or 1, respectively.

In dependence on the type of absorption process (Fig. 2.1), (1) Singlet-singlet absorption $S_0 \longrightarrow S_1$ or $S_0 \longrightarrow S_2$, allowed (2) Singlet-triplet absorption $S_0 \longrightarrow T_1$ or $S_0 \longrightarrow T_2$, forbidden, singlet or triplet excited states are formed. Higher excited triplet states are also accessible from T_1 via (3) Triplet-triplet absorption $T_1 \longrightarrow T_2$, allowed.

Once in the excited state, the molecule tends to return to the ground state, losing energy via radiative (r) or non-radiative (nr) processes. The corresponding parameters describing the dynamic of these deactivation transitions are the lifetimes (τ_r and τ_{nr}) and the rate constants (k_r and k_{nr}), respectively. In general, lifetime and rate constant are related as:

$$\tau = \frac{1}{k}. \tag{2.9}$$

Common radiative processes are: (4) Singlet-singlet emission or fluorescence $S_1 \longrightarrow S_0$, allowed (5) Triplet-singlet emission or phosphorescence $T_1 \longrightarrow S_0$, forbidden.

The nonradiative processes are defined as: (6) Internal conversion (IC) - transitions between states of the same multiplicity - $S_1 \longrightarrow S_0$, $S_2 \longrightarrow S_1$, or $T_2 \longrightarrow T_1$, allowed (7) Intersystem crossing (IS) - transitions between states of a different multiplicity - $S_1 \longrightarrow T_1$ or $T_1 \longrightarrow S_0$, forbidden.

The terms "allowed" and "forbidden" refer to the spin-conservation rule. In reality, $S \longrightarrow T$ and $T \longrightarrow S$ transitions may occur in the presence of an additional internal or external force, which facilitates the momentum intra exchange. Thus, in principle forbidden transitions become weakly allowed. A typical example is the spin-orbit coupling in organometallic complexes, such as PtOEP (2,3,7,8,12,13,17,18-octaethyl-21H,23H-porphineplatinum (II)) or $Ir(ppy)_3$ (tris(2-phenylpyridine) iridium (III)). The presence of heavy metals in the molecular structure induces significant mixing of the singlet and triplet states near the metal atom. Thereby, the triplet lifetime is reduced and the probability for intersystem crossing increases, leading to enhanced efficiency of phosphorescence [30]. The weakly allowed radiative $T_1 \longrightarrow S_0$ transitions are in general characterized by very slow rates resulting in long excited state lifetimes. The typical values of the rate constants, corresponding to various types radiative and non-radiative processes are summarized in Table 2.1.

Additionally, an electron in an excited vibrational level of an electronic state can lose its energy by vibrational relaxation (VR) to the vibrational ground state. At room temperature, the ground state is predominantly populated, since thermal equilibrium corresponds to a Boltzmann distribution over the vibrational levels. In solution, VR is a very rapid process and the excess vibrational energy is converted into heat through collisions with solvent molecules. In the solid state, the vibrational energy of the molecule is lost to its neighbors via phonon modes of the solid, with rate constant $k_v \approx 10^{13}$ s^{-1}.

Process	Rate constant (s^{-1})
Absorption	$\sim 10^{14}$
Fluorescence	10^6 - 10^9
Phosphorescence	10^{-2} - 10^6
Internal conversion	10^8
Intersystem crossing	10^6 - 10^{11}

Table 2.1: Rate constants for radiative and non-radiative transitions [30].

An excited molecule can nonradiatively transfer its energy to a neighboring molecule via dipole-dipole interactions or electron-exchange as well. They are also known as Förster and Dexter transfer, respectively. Detailed discussion about the energy-transfer processes will be presented further in this Chapter.

During the described above photophysical processes, the excited state energy potential surface S_1 is displaced respectively to the ground state S_0 on the nuclear configuration coordinate with ΔR (Fig. 2.2). The vibrational sublevels of the ground and excited states are depicted by dashed horizontal lines with corresponding wave functions ϕ_{0v} and ϕ_{1v}, respectively. Every transition is characterized by a rate constant, whose value is defined by the Franck-Condon principle. Accordingly, since the time required for an electronic transition is negligible compared with that of nuclear motion, the most probable vibronic transition is one which involves no change in the nuclear coordinates. This transition, referred to as Franck-Condon maximum, represents a vertical transition on the potential energy diagram.

In quantum-mechanical terms, the Franck-Condon maximum corresponds to maximum overlap between the ground-state vibrational wave function ϕ_{0v} and the excited-state vibrational wave function ϕ_{1v}, that is when the vibrational overlap integral $\langle \phi_{0v} \mid \phi_{1v} \rangle$ is at a maximum. The squared absolute values of the overlap integrals $|\langle \phi_{0v} \mid \phi_{1v} \rangle|^2$ are referred to as Franck-Condon factors [32]. They determine the intensity distribution in the vibronic progression. Therefore, absorption from the vibrational ground state is strongest for that particular transition into a vibrational level of the excited electronic state whose wave function maximum lies directly over the maximum of the ground state potential diagram (Fig. 2.2). Thus, absorption starts from the bottom of the S_0 potential curve and ends at the S_1^2 sublevel. Transitions to other vibrational terms are also possible but with reduced probabilities. Via vibrational relaxation, the molecule relaxes at the minimum of S_1. The successive fluorescence is vertically accomplished at S_0^2. Finally, the molecule can relax to its lowest sublevel by further emission of phonons. The rate of non-radiative phonon emission is much larger than the radiative transition rate, hence, radiative transitions are most likely to occur from the lowest vibrational level of an electronic state. This principle is known as Kasha's rule.

The absorption of light by molecules in a homogeneous sample of thickness d is

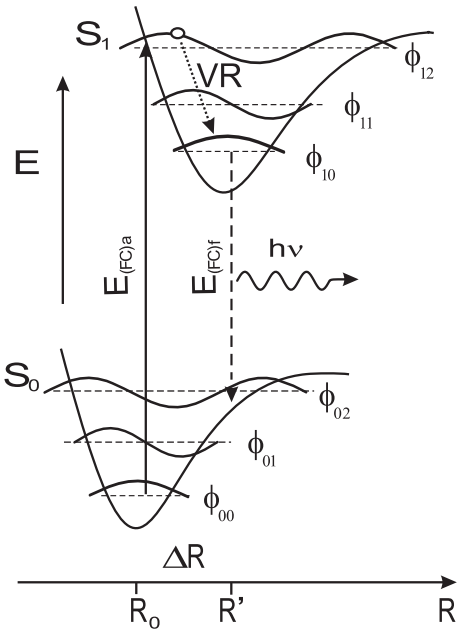

Figure 2.2: Schematic potential energy diagram of electronic ground S_0 and excited S_1 states. Dashed lines represent the vibrational energy sublevels, on top of them are drawn the vibrational wave functions. $E_{(FC)a}$ and $E_{(FC)f}$ denote Franck-Condon maximum in absorption and Franck-Condon maximum in emission, respectively. The equilibrium distance is R_0, and ΔR refers to the nuclear displacement.

governed by the Lambert-Beer law:

$$I = I_0 exp(-\alpha d), \tag{2.10}$$

where I_0 is the intensity of the incident light and I the intensity transmitted by the sample; $\alpha = \alpha(\overline{\nu})$ is an absorption coefficient, characteristic of the absorbing medium and dependent on the wave number of the light. Setting $\alpha = 2.303\varepsilon c$, where ε is the molar extinction coefficient and c is the concentration of the absorbing species, gives the absorbance or optical density OD of the sample:

$$OD = \log(I_0/I) = \varepsilon c d. \tag{2.11}$$

A transition between two electronic states of a molecule includes large number of vibrational and rotational levels. These levels belong to the potential curves of the initial and final states in the molecule and give rise to a frequency range $\Delta\overline{\nu}$ for the transition. Therefore, the intensity of an electronic transition is measured in terms of an integral over the whole absorption band:

$$A = \int \varepsilon \overline{\nu} d\overline{\nu}. \tag{2.12}$$

A is referred to as integral absorption coefficient and is related to the strength of the transition or the transition intensity as:

$$f = 4.319 \times 10^{-9} \int \varepsilon \overline{\nu} d\overline{\nu}. \tag{2.13}$$

The oscillator strength f represents the ratio of the observed integrated absorption coefficient to that calculated classically for a single electron in a three-dimensional harmonic potential well. The maximum value of f for a fully allowed transition is of the order of unity [32]. For an electronic dipole transition between two states n and m with dipole transition moment

$$\mu_{nm} = \int \psi_m e R \psi_n dV, \tag{2.14}$$

where ψ_m and ψ_n are the wave functions of the states, e the elementary charge, R the distance between the centers of charge, and V the volume, the oscillator strength is

$$f \sim \overline{\nu}_{nm} |\mu_{nm}|^2, \tag{2.15}$$

with $\overline{\nu}_{nm}$ the wave number of the transition.

According to the Jablonski diagram, since intersystem crossing and internal conversion compete with fluorescence for deactivation of the lowest excited singlet state S_1, not all potentially fluorescent molecules will return to the ground state S_0 via emission of a photon. The fraction of excited molecules that fluoresce is called quantum yield of fluorescence (ϕ_f) or fluorescence efficiency. In terms of the rates of deactivation processes of S_1, ϕ_f is defined as:

$$\phi_f = \frac{k_f}{k_f + \Sigma k_d}, \tag{2.16}$$

where k_f is the rate constant for fluorescence and Σk_d is the sum of the rate constants for deactivation of S_1 by all competitive non-radiative processes, i.e. $\Sigma k_d = k_{ic} + k_{is}$. Under given conditions of temperature and environment, the fluorescence efficiency is a physical constant of the excited molecular species.

The reciprocal of k_f, $\tau_f^0 = 1/k_f$, is referred as radiative lifetime of the lowest excited singlet state. This is the time required for an initial population of excited molecules to decrease to (1/e) of its original number, assuming that fluorescence is the only deactivation process. The radiative lifetime can be related to the molar extinction coefficient ε, and respectively to the oscillator strength of the electronic transition f, as:

$$\tau_f^0 = \frac{3.47 \times 10^8}{\overline{\nu}_{max}^2} \frac{1}{\int \varepsilon(\overline{\nu}) d\overline{\nu}} \approx \frac{1.5}{\overline{\nu}_{max}^2 f}, \tag{2.17}$$

where $\overline{\nu}_{max}$ is the wave number of the absorption maximum [32]. Since emission shows the same dependence on the transition moment as absorption, it follows that the emission decay time is inversely proportional to the integrated intensity of the absorption. The radiative lifetime is nearly temperature independent, but depends to some extend on the environment.

The reciprocal of $k_f + \Sigma k_d$, τ_f, corresponds to the actual mean time the molecules spend in the excited state. The quantum yield of fluorescence can be thus expressed as:

$$\phi_f = \frac{\tau_f}{\tau_f^0}. \tag{2.18}$$

In general, the greater the number of processes competing with fluorescence for deactivation of the lowest excited state and their rate constants is, the shorter will be the actual lifetime of the lowest excited state.

2.2 Molecule complexes

2.2.1 Dimer

Upon increasing the molecule concentration in a dye solution, due to van der Waals and Coulomb interactions, molecule aggregates can be formed. The smallest complex of molecules is referred to as a dimer. A physical dimer comprises two closely spaced molecules with purely physical interaction between them, no chemical bonding is involved.

Perturbation theory can be treated in order to describe the weak interaction of the molecules forming a dimer [31]. The dimer Hamiltonian can be written as a sum of the Hamiltonians of the isolated molecules H_1 and H_2, and a term V_{12}, describing the intermolecular interaction energy:

$$H = H_1 + H_2 + V_{12}. \tag{2.19}$$

With ψ_1 and ψ_2, representing the ground-state wavefunctions of molecules 1 and 2, the ground-state dimer electronic wavefunction can be approximated as:

$$\psi = \psi_1 \psi_2. \tag{2.20}$$

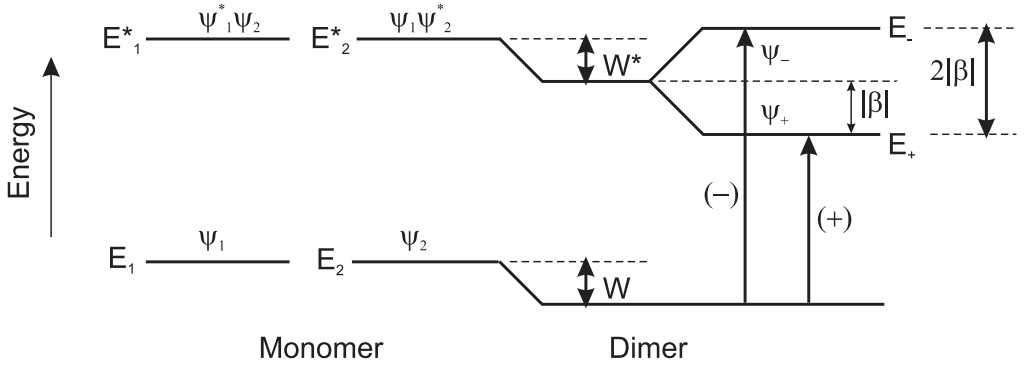

Figure 2.3: Exciton band splitting and energy shift for a dimer. Solid vertical lines represent the two allowed dimer optical transitions (adapted from [31]).

Because of the intermolecular interaction, the total energy of the monomers E_1+E_2 is lowered by the term W (see Fig. 2.3), denoting the Coulombic binding energy for the pair, thus the ground-state energy of the dimer is:

$$E = E_1 + E_2 + W. \tag{2.21}$$

The interaction W arises from the wavefunctions of the isolated molecules and the intermolecular interaction energy V_{12}:

$$W = \langle \psi_1 \psi_2 | V_{12} | \psi_1 \psi_2 \rangle. \tag{2.22}$$

Without interaction, two equivalent excited states ψ_1^* and ψ_2^* of two identical molecules are degenerate with energy $E_1^* = E_2^*$. Switching on the perturbation term V_{12} will lead to lifting of this degeneracy, and will end up in an energetic lowering and splitting of the dimer states:

$$E_\pm^* = E_1^* + E_2 + W^* \pm \beta, \tag{2.23}$$

where

$$W^* = \langle \psi_1^* \psi_2 | V_{12} | \psi_1^* \psi_2 \rangle; \tag{2.24}$$

$$\beta = \langle \psi_1^* \psi_2 | V_{12} | \psi_1 \psi_2^* \rangle. \tag{2.25}$$

The term W^* describes the Coulomb interaction energy (an energy lowering) between the states of the molecules. The exciton splitting term, β, represents the interaction energy due to the exchange of excitation energy between the two molecules. The corresponding dimer states are given as:

$$\psi_\pm = \frac{1}{\sqrt{2}} (\psi_1^* \psi_2 \pm \psi_1 \psi_2^*). \tag{2.26}$$

With dimer formation, the major spectral changes observed are: (i) a displacement of absorption and emission bands relative to the monomer; all dimer maxima lie at lower energy than the corresponding maxima of the monomer spectrum (ii)

the nuclear displacement in the dimer is typically greater with respect to that of the monomer, hence the Franck-Condon maximum of the dimer is represented by the 0-1 transition, as compared to the 0-0 transition in the monomer (iii) changes in the molecular vibrational frequencies and introduction of intermolecular lattice modes; consequently the dimer spectrum is broader and less well defined as compared to the monomer spectrum (iv) variation in the oscillator strength for optical transitions; the luminescence intensity of the dimer is lower than that of the parent monomer.

The selection rules for optically allowed transitions can be derived in a quasi-classical vector picture of transition dipole moments. For the case of identical molecules with coplanar, inclined transition dipoles, the exciton splitting term, β, can be expressed as:

$$\beta = \frac{|\mu|^2}{R^3}(1 - 3\cos^2\theta), \tag{2.27}$$

where μ denotes the transition moments of the molecules, R the distance between centers of the moments, and θ the angle between the direction of the moments and R.

A dimer is called H-aggregate if the molecular transition dipoles are parallel and $\theta > 54.74°$. For $\theta = 54.74°$, the dipole-dipole interaction vanishes, for smaller angles the dimer is called J-aggregate. For the special case of H-aggregates, only transitions to the higher energetic excited state are allowed, whereas in the case of J-aggregates, only transitions to the lower energetic state are allowed. In contrast, for dimer configurations with nonparallel dipole moments, both transitions are optically allowed.

2.2.2 Excimer and Exciplex

In many cases, in solutions of increasing dye concentration, a decrease of the fluorescent quantum yield is observed. Then, the solution features the optical absorption characteristics of a monomer, but also shows a broad, structureless fluorescence with particularly large Stokes shift. The phenomenon is called self- or concentration quenching and is due to the generation of a molecular complex, formed by the combination of a ground-state molecule with an excited state molecule [32]:

$$M^* + M \longrightarrow (MM)^*. \tag{2.28}$$

Such a complex is called an excimer and refers to a dimer that exists only in the excited state, the ground-state of the pair being dissociative. In contrast, in the case of physical dimer, the molecules are fixed with respect to each other, and a definite absorption and fluorescence band can be attributed to the dimer association.

For the system $M+M$ of two molecules, the ground state of the pair is supposed to be dissociative, since, except for a small van der Waals attraction, all interactions are purely repulsive. Thus, even the molecules are free to move, they do not form a physical dimer. Stabilizing interactions are possible if one of the molecules is promoted into the excited state and the highest occupied molecular orbital

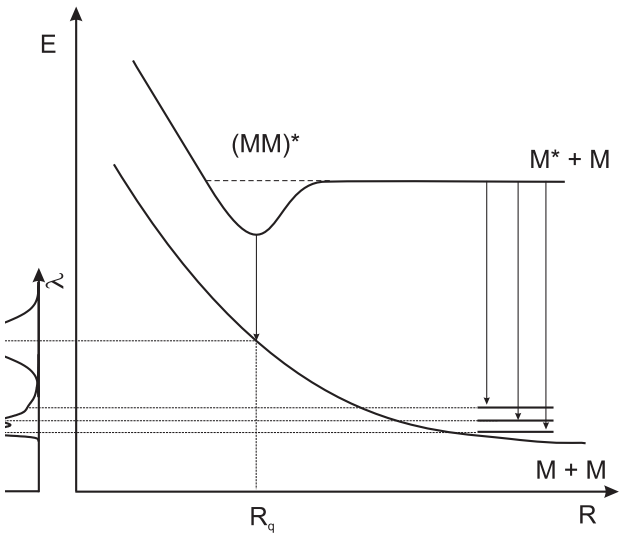

Figure 2.4: Schematic representation of the potential energy surfaces for monomer and excimer as a function of the intermolecular separation R, and of the difference between monomer and excimer fluorescence (adapted from [32]).

(HOMO) and the lowest unoccupied molecular orbital (LUMO) of the combined system are only singly occupied. This gives rise to the relative minimum of the excimer $^1(\mathrm{MM})^*$ on the excited-state potential energy surface. The potential energy surfaces of the ground state $M+M$ and the excited state M^*+M are represented schematically in Fig. 2.4. The excimer gains energy by reducing the molecular separation to the equilibrium distance. As evident from the scheme, the excimer fluorescence is to be expected at longer wavelengths than monomer fluorescence and that the related emission band should be broad and generally without vibrational structure, being a result of transition into the unbound ground state. Since the concentration of the M^* monomer is reduced by excimer formation, the emission intensity from free M^* will be reduced. Hence, excimer formation represents a form of emission quenching.

Excimer fluorescence also appears in crystals. Noteworthy examples are pyrene and α-perylene. In these crystals, there are four molecules per unit cell, representing two physical dimer pairs. In pyrene, adjacent parallel molecules are closely spaced. The interplanar distance between the pairs is 3.53 Å, which lies within the range of an attractive excimer interaction. When the crystal is excited, the excimer is easily formed. Thus the crystal fluorescence is that of the excimer in solution. In β-perylene and in N,N '-dimethylperylene-3,4,9,10-bis-dicarboximide (MePTCDI), there are only two molecules per unit cell, so there are no physical dimers present. Nevertheless, excimer-like fluorescence was observed for MePTCDI as well [33]. Layers with dye coverage much less than a monolayer show monomer-type emission, similar to that of dilute solution. With increasing molecular coverage, the monomer fluorescence decreases and excimer-like emission appears and increases.

If a molecule complex is formed between electronically excited molecule M and

dissimilar type of molecule Q in the ground state, the complex is called an exiplex. In contrast to the excimer emission, the exiplex fluorescence is very sensitive to the solvent polarity. The exciplex emission maxima and intensities depend on the the reduction-oxidation properties of the participating molecules, suggesting that an element of electron transfer is involved in the process of exciplex formation. Detailed discussion of exciplex classification and properties can be found in [34].

2.3 Excitons in organic materials

The optical excitation in inorganic and organic semiconductors results in a mobile, electrically neutral bound electron-hole pair referred to as an exciton. In solids with strong intermolecular interactions, an exciton can be delocalized over a number of molecules. Depending on the degree of delocalization, the excitons are defined as Frenkel, Wannier-Mott (WM) and Charge-Transfer (CT)(Fig. 2.5).

Wannier-Mott excitons appear in weakly correlated, crystalline semiconductors (e.g. Si, Ge, GaAs, etc.), in which the overlap between neighboring lattice atoms reduces the Coulombic interaction between the electron and the hole participating in the exciton. Hence, the electron-hole distance for this type of exciton should be larger than the lattice constant: sometimes it is in the order of many lattice constants (40 - 100 Å). The internal structure of the WM excitons can be represented by hydrogen-like wavefunctions. The medium between the electron and the hole is treated as a dielectric continuum. The WM exciton is not found in organic materials.

The Frenkel exciton corresponds to a correlated electron-hole pair localized on a single molecule. Its radius is comparable to the size of the molecule, i.e. smaller than 5 Å. The Frenkel exciton is considered a neutral particle that can diffuse from site to site. The electric field of the moving exciton polarizes the molecular surrounding and thus produces lattice vibration waves, the so-called phonons. The latter process can also be described as forming a composite quasi-particle, being a combination of an electron plus phonon field, referred to as polaron [30].

The CT exciton is an intermediate case between a Frenkel and a Wannier-Mott state, being neither very extended nor tightly bound to a single molecule. It is sometimes regarded as an unrelaxed polaron pair with both the positive and negative polarons of the charge pair located on discrete and almost adjacent molecules. Yet, this localized picture is only true for a molecular crystal with weak intermolecular interactions and a small overlap between the neighboring orbitals, i.e. each molecule forms a deep potential well in which the charges are confined.

For planar stacking molecules with significant overlap between the π systems of neighboring molecules in the stack, the electronic states can no longer be considered as localized at a single lattice site. Hence, the exciton wave function should be an extended state, with shape and symmetry which are dependent on the crystalline and molecular structures. The CT charge pair becomes delocalized, resulting in a crystalline pseudopotential smaller than the energy bandwidth. In this case, the CT exciton can be represented by a hydrogen-like wave function [35].

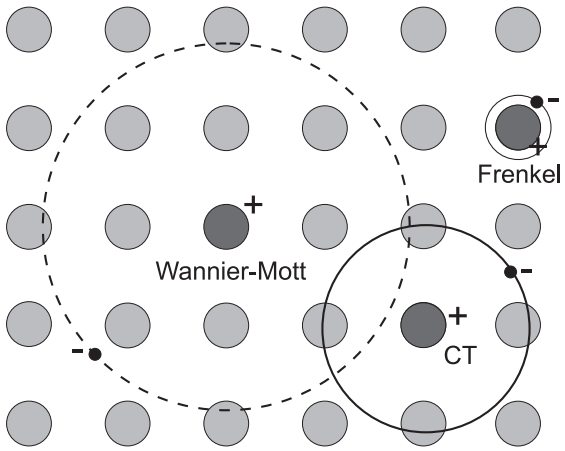

Figure 2.5: Types of excitons in inorganic and organic crystalline semiconductors.

2.4 Energy transfer processes

The radiative and non-radiative processes are not restricted in the space around the excited molecule. Independent of the weak van der Waals interaction between the molecules in the organic film, the excitation energy can be effectively transported to distances substantially exceeding the size of the molecules. Such energy transfer processes are particularly important for doped organic films. The incorporation of even a fraction of a percentage of dissimilar type of molecules during film growth can change considerably the optical and electrical properties of the layer.

The process of any transfer of energy from an excited molecule, donor (D), to another molecule, energy acceptor (A), can be described by the following equation:

$$D^* + A \longrightarrow D + A^* \tag{2.29}$$

As a consequence of this energy transfer, the acceptor is promoted to a higher electronic state. If the donor and the acceptor are the same species, the term "energy migration" is used.

There are number of different energy transfer processes to be distinguished:

1) Radiative energy transfer in which the donor emission is reabsorbed by the acceptor:

$$D^* \longrightarrow D + h\nu,\ h\nu + A \longrightarrow A^* \tag{2.30}$$

No direct interaction of the donor with the acceptor is involved. The process requires that the emission spectrum of D and the absorption spectrum of A overlap. Thus, the efficiency of the transfer is governed by the photoluminescence yield of the donor molecules and the absorption ability of the acceptor, i.e. the extinction coefficient ε_A.

2) Non-radiative energy transfer requires the presence of a specific interaction between D and A. Two types of interaction are identified: the Coulombic interac-

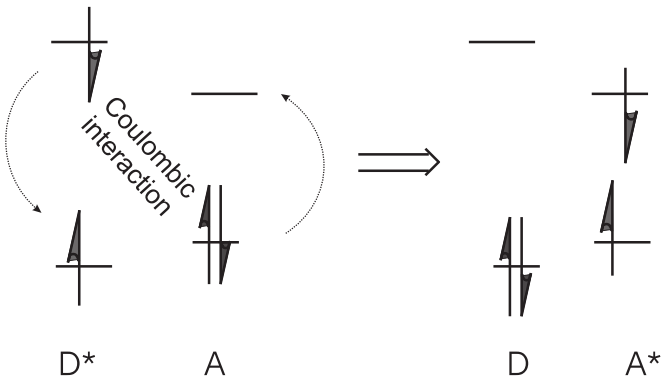

Figure 2.6: Scheme of Förster energy transfer mechanism [34].

tion, known as Förster energy transfer, and electron-exchange, referred as Dexter energy transfer.

The interaction between D* and A can be described by the perturbation Hamiltonian, *H'* [30]. The product of the wave functions of the donor and the acceptor $\psi(D^*)\psi(A)$ characterizes the starting state. Respectively, $\psi(D)\psi(A^*)$ describes the final state. The probability P for an energy transfer process due to weak perturbation *H'* is given by

$$P \propto \rho \langle \psi(D^*)\psi(A)|H'|\psi(D)\psi(A^*)\rangle^2, \tag{2.31}$$

where ρ describes the density of the initial and final states which participate in the interaction. For organic molecules with typically broad spectral features, ρ can be estimated by calculating the overlap integral of donor luminescence and acceptor absorption. The probability P is measured experimentally with the rate constant K_{D-A}. The perturbation Hamiltonian *H'* comprises several terms, of which the most important are the electrostatic (Coulomb) and electron-exchange interactions.

2.4.1 Förster energy transfer

The Coulomb or Förster energy transfer involves a dipole-dipole coupling of the transition dipole moments for excited donor (exciton) and the acceptor dye in its ground state. As the excited donor relaxes, its energy is transferred via the Coulomb interaction with the acceptor dye molecule (Fig. 2.6). A characteristic of this energy transfer process is that the dipole-dipole interaction covers large distances, thus efficient transfer is possible over distances up to 100 Å.

A measure for the efficiency of the process is the value of the rate of energy transfer relative to the radiative relaxation of the donor molecule. A high rate of the energy transfer relative to radiative relaxation will lead to emission exclusively from the acceptor. For the rate of energy transfer between a donor and acceptor molecules separated by distance r, Förster has derived the following quantitative

expression in terms of experimentally obtainable parameters:

$$K_{D-A} = \frac{B\phi_D J}{\tau_D r^6} = \left(\frac{1}{\tau_D}\right)\left(\frac{R_0}{r^6}\right), \tag{2.32}$$

where ϕ_D is the fluorescence quantum yield of the donor in the absence of acceptor and τ_D is the excited state lifetime of the donor. B is a constant which depends on the donor refractive index n, Avogadro's number N_A and a factor k_p, associated with the relative orientation of the donor and acceptor dipoles:

$$B = \frac{\{9000(ln10)\}k_p^2}{128\pi^5 n^4 N_A}. \tag{2.33}$$

The orientation factor k_p^2 has a value of 2/3 for random donor - acceptor orientations. J is the overlap integral between the donor and acceptor over the whole spectrum; J is defined as:

$$J(\lambda) = \int F_D(\lambda)\varepsilon_A(\lambda)\lambda^4 d\lambda, \tag{2.34}$$

where $F_D(\lambda)$ is the fluorescence spectrum of the donor, and ε_A (λ) is the molar extinction coefficient spectrum of the acceptor molecules in dilute solution. The integral J measures the degree of spectral overlap between the donor fluorescence and acceptor absorption spectra. A high degree of overlap is favorable for high rate of energy transfer.

Yet, it is difficult to determine the rate of energy transfer for randomly doped systems, e.g. those used in OLEDs. The problem arises from the fact that the dipole-dipole interaction and, hence, the energy transfer will have strong distance dependence. A broad distribution of distances in a randomly doped sample will lead to a broad distribution of rates [36]. Therefore, a more ordinary approach for evaluation of Förster transfer is to determine the Förster radius R_0. This is the critical transfer distance at which the rate of energy transfer is equal to the decay rate of the donor:

$$K_{D-A}(at\ R_0) = \frac{1}{\tau_D}. \tag{2.35}$$

A large Förster radius refers to efficient transfer process, competing very effectively with unimolecular relaxation at distances shorter than R_0. A short Förster radius indicates very inefficient transfer process that requires short donor-acceptor distances to be efficient.

In Förster energy transfer, the spin of both donor and acceptor is conserved. Therefore, allowed transitions are

$$^1D^* + {}^1A \longrightarrow {}^1D + {}^1A^* \tag{2.36}$$

and

$$^1D^* + {}^3A(T_n) \longrightarrow {}^1D + {}^3A^*(T_m), \tag{2.37}$$

where $n{>}m{\geq}1$. The triplet-singlet transition

$$^3D^* + {}^1A \longrightarrow {}^1D + {}^1A^* \tag{2.38}$$

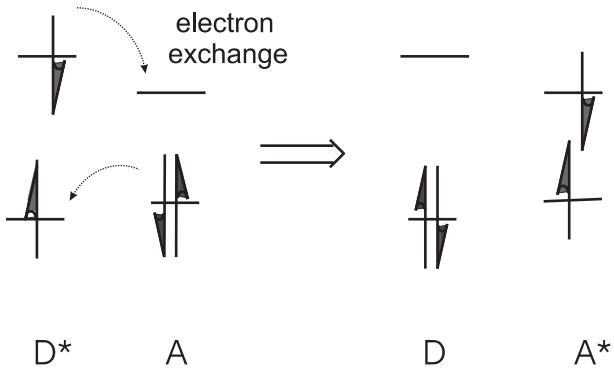

Figure 2.7: Schematic presentation of Dexter energy transfer mechanism [34].

is forbidden. However, since ^{3}D* has a long lifetime and K_{D-A} can exceed the ^{3}D$^* \longrightarrow {}^1$D transition rate, it has been also observed [30]. This process is also called sensitized fluorescence.

2.4.2 Electron-exchange energy transfer

The electron-exchange or Dexter transfer involves an electron transfer mechanism in which the excited electron on D* transfers into the LUMO of A with a simultaneous transfer of an electron from the HOMO of A into the corresponding orbital on D (Fig. 2.7). Thus, in contrast to the Förster transfer, the Dexter transfer requires much closer contact between the excited donor and the acceptor allowing for overlap of the electron orbitals involved. Dexter energy transfer does not have a singlet requirement and can effectively act to transfer energy between triplet states or between singlet and triplet states.

The transfer probability from the donor to the acceptor is expressed as:

$$P_{D-A} = \frac{2\pi}{\hbar} Z^2 J', \tag{2.39}$$

where J' is the overlap integral, however calculated with the normalized emission spectrum of the donor and the normalized absorption spectrum of the acceptor. Therefore, the rate of Dexter energy transfer is independent of the strength of dipole-dipole interaction. The parameter Z is related to the separation between donor and acceptor molecules R and the van der Waals radius L of the donor-acceptor pair [32]:

$$Z^2 \propto exp(-2R/L), \tag{2.40}$$

Thus, since Z^2 respectively P_{D-A}, are rapidly decreasing functions of the D-A separation distance, Dexter transfer occurs only over a short distance, typically $\sim$ 10 Å, and is effectively restricted to neighboring molecules.

In the Dexter transfer process, only the total spin of the D*-A system is conserved. Triplet-triplet energy transfer

$$^3D^* + {}^1A \longrightarrow {}^1D + {}^3A^*, \tag{2.41}$$

which is forbidden in the Förster approximation is now allowed.

2.5 Solvent effects in solid organic films

Solvents influence the absorption and emission spectra of many organic dyes through their electrostatic properties [37]. The solvent interaction with the solute molecules, referred to as "solvation effect", may be dipole-dipole, dipole-induced dipole, induced-dipole induced-dipole, or hydrogen bonding in dependence on the molecular structures of solvent and solute. The solvent-solute interactions lead to an alteration of the energy difference between ground and excited states of the solute molecule.

Theoretical modelling of the solvation effect is limited by the complexity of the solvent-solute system, however qualitative treatments have established that the polar solvent strongly affects the more polar state of the molecule.

Since molecular electronic transitions lead to redistribution of charge, the dipole moment of the ground state μ_0 and of the excited state μ_1 will, generally, be different. Light absorption alters the electronic distribution of the solute so that the electronic dipole moment of the electronically excited molecule is altered with respect to that of the molecule in its ground state. Since the absorption process is fast, it ends up with the excited molecule still surrounded by the ground electronic state equilibrium solvent cage and in the ground electronic state equilibrium geometry, i.e. in a Franck-Condon state. If the solute molecule becomes more polar in the excited state, i.e. $\mu_1 > \mu_0$ (Fig. 2.8a), there will be a greater electronic stabilization of the electronically excited state, relative to the ground state by interaction with the polar solvent. Assuming that the molecular geometry does not change subsequently to excitation, the greater the polarity of the solvent, the lower will be the energy of the electronically excited state. This type of behavior tends to shift the absorption band to longer wavelengths with increasing solvent polarity. If the electronic dipole moment is lower in the electronically excited state than in the ground state ($\mu_0 > \mu_1$), increasing solvent polarity stabilizes the ground state to a greater degree than the electronically excited state, and the absorption spectrum tends to shift to higher energies with increasing solvent polarity (Fig. 2.8b).

When the position of emission bands in dependence on the solvent is considered, one has to take into account the finite relaxation time τ_R for the rearrangement of the solvent molecules surrounding the solute molecule in the Franck-Condon excited state as well as the lifetime τ_e of the molecule in the excited state. Immediately after excitation, the Franck-Condon solvent cage [38] and the molecular geometry relax to conform to the new electronic distribution of the excited molecule. Since nuclear motions are involved, solvent relaxation is nearly simultaneous with rotational and vibrational relaxation, i.e. about 10^{-13} - 10^{-11} s in solvents of viscosity comparable to that of water at room temperature. In comparison to the deactivation of the lowest excited singlet state, typically of the order of 10^{-8} s, solvent relaxation is usually fast. As a consequence, emission occurs from the excited solute molecule in a thermally relaxed solvent cage configuration S_1

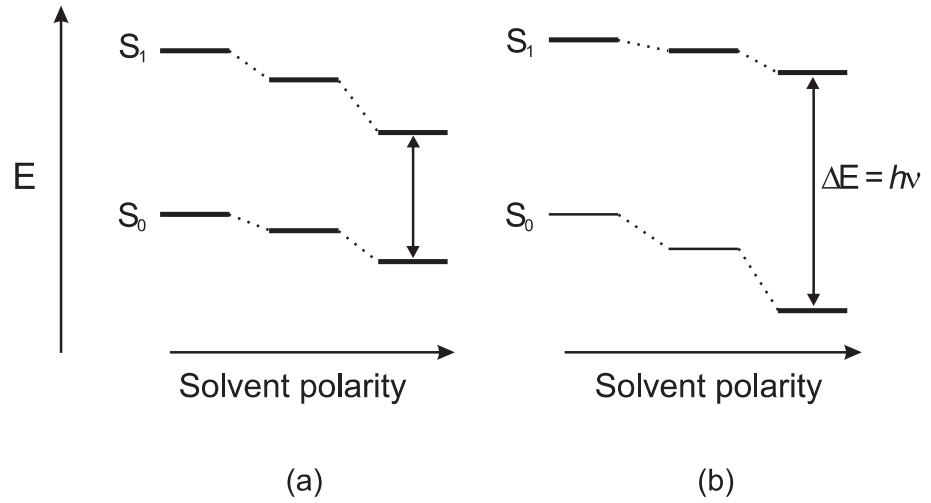

Figure 2.8: Schematic presentation of solvatochromism. (a) The dipole moment of the Franck-Condon excited state μ_1 is larger than those of its ground state μ_0. (b) The opposite holds (adapted from [37]).

that is lower in energy than the Franck-Condon excited state S'$_1$ (Fig. 2.9). The fluorescent transition ends up in the ground electronic state of the molecule S'$_0$, however due to the rapidity of the electronic transition, the molecule is still in the solvent cage of the electronically excited state equilibrium. The latter is higher in energy than the thermally equilibrated ground state. Then, rapid solvent and geometrical relaxation occur and the solute molecule returns to the ground-state equilibrium solvent cage and geometry S_0. When the dipole moment of a fluorescent molecule is larger in the excited state than in the ground state ($\mu_1 > \mu_0$), the relaxed excited state S_1 will be energetically stabilized relative to the ground state S_0 and a significant red shift of the emission band will be observed. The stronger the solute-solvent interaction, the larger the red shift of the fluorescence band and the corresponding Stokes shift.

In the particular case of non-polar solute in a non-polar solvent, only dispersion forces contribute to the spectral changes, causing a shift to longer wavelengths. For aromatic compounds, its magnitude is found to be in linear correlation to the solvent refractive index n via the function

$$(n^2 - 1)/(2n^2 + 1). \tag{2.42}$$

Similarly to liquid solutions, a solvation effect was observed for dye molecules doped in solid matrices. Bulovic et al. [39] have shown for DCM2 doped Alq_3 and zirconium 8-hydroxyquinoline (Zrq_4) thin films that the luminescence peak shifts to the red upon increasing DCM2 concentration (Fig. 2.10). The energy shift is explained by a self-polarization effect of the dopant molecules due to dipole-dipole interactions. As the highly polar DCM2 ($\mu_0 = 11.3$ D as referred in [39]) is dispersed in the relatively non-polar matrices at higher concentrations, the distance between the neighboring DCM2 molecules decreases. Thereby the local electric

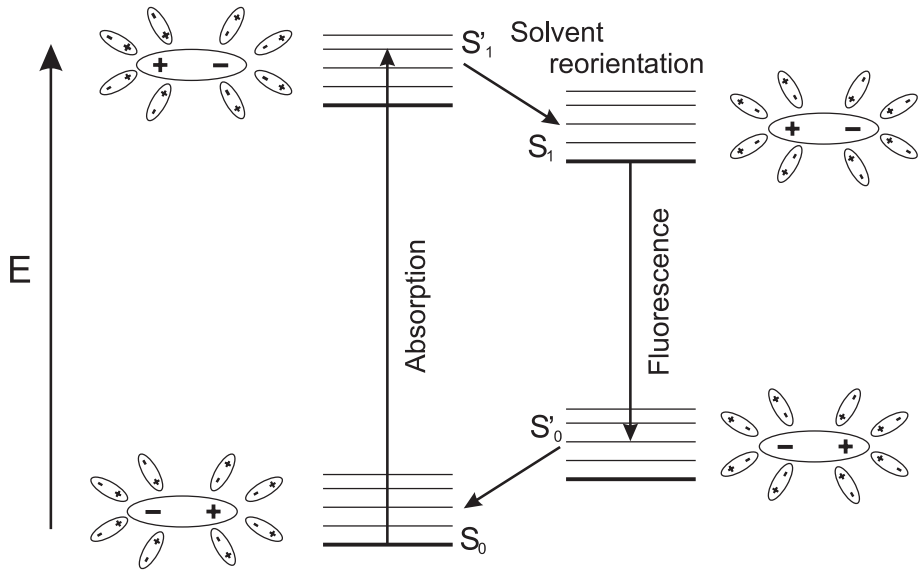

Figure 2.9: Schematic representation of solvent change due to excitation or emission. S'$_1$ and S'$_0$ are the Franck-Condon excited and ground states, respectively. S$_1$ and S$_0$ are the corresponding equilibrium states; $\tau_R \ll \tau_e$ [38].

field increases. This field perturbation tends to shift the emission peak of DCM2 to the red. For DCM2 concentrations above 10 %, the position of the emission maximum is independent of the host material (Fig. 2.10) as the local electric fields are determined basically by the polar DCM2 molecules, while below 10 % doping the local fields are determined by the host. Thus, the emission in Alq_3 is shifted to lower energies with respect to that in Zrq_4 since Alq_3 has the larger ground state dipole moment ($\mu_0(Alq_3) = 5.5$ D, while $\mu_0(Zrq_4) \sim 0$ D).

Likewise, when DCM2 is doped in the non-polar N,N'-dyphenyl -N,N'-bis(3-methylphenyl)-1,1'-biphenyl-4,4'-diamine (TPD), the electroluminescence peak undergoes a shift of $\Delta\lambda_{max} = 75$ nm for DCM2 concentrations from 0.9 to 11 %. As in Zrq_4, this large shift is due to the small TPD dipole moment of 1.5 D, associated with its almost symmetric structure [30].

Another example of a self-polarization-induced solid-state solvation effect is the observed luminescence shift of Alq_3 when distributed in TPD [40]. Due to the small dipole moment of Alq_3 in the ground state, the increase of the Alq_3 concentration in the mixed Alq_3/TPD films leads to shift of the luminescence peak from 498 nm (1 % Alq_3) to 522 nm (100 % Alq_3).

The adjustment of the strength of dipole-dipole intermolecular interactions in doped host-guest molecular organic thin film systems is proven to be an effective method for tuning the emission spectrum of dipolar molecules.

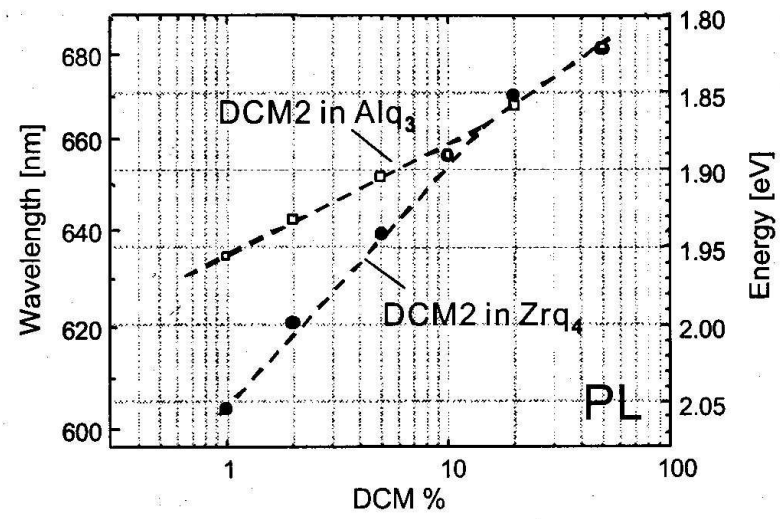

Figure 2.10: Fluorescence peak position of DCM2 doped Alq_3 and Zrq_4 thin films as a function of DCM2 concentration (from [39]).

2.6 Photostability

The lack of photostability, i.e. the photobleaching, is a dynamic, mostly irreversible process in which fluorescent dye molecules undergo photoinduced chemical destruction upon absorption of light, thus losing their ability to fluoresce.

A measure for the efficiency of the photobleaching reaction is the quantum yield of photobleaching, which by definition is the number of molecules that have been photobleached, divided by the total number of photons absorbed during the same time interval:

$$\phi_b = \frac{number\ of\ photobleached\ molecules}{total\ number\ of\ absorbed\ photons}. \tag{2.43}$$

The mean number of survived absorption cycles μ is equal to

$$\mu = \frac{1-\phi_b}{\phi_b} \approx \frac{1}{\phi_b}. \tag{2.44}$$

There are multiple chemical reaction pathways for the alteration of a chromophore. Some of them only change the fluorescent properties, whereas others produce nonfluorescent species. The irreversible photobleaching reactions can be divided into three categories: unimolecular reactions, multi-photon photolysis, and bimolecular reactions ([41] and the references there). The fluorescent dye molecule M may either be in the first excited electronic singlet state $^1M_1$ or in the triplet state $^3M_1$. However, the bleaching mechanism may well vary from one class of dyes to another.

The unimolecular reactions are important for vibronically excited as well as for relaxed states (thermally activated reactions). They depend solely on the properties of the chromophore and the solvent environment. Unimolecular reactions are

the rearrangement and isomerization reactions (e.g. *cis-trans* interconversions in double-bonded systems like stylbenes) or photochemical fragmentation reactions such as homo- and heterocyclic dissociation reactions producing radicals ($X^{\bullet}$, $Y^{\bullet}$), or ions (M^+e^-).

The application of high irradiances might result in an increasing probability for multi-photon absorption with high probability of a photobleaching reaction from the excited electronic state. As an example, in single-molecule spectroscopy, such processes occur when the irradiance exceeds 10^5 W/cm^2. Thereby, subsequent heterocyclic dissociation forming a radical ion pair (M^+e^-) is favored. Two-quantum photoexcitation can be achieved by (i) two-step excitation as a result of successive absorption of two photons via a real intermediate state (e.g. S_1 or T_1) or (ii) two-photon absorption as a result of a simultaneous absorption of two photons via a virtual state. Especially in the UV, two-photon excitation can produce highly lying excited molecular states close to or even above the ionization threshold of 5 - 8 eV [42].

The bimolecular reactions cover the photoinduced reactions, proceeding via the formation of an encounter complex [32]. In variable distances, all chemical reactions can subsequently take place, such as energy transfer with follow-up reactions (sensitized reactions), electron transfer, proton transfer, short-range electron exchange energy transfer, etc. The reaction partner may be a solvent molecule, an added reactant (e.g. a quencher, a proton donor), an impurity, another dye molecule, or molecular oxygen (O_2). The latter is probably the most important reactant at room temperature.

Oxygen has a triplet electronic ground state $^3O_2$ with unpaired electrons and a very low singlet excited state. In contrast, most stable organic dyes show singlet spin multiplicity in the electronic ground state. Thus, the reaction of these compounds with oxygen is generally slow without the presence of light. The formation of singlet oxygen is represented by the following reaction:

$$^3M^* + {}^3O_2 \longrightarrow {}^1M + {}^1O_2^*, \tag{2.45}$$

the oxygen quenching the triplet state of an organic molecule M. Afterwards, the singlet oxygen can readily chemically react with other molecules in the singlet state. The photodestruction reaction can take place (i) as a follow-up reaction in the reaction complex with the dye molecule just quenched or (ii) due to the long lifetime (3 - 7 μs) of singlet oxygen, as a reaction of a freely diffusing oxygen with another singlet dye molecule. Hence, the diffusion constant and solubility of oxygen in the host matrix are important factors in the efficiency of photooxidation reactions. Table 2.2 presents examples for the latter properties of O_2 in some hosts.

Upon photon absorption, bimolecular photobleaching reactions and two-photon absorption compete with other molecular deactivation processes. Most of the photobleaching reactions of electronically excited molecules take place in the long-lived (vibronically relaxed) states, i.e. in the first excited singlet state S_1 or in the first excited triplet state T_1. Compared to the singlet states with typical lifetimes on the order of 1 to 20 ns, the triplet state is in particular prone to photobleaching due to its long lifetime of several μs or longer.

Host	Solubility/ concentration of O_2 (cm^{-3})	Diffusivity of O_2 (cm^2/s)
Air (pores in solid host)	6 x 10^{18}	10^{-1}
Solvent	1.2 x 10^{18}	$\approx 10^{-4}$ - 10^{-5}
PMMA	$\approx 10^{-18}$	10^{-8}
SiO_2 glass	-	$\approx 10^{-18}$ - 10^{-23}

Table 2.2: Solubility and diffusivity of molecular oxygen in various hosts; data from [43, 44].

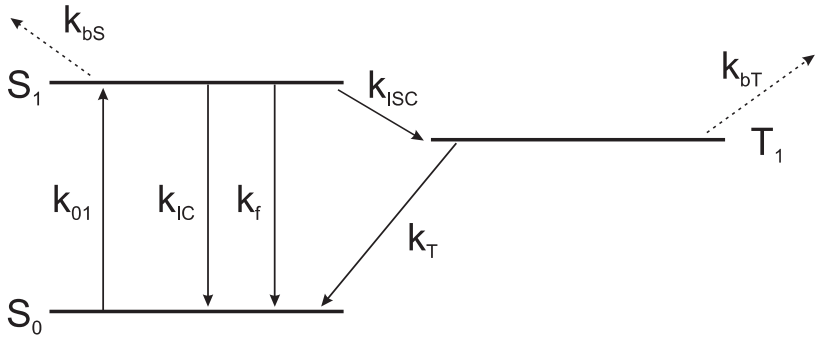

Figure 2.11: Electronic energy diagram of a dye molecule with three electronic levels regarding photobleaching from every excited electronic level [41].

The number of irreversibly photobleached molecules results in a decrease in dye concentration, *c(t)*, with time *t*. Assuming a quasi-unimolecular character of the photobleaching reaction, an exponential dye concentration decrease should be observed [41]:

$$c(t) = c_0 \exp(-k_z t), \tag{2.46}$$

where c_0 is the initial (t = 0) concentration, and k_z denotes the effective pseudo first-order bleaching rate constant. Actually, such a dependence has been observed for fluorescing dyes in liquid solutions. Figure 2.11 presents the electronic energy diagram of a dye molecule with three electronic levels: ground singlet state, S_0, first excited state, S_1, and lowest excited triplet state, T_1. Photobleaching reactions are assumed to be possible from all excited states with the microscopic rate constants k_{bS} and k_{bT} respectively. As long as the fluorescence intensity depends linearly on the excitation irradiance, the photophysical processes are limited to a three-level system of the electronic states S_0, S_1 and T_1. In that range, the corresponding quantum yield of photobleaching ϕ_b is

$$\phi_b = \frac{k_b}{k_0}, \tag{2.47}$$

where $k_b = k_{bS} + k_{bT} k_{ISC}/k_T$ represents the composite microscopic rate responsible for the photobleaching in both singlet and triplet states and k_0 is the deactivation

rate of S_1 ($\tau_0 = 1/k_0$ - fluorescence lifetime of S_1).

Studies on the optimization of organic-based systems as active media for solid-state laser applications have established that some of the deactivation pathways can be suppressed by incorporating the dyes in a solid host [45, 46, 47]. Organic dyes have been incorporated in various solid-state hosts such as polymers (e.g. poly(methyl methacrilate)(PMMA), polyurethane acrylate, poly(vinyl alcohol etc.), porous glasses, sol-gel derived glasses (mostly inorganic silica glasses).

In general, the increased photostability in such solid hosts is due to (i) a lack of translational freedom for the dye; intermolecular collisions deactivation is thus avoided. Each molecule is trapped in his own cage (ii) initial impurities in the dye are isolated and do not interfere by destructive (photo)processes (iii) photodecomposition products do not migrate and thus cannot facilitate further decomposition (iv) in particular for inorganic glass matrices, the dye molecule is totally isolated from the surrounding gas or liquid; the solid cage reduces internal rotation modes in the dye to a greater extent than the relatively flexible organic polymer molecules. It has to be noted, however, that photobleaching decays of dye molecules in solid matrices are generally difficult to predict. In addition to the variety of possible degradation mechanisms, there is a large heterogeneity of molecular environments, hence the assumption for first-order rate constant of photobleaching is rather inadequate [48]. Mostly, the experimental curves of fluorescence decay in time under continuous irradiation can be analyzed by a multi-exponential function [47, 49]:

$$I_F(t) \sim \sum A_i \exp(-t/\tau_i), \tag{2.48}$$

where $I_F(t)$ is the time-dependent fluorescence intensity, proportional to the electronic ground state population, A_i is the pre-exponential factor, interpreted as proportional to the relative contribution of each rate constant, corresponding to different photobleaching processes, and τ_i is the lifetime defined as the time necessary for the emission to reach 1/e of its initial value.

Since many of the organic dyes react with oxygen, leading to their degradation, an oxygen-free environment increases the photostability of the organic molecules. Therefore, some of the techniques proposed for improving the photostability of the dye molecules include increasing dye caging in order to prevent dye diffusion or oxygen diffusion, controlling the chemical environment, covalently attaching the dye to the host, removing the porosity of the host, or incorporation of additives such as interceptors [43, 50]. The latter are molecules which preferentially react with O_2, or quench the excited state of O_2.

A parameter which also influences the photostability is the temperature. Lowering the temperature results in drastic decrease of photobleaching (up to one order of magnitude decrease of the photobleaching efficiency at 193 K compared to that at 300 K [51]). Since the most photobleaching processes are chemical in nature, they have to overcome an activation barrier. The immobilization of reactive molecules, such as water, at low temperatures can also further lead to increased photostability.

2.7 Multi-component systems

The multi-component systems we refer here to are vacuum deposited thin films comprising two or more materials. The latter can be either only organic or a mixture of both organic and inorganic.

2.7.1 Organic guests in inorganic host materials (metal halogens, metal oxides, etc.)

This group of multi-component systems was first introduced by Böttcher et al. ([25] and Refs. 4-7 presented there) and termed as "norganics". In general, compared to the corresponding liquid solutions of the organic dyes, these systems show a broadening of the absorption bands. The PVD technique assures low-order arrangement and thus enables the formation of various aggregate modifications, resulting in both blue and red shift and broadening with respect to the absorption band of the monomer. The distribution of aggregates is defined by the deposition conditions, substrate temperature, annealing processes, as well as by the individual structure of the organic molecules.

The size of the molecular aggregates can be influenced by changing the volume fraction of the inorganic material. Studies on the Merocyanine dye MC1 incorporated in the polycrystalline host NaF show that the dilution of the dye in the host leads to a steady decrease in the size of the aggregates formed [24]. Structural and morphological investigations of Cu-phtalocyanine (CuPc)/SiO_2 VD films reveal that in films with dye fractions > 50 vol%, the dye microcrystallite sizes are typically in the range 30 - 80 nm, while at smaller CuPc contents (< 25 vol%) the organic molecules are almost completely isolated in the inorganic SiO_2 matrix [22]. As a general trend, with increasing size of the matrix crystallites, lower dye contents are required in order to obtain mixed films with predominantly isolated molecules. Such behavior is easy to understand, taking into account the possibility for phase separation in the crystalline matrix.

For a strongly polar dye such as MC1, it is established that upon dilution in various types of matrices, solvatochromic effects become active, and hence absorption shifts of up to 200 nm can be realized [25]. In the case of non-polar dyes, the observed shifts in the absorption are only minor.

Similarly, the luminescence spectra are affected by the molecule distribution in dimers and higher order aggregates and can be likewise interpreted by exciton models (Fig. 2.12). As argued in Section 2.2, only luminescence of red-shifted dimers and aggregates is allowed. Hypsochromic shifted excited states are mostly thermally deactivated or transfer their energy to low lying emitting states. The latter effects can be followed by comparison of the luminescence spectra recorded upon various excitation wavelengths.

Additionally, due to the small separation between molecules in highly concentrated mixed samples, the excitation energy can migrate either by exciton diffusion or by Förster energy transfer to luminescence traps. As such, surface or lattice defects are considered. Steady-state and transient luminescence measurements have proven that low-energy excitation states can also act as energy traps and thus can

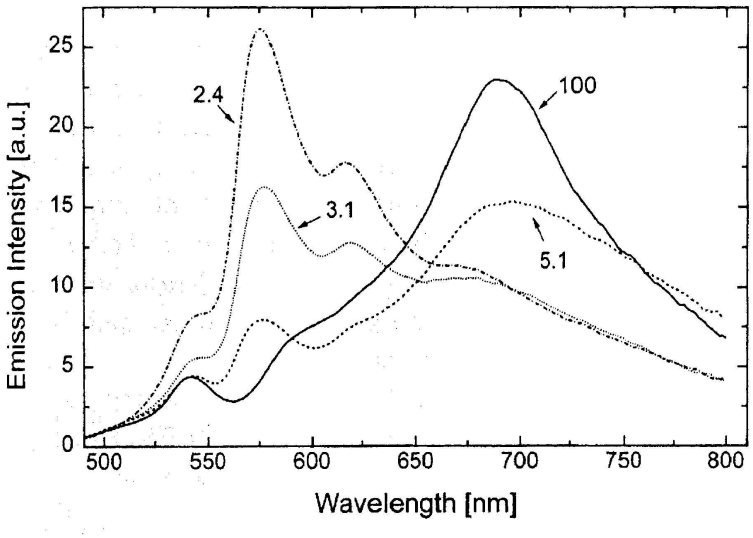

Figure 2.12: Fluorescence spectra of mixed perylene derivative MePTCDI-NaF layers at various dye volume concentration. The total MePTCDI amount in the solid layers is constant (from [21]).

explain the low luminescence efficiency of the dyes in the solid state [24]. For several dyes in inorganic hosts, it has been shown that in the region between 10 to 50 vol% dye content, the PL quantum efficiency has a minimum, which is attributed to both the presence of a high fraction of non-luminescent dye aggregates and a disordered matrix structure [25, 52]. Dilution below 2 vol% results in predominant monomer emission and enhanced PL efficiency, respectively.

For inorganic hosts with low gap energies, it is established that electron transfer from the excited embedded dye is possible. This is supported by observation of largely quenched luminescence from MC1 molecules in $PbBr_2$ (E_g = 3.84 eV) and PbI_2 (E_g = 2.5 eV) matrices [24].

An additional effect, following from the modified absorption in the visible spectral region, is alteration of the color coordinates of the mixed films. The magnitude depends on dye concentration and matrix materials [23].

2.7.2 Organic molecules distributed in organic hosts (polymers or small molecules)

Polymeric materials have shown promising properties as matrices for incorporation of active organic molecules. Reported are results for application of molecularly doped polymer thin films as active layers in OLEDs [53], plastic scintillator detectors [54], microcavities [130], etc. As polymer matrices, polyimides are commonly used, since the variety of existing monomers offers broad possibilities for obtaining the desired matrix properties. Additionally, the vacuum deposition polymerization (VDP) technique enables an easy incorporation of the dopant molecules within the

polymer host. In general, the polymer matrix is optically inactive, due to the low absorption in the visible spectral range. However, when the polyimide matrix itself is fluorescent and there is sufficient spectral overlap with the absorption of the dye molecules, a transfer of the exciting energy of the matrix to the guest molecules can take place. For polyimide hosts, the thermal treatment procedure could influence not only the properties of the matrix, e.g. thermal and mechanical stability [53], but also the optical properties of the dopant molecules. For example, the increase of curing temperature leads to preferential formation of H-dimers of rhodamine B due to steric hindrance [54].

Selective doping of thin films of low molecular weight organic compounds with guest organic molecules known for their high fluorescence quantum yield has proven to be an effective approach for obtaining high luminescence efficiencies [55, 56]. Additional effects achieved by doping are color tuning and white light emission [36, 57]. For this purpose, laser dyes such as (dicyanomethylene)pyran derivatives (e.g. DCJTB, DCM1, DCM2) [58, 59, 60, 61, 62], coumarines (e.g. C540) [63, 64] or N,N-diethyl quinacridone (DEQ) are commonly used [65]. The dye doping technique has been successfully applied to fabricate OLEDs whose colors cover the entire visible spectrum, with good efficiencies and device lifetimes.

As organic hosts, mostly blue or green luminescent materials are employed, such as the metal chelate Alq_3 or its methylene derivative $Almq_3$, the aromatic diamines TPD, 4,4",4"-tris(1-naphtylphenylamino) triphenylamine (1-TNATA) and N,N'-dyphenyl-N,N'-bis(1-naphthyl-phenyl)-1,1'-biphenyl-4,4'-diamine (NPB), etc.

Red emitting materials with planar molecular geometry are commonly used as dopants. Dyes that emit at longer wavelengths, above 610 nm, are usually polar such pyran-containing compounds, or non-polar but extensively π-conjugated [56]. Although some of them are highly luminescent in solution, such as DCM1, they tend to aggregate in the solid state due to either attractive dipole-dipole interactions or effective intermolecular π-stacking. Planar red emitters are thus prone to concentration quenching and are only weakly emissive in the solid state.

Many studies are dedicated to the emission mechanism in organic doped systems. The process of energy transfer from the host to the dopant may involve several different processes, including carrier trapping as well as Dexter or Förster energy transfer. Even small numbers of guest molecules (from a fraction of a percent to a few percent doping concentrations) are sufficient to change the luminescence spectrum, often completely quenching the host emission. Low doping ratio means a large average distance between the guest molecules, reducing exciton quenching due to dopant-dopant interactions, and thus yielding high luminescence efficiency. The lifetime and the efficiency of doped OLEDs are found to depend strongly on the combination host/guest pair and the doping ratio.

For example, Förster transfer is an efficient process in Alq_3 OLEDs doped with 2 % DCM2 leading to orange electroluminescence [64], while Dexter transfer in 6 % PtOEP/Alq_3 OLEDs results in highly efficient red phosphorescence [30]. In contrast, coumarin 6 improves the color saturation and the efficiency of green Alq_3 OLEDs due to carrier trapping [64].

When more than one dopant is present in the organic thin film, an exciton can

transfer its energy in a multistep process from the host to the first dopant, and subsequently to a second dopant, etc. This process is known as cascade energy transfer [162] and requires sufficient overlap of the luminescence and absorption of the participating species at each step in the Förster transfer so that the integral in Eq. (2.34) is non-vanishing. Also, the host exciton can transfer its energy to other molecular species, lying in adjacent layers, resulting in interlayer energy transfer [66]. Both these processes are used to tailor the luminescent properties of the organic thin films.

3 Materials and experiment

This Chapter contains a brief characterization of some of the basic organic dyes studied in the thesis - MePTCDI, Alq_3, and the 2,2-Difluoro-1,3,2-dioxaborine derivatives GG142B, GG277, GG247 - as well as of SiO_2 and polyimide as matrix materials. Furthermore, we present a description of the experimental methods and set-ups applied in this study.

3.1 Dyes to be embedded in matrices

The used perylene derivatives N,N '-dimethylperylene-3,4,9,10-bis-dicarboximide (MePTCDI) and 3,4,9,10 -perylenetetracarboxylic-dianhydride (PTCDA), as well as tris(8-hydroxyquinoline) aluminium (Alq_3) are trade products of Aldrich. 4-dicyanomethylene-2-methyl-6-(p-dimethylaminostyril)-4H-pyran (DCM) is delivered by Radiant Dyes Chemie and 5,6,11,12- tetraphenyl - naphthacene (rubrene) by Fluka, respectively. The 2,2-Difluoro-1,3,2-dioxaborines GG142B, GG274, and GG277 are synthesized by Prof. H. Hartmann and co-workers at the IAPP, TU Dresden. Purification of the compounds MePTCDI, PTCDA and Alq_3 was carried out by gradient sublimation in vacuum. All other dyes were used as received without further purification. The chemical structures of the dyes are presented in Fig. 3.1.

3.1.1 MePTCDI

MePTCDI, a model organic material in our study, belongs along with PTCDA to the group of the perylene derivatives. Both MePTCDI and PTCDA molecules are known to form quasi-one dimensional (quasi-1D) crystals [69]. In such a crystal structure, the interactions along one lattice constant are significantly stronger than along the other two. Hence, the crystal can be considered as a two-dimensional array of one-dimensional stacks. The lattice constant along the stacks in MePTCDI and PTCDA crystals is approximately 3.7 - 3.9 Å, and thus fairly shorter than both the other lattice constants (>12 Å, see Fig. 3.2) and the dimensions of the molecules (for example the N-N'-distance in MePTCDI equals 11.3 Å).

A characteristic property of the MePTCDI and PTCDA quasi-1D crystals is their strong intermolecular overlap in the one-dimensional stacks. In MePTCDI, the molecular planes have a distance of 3.40 Å [67]. That is, a nearest neighbor pair within the stack has a sandwich-like geometry with the molecules shifted with respect to each other within the molecular plane (cf. Fig. 3.3). However, about 50% of the conjugated electron system lies directly above each other [68], thus leading to strong mutual overlap of the molecular wave functions. A direct result of the strong intermolecular overlap is a large electronic bandwidth. Consequently, such materials should develop qualitative similarities to covalent crystals.

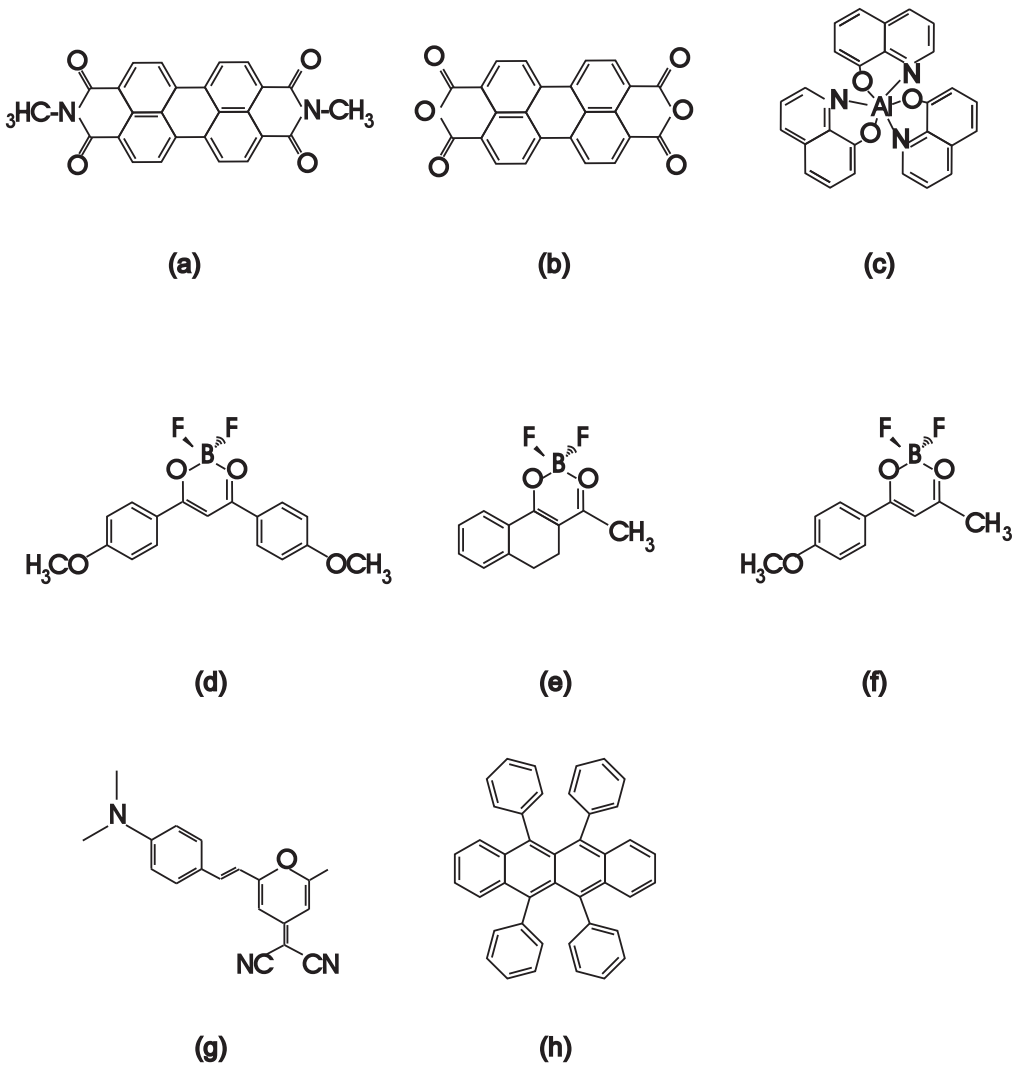

Figure 3.1: Chemical structures of (a) MePTCDI, (b) PTCDA, (c) Alq_3, (d) GG142B, (e) GG274, (f) GG277, (g) DCM, and (h) rubrene; full names in text.

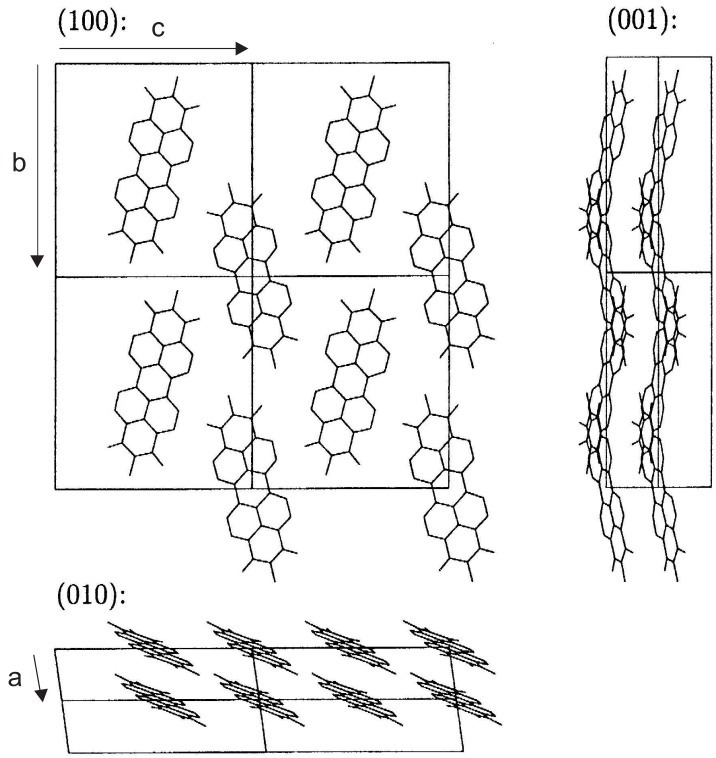

Figure 3.2: Crystal structure of MePTCDI. Shown are the projections of 2 x 2 unit cells onto the b-c-plane (100), the a-b-plane (001), and onto the a-c-plane (010). The crystal structure is monoclinic, space group $P2_1/c$, Z = 2 molecules per unit cell, a = 3.874 Å, b = 15.580 Å, c = 14.597 Å, $\beta = 97.65°$ (data from [147]).

Because of its higher sublimation temperature (around 320°C - 350°C), MePTCDI is easier to handle in high vacuum and is thermally more stable than other dyes, which is very important for preparation of VD films with well reproducible parameters such as composition, structure, dye distribution in the matrix, etc.

In the framework of this thesis, we mainly studied MPTCDI thin films, grown by PVD in high vacuum (HV) on glass substrates at room temperature (RT). The thickness of the films varied between 10 and 200 nm. Atomic force microscopy (AFM) and X-ray diffraction measurements on vacuum deposited MePTCDI and PTCDA thin films (100 nm) on various substrates at RT have shown that the films are polycristalline [69]. The average size of the polycrystallites within the layers is estimated to be in the range of 20 - 100 nm.

3.1.2 Alq_3

Since the fundamental work of Tang and Van Slyke [2], the interest in Alq_3 is persistent. It is a key OLED material, most often used as electron transport and emitting layer [70, 71, 72]. In this regard, many studies were devoted to an

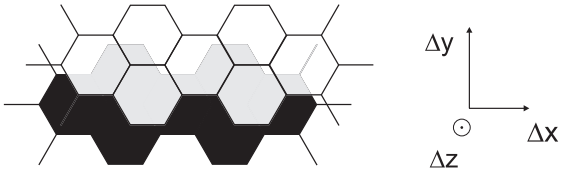

Figure 3.3: MePTCDI pair within the 1D stack. The second molecule is displaced by Δx = 0.94 Å, Δy = 1.60 Å, Δz = 3.40 Å (data from [67]).

understanding of the charge-transport mechanisms in Alq_3 thin films and to an improvement of the device performance [73, 74, 75]. Yet, systematic investigations of the structural and optical properties of the material in the solid state, as well as of the influence of the preparation conditions on these properties, were carried out only recently [27, 76, 77].

Alq_3 is a metal quinolinate based on 8-hydroxyquinoline [78]. The Alq_3 molecule consists of a central Al atom coordinated by three quinolate ligands (Fig. 3.1). Every one of them binds to the metal site via oxygen and nitrogen atoms, thereby giving pseudo-octahedral environment of the metal atom.

Theoretical calculations which have recently been proven experimentally [28, 29], established that Alq_3 can exist in either of the two geometrical isomers: the meridional (*mer*) or the facial (*fac*) isomer. They differ in the relative position of the nitrogen and the oxygen atoms of the metal coordination shell. A more detailed description of the isomers will be presented in Chapter 4.

Investigations of crystalline Alq_3 powders have shown that Alq_3 has three polymorphs - α-Alq_3, β-Alq_3 (Fig. 3.4), and the high-temperature γ-Alq_3. Brinkmann et al. [27] gave a detailed structural characterization of these three phases, investigating the correlation between the molecular packing and the optical properties of Alq_3 in various systems. The structures of both α- and β-Alq_3 phases have triclinic symmetry with a unit cell containing four molecules with meridional structure. They are characterized by different molecular densities, the α-phase having less density. Both phases emit yellowish-green light, with a peak positioned around 500 nm. X-ray diffraction analysis have shown the existence of close contacts between pairs of quinolate ligands belonging to neighboring Alq_3 molecules, the interligand spacing being in the range 3.5 - 3.9 Å. However, the β-phase exhibits stronger overlap of the π-electron systems (distance between adjacent ligands of 3.5 Å) and is the one showing red-shifted fluorescence with respect to the α-phase. Despite the short distances between the quinolane ligands of adjacent Alq_3 molecules, neither excimer nor dimer emissions were observed in the crystalline phases of Alq_3. In fact, a study of the absorption and emission spectra in solvated and condensed phase systems shows that the spectra are largely independent of the molecular environment and the emissive states are localized on individual molecular sites [79, 80]. Theoretical investigations support the localized nature of the orbitals involved in the lowest energy electronic transition [152].

Lately, experimental findings demonstrated the existence of a δ-phase, containing facial-Alq_3 molecules [81, 82]. Brütting et al. managed to produce blue-

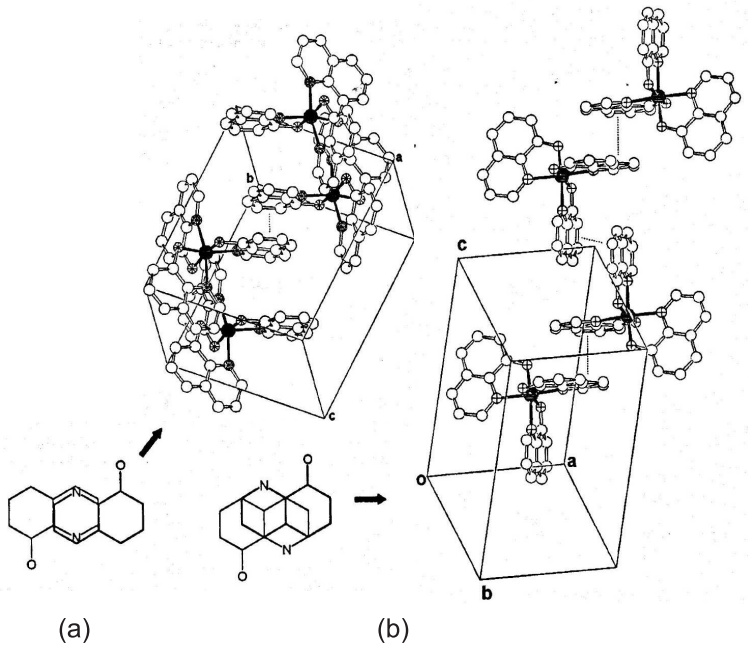

Figure 3.4: Crystal packing of (a) the Alq_3 α-phase (down (3-11)) and (b) the Alq_3 β-phase (down (121)) showing the short π-π contacts between neighboring molecules, along with the relative shifts of the stacked π-π aromatic rings (from [27]).

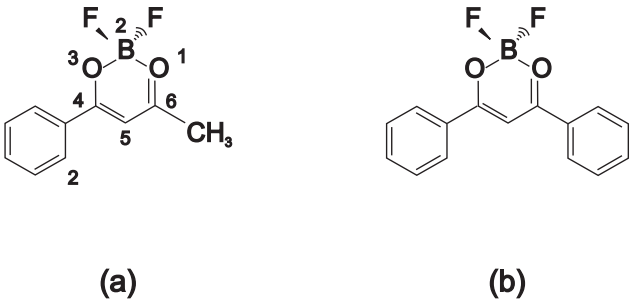

Figure 3.5: Chemical structure of (a) ABMBF and (b) DBMBF.

luminescent Alq_3 by simply annealing α-Alq_3 powder in HV at temperatures between 380°C and 400°C [83]. Isomer conversion was later confirmed for another metal quinolinate, namely tris(8-hydroxyquinoline)gallium(III) (GaQ_3) [84].

Alq_3 sublimes in high vacuum at temperatures around 180°C - 220°C to produce stable and smooth thin films. Concerning the morphology of the sublimed Alq_3 films, there are ambiguous reports in literature. In [2, 85], a microcrystalline structure with average grain size of about 500 Å is established. In contrast, for example in [27], results are presented which show that the Alq_3 films are characterized by an amorphous-like structure, comprising a mixture of the two geometrical isomers. The structure represents disordered media, without any well-defined molecular organization, yielding inhomogeneously broadened spectra. The amorphous character is favored by the intrinsic polymorphism of Alq_3, fluctuations in the isomers concentration during the evaporation process, as well as strong dipolar interactions between the Alq_3 molecules.

Thin Alq_3 films have an absorption maximum at 390 - 400 nm and emit light upon excitation with a maximum at about 517 - 530 nm. In the present thesis, in some of the investigations Alq_3 is used as optically active matrix material, doped with the highly luminescent dyes DCM and rubrene. Both dopants are chosen with respect to their energy level alignment toward Alq_3, which is favorable for resonant energy transfer from the host to take place.

3.1.3 2,2-Difluoro-1,3,2-dioxaborine derivatives

GG277 and GG142B are derivatives of 4-methyl-6-phenyl-2,2-difluoro-1,3,2- dioxaborine (acetylbenzoylmethanatoboron difluoride, ABMBF) and 4,6-diphenyl-2,2-difluoro-1,3,2-dioxaborine (dibenzoylmethanatoboron difluoride, DBMBF) (Fig. 3.5), respectively, substituted in para position on the phenyl ring. The initial compound ABMBF absorbs at 330 nm in cyclohexane solution and at 354 nm in the solid state [86]. At room temperature, it does not fluoresce in solution. When the temperature of the medium is decreased, the molecule shows a well-structured absorption spectrum and a strong fluorescence emission. On the other hand, DBMBF fluoresces only weak in non-polar solvents, but somewhat stronger in polar solvents ($\phi_{PL} = 0.046$ in cyclohexane vs. $\phi_{PL} = 0.10$ in acetonytrile)[86].

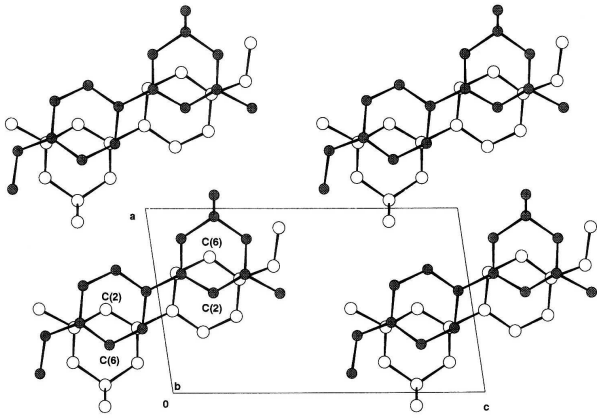

Figure 3.6: Packing diagram projected on the a-b-plane for GG277 (from [87]).

The molecules ABMBF and GG277 are found to be planar in their crystal structure [87]. In addition, they lie in parallel planes. In GG277, the separation distance is 3.536 Å. The molecular packing is such that the molecules are stacked, each molecule being in a different plane. For both compounds, the molecules are linked by a symmetry center. The closest two molecules lying in parallel planes are oriented in opposite directions, the benzenic part (A) of one molecule lying above the boron-containing heterocyclic part (B) of the other molecule, and reciprocally (Fig. 3.6).

The two molecules in parallel planes are shifted with respect to each other. The C(6) carbon atom of the benzenic part of the first molecule projects itself in the center of the boron-containing heterocycle of the second molecule, while the C(2) carbon atom of the heterocycle of the first molecule projects itself in the center of the benzene ring of the second molecule. In the monoclinic crystal of GG277, the distance between the C(6) carbon atom of one molecule and the nearest fluorine atom of a second molecule is 3.325 Å [87]. The stacking of both molecules constitutes of piles of infinite chains as follows:

A...B...A...B...A...B
| | | | | |
B...A...B...A...B...A,

oriented parallel to the b axis. Additionally, the monoclinic compound GG277 contains two molecules in the elementary cell.

The molecules DBMBF and GG142B show similar crystal structure [88]. In the crystal, the GG142B molecules are arranged in layers, comprising parallel molecules. In the out-of-plane direction, the layers are separated by 3.52 Å. The nearest molecules of adjacent layers lie antiparallel to one another and overlap in such a way that the diketonate ring of one molecule is located above the phenyl ring of another molecule and vise versa (Fig. 3.7). The overlapping molecules are arranged in a staircase fashion; the degree of overlap is 27 % of the surface area of the phenyl ring.

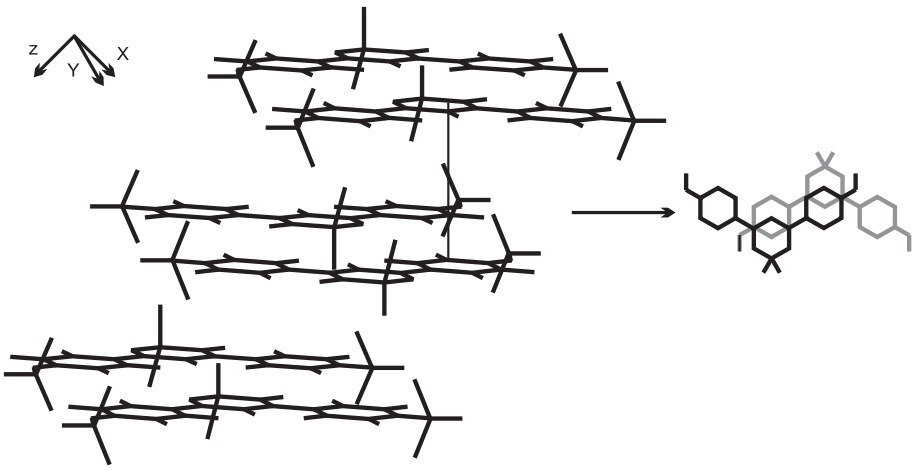

Figure 3.7: Molecular packing of GG142B in the crystal; shown is the way the molecules overlap (adapted from [88]).

The GG274 dye represents another class of derivatives of ABMBF. In this molecule, alkyl groups close the bridge between the 5th position of the heterocycle and the 2nd position of the aryl moiety by formation of a sixring (see Fig. 3.5a). The bridge fixes the phenyl ring in the π-plane, although this is slightly disturbed by the formation of the sixring since the sp^3-C-atoms of the ring strive for ideal bond angles [89]. Thus, the GG274 molecule has nearly planar configuration. Blocking of the phenyl ring results in strongly fluorescent molecules in both slightly polar and non-polar solvents [90, 91].

3.2 Sample preparation

3.2.1 Vacuum unit

All samples were prepared by evaporation of dye and matrix in oil-free HV and their condensation on the substrates. For all experiments, the substrates were kept at RT. The base pressure in the deposition chamber was less than 5 x 10^{-6} mbar during deposition. The evaporation chamber is equipped with an electron gun and three thermal sources, which enable the incorporation of several dyes simultaneously in the matrix and allow various opportunities for design of the deposited films. The deposition rates and final film thickness as a measure of the dye concentration in the investigated dye/SiO_2, dye/PI or dye/dye systems are monitored by quartz oscillators.

For evaporation of SiO_2, the density was set to 2.6 g/cm^3, while for the organic materials, it was set to 1.6 g/cm^3. The latter value was chosen with respect to the results of Hoffmann [69], who determined 1.62 g/cm^3 for evaporated MePTCDI films. With the quartz oscillators and shutters, the deposition rate, the distribution and the deposited amount of each material can be easily controlled independently.

3.2.2 Substrates

As substrates, for most of the experiments we used adhesion glass micro slides with thickness 1 mm, a trade product of Superior. In some specific cases, however, samples were prepared on KBr pellets (for IR spectrometry) or Si-wafers (for scanning electron microscopy).

The substrates were cleaned in two steps. First, they were treated in Extran MA 01 solution (Merck KGaA) at 40°C, combined with ultrasound at 35 kHz for 15 minutes. Second, substrates were washed in deionized water (14MΩ) in 35 kHz ultrasound for 15 minutes. After that, they were dried at 105°C for 60 minutes in air.

3.2.3 Deposition of the SiO_2 matrix

The SiO_2 used is a trade product of Prof. Feierabend GmbH and was employed as received. The purity of the material according to the manufacturer is 99.997 %. Because of the high temperature melting point of SiO_2, the matrix was grown using an electron beam. An important advantage of this method is the feasibility to obtain high deposition rates (0.1 - 20 Å/s) on a large area. Thereby, it is possible to prepare thick films in reasonable time. The energy deposited within the layer is a function of the energy of the impinging ions and their flux density. In this process, the purity of the deposited material is determined by the purity of the target material. However, it has to be noted that an additional process accompanying the film growth - the secondary electron radiation - could influence the structure of the organic substances and thus the properties of the obtained layers. In the case of mixed dye/SiO_2 films, the matrix is obtained at evaporation rates in the range 0.2 - 10 Å/s.

SiO_2 is stable against e-beam evaporation and the grown films are quite homogeneous. Structure investigations of vacuum deposited SiO_2 films show that they are amorphous [92], which should favor the isotropic distribution of the embedded dyes. In Chapter 4, we present concise comments on the structure of the studied neat SiO_2 films. Thin SiO_2 films show only slight absorption in the visible spectral region, which is a prerequisite for an optically inactive matrix.

3.2.4 Deposition of the PI matrix

The PI matrix was prepared by the so-called vacuum deposition polymerization [109, 130, 131, 135, 138]. The initial monomers pyromellitic dianhydride (PMDA) and oxydianilline (ODA), trade products of Fluka, were thermally co-deposited in HV. Typical evaporation temperatures were 140°C for ODA and 160°C - 180°C for PMDA, used in order to achieve deposition rates of 1 Å/s for each precursor. Thus, the optimal ratio in the flux of 1:1 for the ODA:PMDA vapors was ensured [26]. Upon condensation on a substrate, the monomers ODA and PMDA polymerize to form the polyamic acid. After deposition, the films undergo subsequent thermal treatment in order to accelerate the polycondensation solid state reaction between the monomers and to convert the polyamic acid to PI, according to the reaction scheme in Fig. 3.8.

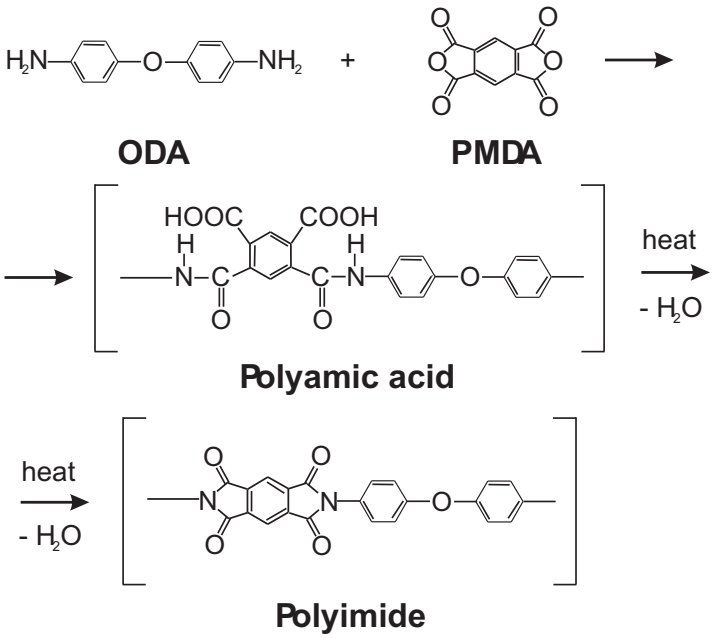

Figure 3.8: Reaction scheme of the chemical process leading to the formation of PMDA-ODA polyimide [94].

Thermal treatment was carried out in ambient air in a laboratory drying oven (Series 7000 Function line Heating and Drying Oven by Kendro). It allows tempering up to 250°C. The neat matrix and the mixed dye/matrix films were cured at carefully controlled temperatures and time intervals depending on the experimental goals.

Scanning electron microscopy (SEM) of cured VD films with ODA:PMDA ratio 1:1 show that the surface of the films is smooth, without clear crystalline structure and structural defects [26]. AFM investigations confirm that the surface roughness of vapor deposited PI films is smaller than that of films produced by wet methods [93]. In Chapter 4, we present some additional results from Fourier transform infrared spectroscopy (FTIR) measurements, giving details about the quality of the obtained PI films.

3.2.5 Deposition of the "guest" dyes

Dyes were thermally evaporated from quartz crucibles. The rate of heating, the evaporation temperature, as well as the stability of the temperature were controlled by Eurotherm Controls Inc units (94 Temperature Controller, 2216E Temperature Controller with Digital Communication).

The evaporation rate was chosen in dependence on the goal of the experiment and was commonly between 0.02 and 2 Å/s. The concentration of the dyes in the prepared layers was varied in the range 0.2 - 100 vol%, according to the experiment as well. For MePTCDI, this corresponds to 8 x 10^{-3} - 4 x 10^{0} mol/l. In the case of doped Alq_3 films, the concentration of the guest (DCM, rubrene) was controlled

by adjusting the rate of deposition for the dopant with respect to that of the Alq_3 host.

3.2.6 Preparation approaches

Generally, the reported studies on VD organic solid solutions are restricted to thin films prepared by simultaneous condensation of matrix and guest dye on a substrate in a static state. In contrast, for most of our experiments, the glass substrate was mounted on a rotating substrate holder during sample preparation. Thus, in addition to the classical method, we were able to apply two different sample preparation approaches.

For the first one - co-evaporation on rotating substrate - dye and matrix particles condense at the same time on a substrate in dynamical state.

The second one includes additional disk, situated under the one on which the substrate is attached. This additional disk has apertures, which can be varied from 180° to 18° and thus allow (i) to decrease the evaporation rate from two to twenty times and (ii) to separate the condensation of dye and matrix particles. For this, the substrate holder rotates in such a manner that for a part of the rotation period, the substrate sees only the dye crucible and for another part, for example, the e-gun for the SiO_2. The film obtained is built up of many very thin sublayers of guest and host material. Moreover, by variation of the initial deposition rate, we are able to control the thickness of each dye or matrix sublayer, i.e. the distance between the single molecules. We will denote the separate condensation of matrix and dye on rotating substrate as "layer-by-layer" film growth. A scheme of the evaporation geometry is given in Fig. 3.9b. An evaporation source to substrate distance of about 30 cm assures good film homogeneity. The films deposited on substrates in dynamical mode are uniform in thickness and have low surface roughness [95]. In Chapter 4, we compare the optical properties of samples prepared using layer-by-layer film growth with samples at the same dye concentration obtained by co-evaporation on rotating substrate and by the classical condensation on static substrate (Fig. 3.9a).

3.2.7 Liquid solutions

For preparation of the liquid solutions, usually dimethyl sulfoxid (DMSO), chloroform, chlorobenzene, or dimethylformamid (DMF) as solvents were used. Dyes were dissolved at concentrations in the range 10^{-4} - 10^{-5} mol/l. Yet, in the case of MePTCDI, which is known to have poor solubility, it was rather demanding to obtain solutions at a defined concentration. It was necessary to wait for 6 - 24 hours, and in order to increase the efficiency of dilution, to resort to ultrasound and heating. To avoid thermal destruction, heating was carried out at up to 40°C under continuous stirring.

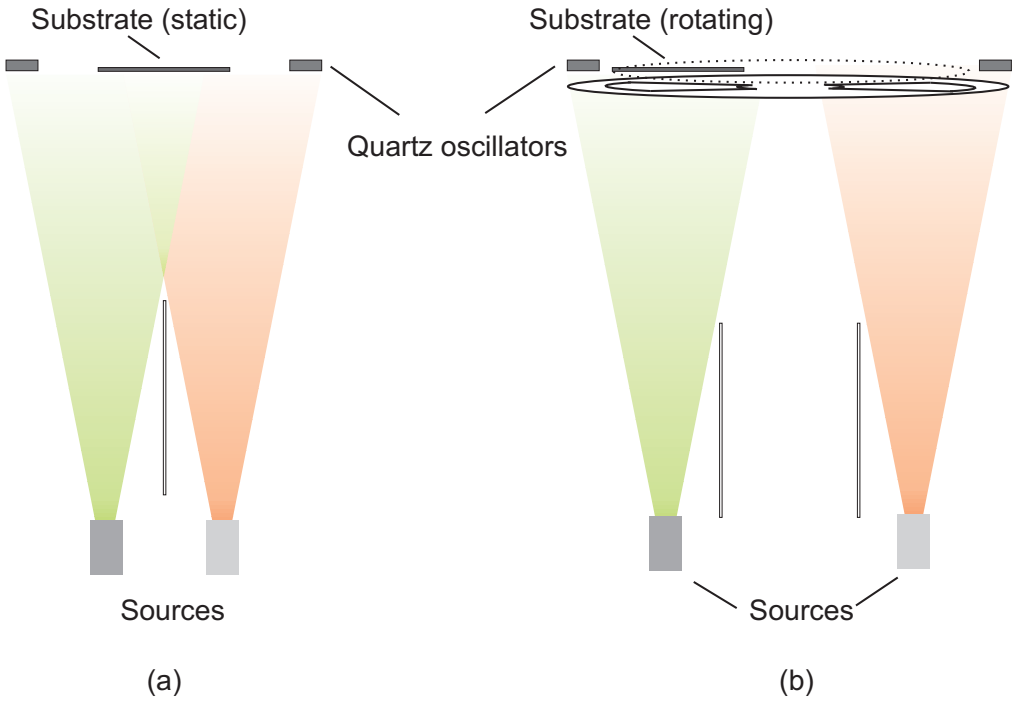

Figure 3.9: Scheme of the evaporation geometry. (a) Co-deposition on static substrate. (b) Layer-by-layer condensation on rotating substrate.

3.3 Methods and measuring apparatus

3.3.1 Optical characterization of the films

Absorption spectroscopy. Reflectance (R) and transmittance (T) of the samples were recorded using a commercial two-beam spectrophotometer UV-3101 PC (Shimadzu). It is equipped with a compartment for reflectance measurements, operating in the spectral region 190 - 3200 nm.

Transmittance and reflectance were measured in a collimated beam at normal or quasi-normal incidence (R under 5° angle) in the range from 290 to 1500 nm. The spectral resolution for the transmittance spectra was 2 nm, while reflectance was measured with 8 - 12 nm spectral resolution. Using both T and R, one can further define the Absorption (A) from the energy conservation law:

$$A = 1 - T - R \tag{3.1}$$

In some graphs, as a measure for the absorption of the studied samples, we present the spectral dependence of the optical density OD. Substrate substraction is carried out beforehand.

We have to note that most of the investigated dye/matrix thin films were 1000 Å thick. At this thickness and particularly at the high dilution range, the optical density of the samples is too low to be measured directly. Therefore, conclusions about absorption are drawn on the basis of the corresponding luminescence exci-

tation spectra, which can be recorded even at low intensity. It is then assumed that the results from absorption and excitation measurements are equivalent, i.e. luminescence spectrum and quantum yield are independent of excitation wavelength.

Evaluation of the optical constants using Film Wizard®. The software program Film Wizard (Scientific Computing International) was applied for correction of the experimental film thickness d of the samples, and in the case of thick ($\geq$ 6000 Å) MePTCDI/SiO_2 films additionally for determination of the optical constants. In order to define d and the real and imaginary part of the index of refraction, n and k, in the spectral region where the studied dyes do not absorb (800 - 1500 nm), the measured transmittance and reflectance spectra were fitted using the Cauchy approximation

$$n(\lambda) = A_n + \frac{B_n}{\lambda^2} + \frac{C_n}{\lambda^4} \tag{3.2}$$

$$k(\lambda) = A_k + \frac{B_k}{\lambda^2} + \frac{C_k}{\lambda^4}. \tag{3.3}$$

In these equations, A, B and C are the model constants and λ is the wavelength. For transparent or only weakly absorbing materials A_k, B_k, and C_k are assumed to be 0. Accordingly to the fitted data, the experimental and real thickness of the studied samples differ on the average by 15 to 20 %; the experimental d was corrected by this factor.

In the absorption region, we modeled the optical constants of the mixed MePTCDI/SiO_2 layers using the Effective Medium Approximation (EMA). The EMA theory was first introduced by Maxwell Garnett in 1904-6 [96], who considered a discontinuous metal film as a dispersion of small spheres embedded in ambient medium with dielectric function ε_h. The distribution in space of the particles is assumed random, i.e. the medium is isotropic, and the density is characterized by factor f giving the fractional volume occupied by the metal. When an external electric field is applied, the spheres will be polarized by the field and will thus generate an additional field. By means of the Clausius-Mosotti equation which incorporates the contribution of the additional field to the total polarization P, the effective dielectric function ε of the metal film can be related to the dielectric function of the bulk material and to the volume fraction of the material f by

$$\frac{\varepsilon - \varepsilon_h}{\varepsilon + Y\varepsilon_h} = \sum f_j \frac{\varepsilon_j - \varepsilon_h}{\varepsilon_j + Y\varepsilon_h} \tag{3.4}$$

$$Y = \frac{1}{q} - 1$$

The shape factor q introduced in the parameter Y allows a wide range of possible particle shapes, e.g. shape factor of 0 represents a flat disk, and q of 0.5 represents a columnar microstructure. The self-consistent EMA ($\varepsilon_h = \varepsilon$), referred to as Bruggeman model, describes accurately the optical properties of composite

materials of random or aggregated microstructure. In this case, the participating materials are treated as embedded in the effective medium and thus play equivalent roles. The EMA equation reduces to:

$$\sum f_j \frac{\varepsilon_j - \varepsilon}{\varepsilon_j + Y\varepsilon} = 0, \tag{3.5}$$

where ε is the effective dielectric function of the total system.

Accordingly, the MePTCDI/SiO_2 layers were modelled as a mixture of Cauchy host (SiO_2) and organic material (MePTCDI). In the region where the dye is absorbing (only the spectral range 400 - 800 nm was considered), it can be modeled with several Lorentz oscillators peaks added to the Cauchy expression. In the Lorentz oscillator model (LOM), the real and imaginary part of the complex dielectric function $\varepsilon = \varepsilon_1 + \mathrm{i}\varepsilon_2$ are given by

$$\varepsilon_1(\omega) = \varepsilon_{1\infty} + \sum_j \frac{F_j(\omega^2 - \omega_j^2)}{(\omega^2 - \omega_j^2)^2 + (\omega\Gamma_j)^2} \tag{3.6}$$

$$\varepsilon_2(\omega) = \sum_j \frac{F_j\omega\Gamma_j}{(\omega^2 - \omega_j^2)^2 + (\omega\Gamma_j)^2}, \tag{3.7}$$

where j denotes a transition with frequency ω_j and lifetime $1/\Gamma_j$, $F_j = f_j\omega_j^2$ is a parameter associated with the oscillator strength f_j, and $\varepsilon_{1\infty}$ is the dielectric constant arising from higher-lying transitions [97].

We have to remark here that the spectral response depends strongly on the molecular packing. Hence, in dependence on dye concentration, the embedded organic molecules can show either monomer or collective response as molecular complex. Increasing the dye content will lead to a variation in the oscillator strength of the transitions, and accordingly in a different contribution of the individual oscillators to the dielectric function. That is, at low concentrations, application of the EMA model using directly the optical constants of polycristalline MePTCDI by only changing the volume fraction is inconsistent.

Absorption spectroscopy studies on vacuum deposited DCM films indicate that the grown films differ in structure, however, not only in dependence on the final film thickness. Though keeping a constant thickness, very slight changes in the growing conditions lead to films with different microstructure. In the grown film, even without the help of an optical microscope, we were able to distinguish between regions with amorphous and obviously crystalline structure. Thus, for correct determination of DCM optical constants, it was necessary to carry out thorough investigations of DCM film growth, taking into account all possible factors influencing the final film structure and analyzing the precise crystallographic composition. On the other hand, as composite layers of Alq_3 doped with DCM molecules were our main interest, it was rather difficult to predict what kind of structures DCM would form when growing together with Alq_3. Since relatively low doping DCM levels were investigated, the experimental T and R spectra of the doped at around 2 vol% DCM concentration films were compared with calculated spectra for neat host film at equal thickness (n and k of Alq_3 are defined via an

algorithm developed by T. Fritz, IAPP - TU Dresden, [98] and implemented in a computer program). In the spectral region 300 - 430 nm, the maximal difference between calculated and measured spectra is around 1.5 %. That is, in this region the doped films can be sufficiently described by the optical constants of the host Alq_3.

Luminescence spectroscopy. Steady-state photoluminescence excitation and emission spectra were recorded at RT with a luminescence spectrometer FluoroMax (Spex). The device has separated Czerny - Turner monochromators in excitation and emission positions. In each monochromator, light is dispersed by a grating. The excitation source is 150 W Xenon Lamp. Light leaving the emission monochromator is detected by a photomultiplier (R928P Hamamatsu), operating in photon-counting mode.

The spectra of the VD films were recorded using front-surface optical arrangement [99]. The samples are irradiated at normal incidence and the resulting luminescence is detected under an angle of 22.5°.

The luminescence spectra of the liquid dye solutions, placed in quartz cuvettes (10 mm path length) were obtained using the 90° optical configuration. In this configuration, the samples are excited at normal incidence, the luminescence propagates in all directions and only the portion of the emitted at right-angles to the incident beam is collected from the detector.

All measurements were carried out with a spectral resolution of about 4 nm. A suitable edge filter was used for suppression of stray-light effects. The collected data were corrected for the lamp spectral emission and for the detector and monochromator spectral efficiencies.

3.3.2 SEM, AFM and FTIR spectroscopy

The surface morphology of the studied films was investigated by SEM and AFM. The SEM micrographs were taken using an X-ray microanalytical system Philips SEM 505 EDA 9100/MicrospecWDX2A. The investigations were carried out in the Central Laboratory of Photographic Processes at the Bulgarian Academy of Sciences, Sofia.

AFM images were recorded at the IAPP - TU Dresden, with a NanoScope IIIa (Digital Instruments) in tapping-mode. Analysis of the images was done using WSxM Scanning Probe Microscopy software, http://www.nanotec.es.

FTIR spectroscopy was applied for the characterization of the neat PI films. The measurements were carried out in the University of Chemical Technology and Metallurgy, Sofia. The FTIR spectra were recorded on a Perkin-Elmer 1600 spectrometer in transmission mode in the range 2000 - 650 cm^{-1}, with a resolution of 4 cm^{-1}.

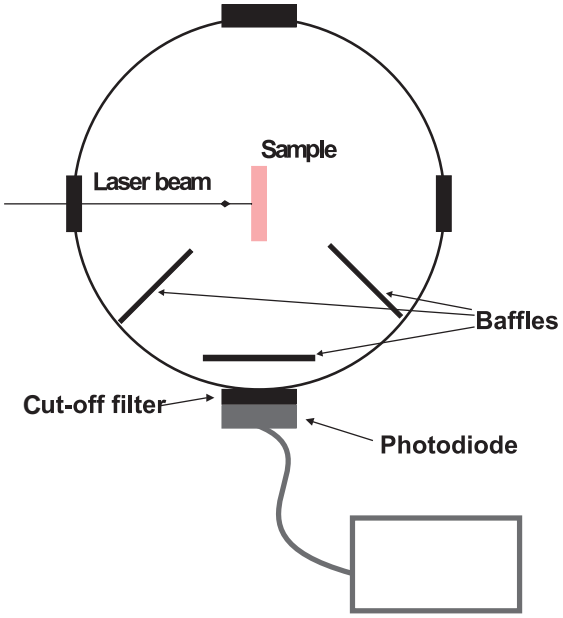

Figure 3.10: Scheme of the experimental set-up for measurement of the PL quantum efficiency.

3.3.3 Measurements of the photoluminescence quantum yield

Measurements of the PL quantum yield of the studied films were carried out following the procedure described in [65, 100]. Since the angular distribution of the luminescence is sensitive to the refractive index of the material and to the orientation of the emitting dipoles within the film, the usual approach is to collect the emitted light over the whole solid angle using an integrating sphere. A scheme of the experimental set-up is presented in Fig. 3.10. Accordingly, the procedure includes three steps. In the first one, the integrating sphere is empty; the laser beam is directed toward the sphere wall, the light is then scattered by its surface and the resulting signal is measured at the sphere exit port. Second, the sample is placed in the sphere, the laser being directed to the sphere surface in such a way, that the sample is excited only by scattered, but not by direct laser light and the corresponding PL signal is measured. Third, the laser light passes through the sample and the luminescence, scattered within the integrating sphere and leaving the exit port, is measured. In the latter two steps, a cut-off filter for the laser wavelength precedes the detector. Thus, the external PL efficiency is determined from:

$$\phi_{PL} = y^{-1} \frac{X_{samp} - (R+T)X_{sph}}{(1-R-T)X_{laser}}. \tag{3.8}$$

X_{laser} corresponds to the signal of the laser itself; X_{samp} denotes the emitted from the sample light when the laser irradiates directly the sample; X_{sph} is the PL intensity measured when the sample is diffusely irradiated from the laser light, impinging on the sphere walls. T and R denote the transmittance and reflectance

of the sample. All these signals are normalized to the spectral response of the experimental set-up via the term y, taking into account the spectral response of the integrating sphere, the efficiency of the photodiode over the near-UV-visible spectrum and the transmission spectrum of the cut-off filter [100].

In the experiments carried out, we used a cw - HeCd laser (325 or 442 nm) for excitation. Typical laser powers were in the range 0.12 - 12 mW, with a beam diameter at the sample of approximately 1 mm. The reflectance and transmittance of the investigated samples at the excitation wavelength were measured at near normal incidence. The luminescent light from the sample was scattered within an integrating sphere RTC-060-SF (Labsphere) with 6 inch diameter. The sphere has 3 baffles, situated above the exit port in such a way that the PL light could not be seen directly from the detector. The PL signal was detected at the exit port of the sphere by Newport Power Meter 1815-C with measure head 818-UV. The cut-off wavelength of the filter was chosen 360 or 495 nm in order only the luminescence signal to be transmitted to the detector.

The measurements were carried out in air, but the values of the PL signal were recorded after 5 to 10 s of excitation in order to reduce the influence of the luminescence degradation.

3.3.4 Photobleaching measurements

The photobleaching of the mixed layers was studied upon continuous laser irradiation. In dependence on the optical absorption of the samples, we used the following cw-lasers: HeCd with lines at 442 (P_{max} = 80 mW) nm or Ar^+ at 488 nm (P_{max} = 170 mW). The layer under study was placed in the sample compartment of the FluoroMax spectrofluorometer. The excitation beam was directed to the sample via Al mirrors. For some of the experiments, the laser light was focused on the sample surface using f = 150 mm. The photobleaching reaction was measured following the intensity at the fluorescence maximum. The decay curves were recorded using the emission monochromator and the photomultiplier of the FluoroMax in the "Time-based scan" regime. Suitable cut-off filters for the excitation wavelength were put in front of the entrance slit of the detecting system. The experimental data were collected at intervals of 0.1 to 2 s during a time span of 5400 s.

4 Solid solutions of organic molecules in SiO_2 and polyimide matrices

This Chapter reports organic dyes distributed in the optically inactive matrices SiO_2 and polyimide. In the first part of the Chapter, we present results about solid solutions of various dyes in SiO_2. The surface morphology of the films is described. Afterwards, the optical response of mixed MePTCDI/SiO_2 films, grown by co-deposition of both materials, in dependence on dye content is reported. We motivate the introduction of layer-by-layer deposition geometry and discuss its advantages for preparation of films with increased PL efficiency at higher dye content. Further, we consider the influence of the inorganic matrix for the occurrence of meridional to facial isomer transformations of Alq_3 molecules during film growth. Finally, we present results about the luminescence behavior of 2,2-difluoro-1,3,2-dioxaborine dyes embedded in SiO_2.

The second part of the Chapter is concerned with mixed dye/polyimide films. First, in order to motivate the choice of matrix material, we present results related to the photo physical properties of the neat polyimide films. We then address the absorption and luminescent properties of the model dye MePTCDI dispersed in the organic polyimide matrix. The influence of the embedded dye concentrations and the thermal treatment conditions on the optical properties of the mixed layers are discussed. Next, the photoluminescence of Alq_3 in the PI matrix is compared with that in SiO_2. Conclusions about the incorporation conditions in both matrices are drawn.

4.1 Organic dyes in SiO_2 matrix

4.1.1 Surface morphology of the mixed films

Information about the morphology of the grown mixed dye/SiO_2 thin films is obtained from SEM and AFM measurements. As an example, we present results of pure SiO_2 and mixed with Alq_3 or MePTCDI as embedded dye layers.

Figure 4.1 shows SEM micrographs of the surface of the neat host and mixed Alq_3/SiO_2 films. Both samples were deposited at 5 Å/s on Si wafers. The total film thickness is 5000 Å, and the concentration of Alq_3 in the mixed layer is about 2 vol%. The diluted dye film is prepared using layer-by-layer growing mode. Comparison between the layer-by-layer sample and Alq_3/SiO_2, prepared by co-evaporation on static substrate shows that both films have a similar structure, hence a micrograph of the latter sample is not presented here.

The micrographs show that the films are homogeneous, characterized by a fine grain microstructure. Close examination, however without statistical processing, established a difference in the grain size of the films. The mean grain size of the neat matrix film is larger compared to that of the mixed samples. The grains of

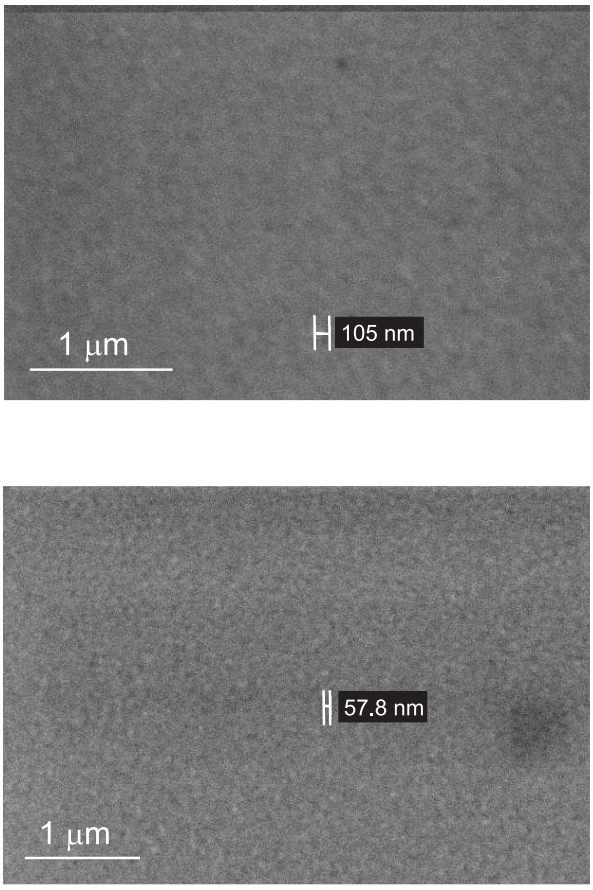

Figure 4.1: SEM micrographs of the surface of (a) a neat SiO_2 film, 5000 Å film thickness and (b) 2 vol% Alq_3/SiO_2 film, 5000 Å total film thickness.

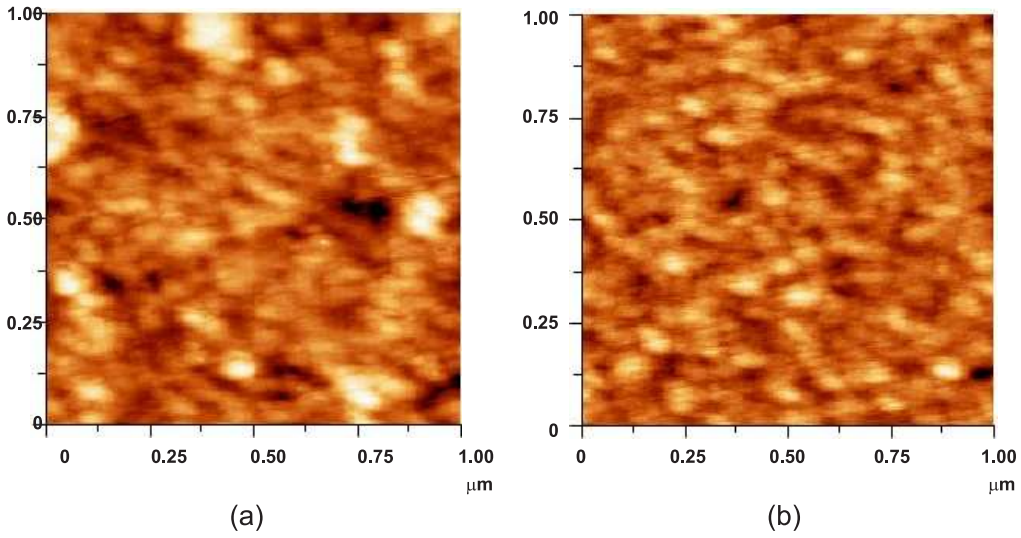

Figure 4.2: AFM images of vacuum deposited (a) pure SiO_2 and (b) 2 vol% MePTCDI/SiO_2 films on glass substrate (image section: 1.00 x 1.00 μm, Z-range: (a) 6.2 nm, (b) 5.1 nm). The total film thickness is 1000 Å.

the SiO_2 film have an average size of 100 - 120 nm, while the size of the mixed layer grains has an average of 70 to 100 nm. Additionally, the mixed samples are characterized by slightly higher film density with respect to the pure matrix film.

The established higher porosity of the pure host film is in agreement with our experimental findings concerning the growth of SiO_2. Upon venting of the vacuum chamber, we observe an increase of the thickness of deposited film measured with the quartz oscillator. Yet, the effect is reversible upon evacuation. Therefore, we attribute this phenomenon to an instant absorption of mostly water from the pores within the thin film volume, resulting in increased density of the deposit, which the monitor interprets as increase of thickness. Upon pumping, the absorbed water is again desorbed. The enhanced density of the mixed layers is due to the incorporation of foreign species, i.e. dye molecules, admixed with the matrix particles, which inhibit the mobility of the SiO_2 particles, thus impeding the formation of large SiO_2 clusters and encouraging a denser microstructure [101]. As a result, the structure which is formed has less micro pores in contrast to the neat SiO_2 layer.

Furthermore, Figure 4.2 presents AFM images of neat matrix and mixed 2 vol% MePTCDI/SiO_2 samples at total film thickness of 1000 Å. The images also indicate that both films are amorphous and the surface is relatively flat. Roughness analysis does not show considerable differences in the surface roughness. However, the latter is slightly smaller for the mixed layer, i.e. the RMS (Root Mean Square) roughness is 0.5 nm compared to 0.9 nm. Thus, the results are consistent with those obtained from SEM.

4.1.2 MePTCDI in SiO_2 matrix

Isolated molecules vs. crystalline film

As we noted in the introduction, the PVD method allows the growth of mixed dye/matrix layers, independent of the dye solubility in the matrix. Hence, it is possible to study a wide range of dye concentrations, from a neat dye film to single dye molecules isolated in the solid matrix. However, before discussing extensively the results on mixed MePTCDI/SiO_2 and further on MePTCDI/PI layers, it is essential to first present briefly the two borderline systems: an isolated MePTCDI molecule (monomer) and MePTCDI molecular crystal. We compare their optical behavior in order to provide a basis for assignment the spectral features of the mixed layers.

Figure 4.3 shows the normalized absorption and emission spectra of MePTCDI, dissolved in DMSO. Since it is known for diluted liquid solutions that excitation spectra of isolated molecules are identical or rather similar to their absorption spectra [102], the corresponding luminescence excitation spectrum is presented instead of the absorption spectrum. Both spectra are characterized by a mirror symmetry. It thus reflects the relatively simple electronic and vibronic structure of MePTCDI. The observed three bands are assigned to one electronic transition and its vibronic progression. The S_0 - S_1 transition with S_0[0-0] peak positioned at 2.36 eV is a strong π - π^* transition which is polarized along the long molecular axis [156]. The vibronic progression is due to the coupling of the first singlet excited state S_1 to several vibrational modes of the molecule. An understanding of the vibronic structure of perylene derivatives is possible by a combination of IR, Raman, and Resonant Raman spectroscopy (RRS) and theoretical models [157, 158, 159]. For example, in Ref. [159], the most intense vibronic modes in the RRS spectra of PTCDA are assigned to the in-plane vibrational modes from a theoretical prediction. However, only few modes of comparable energy contribute with large oscillator strength to the absorption. The absorption spectrum can thus be sufficiently described by one effective vibrational mode. Hence, the spectrum is treated as the electronic transition with the vibronic progression of this effective mode. The weak feature at around 3.4 eV in the luminescence excitation spectrum corresponds to the next highest dipole allowed singlet state S_2.

Figure 4.4 presents the absorption and luminescence emission spectra of a MePTCDI thin film. In contrast to solution, no vibronic progression can be assigned to the thin film absorption spectrum: It is considerably broader. Additionally, the absorption edge is strongly red-shifted. The thin film is crystalline in nature, but the interactions between the molecules in the crystal are much weaker than the covalent in origin intramolecular interactions. As a result, the electronic structure of the individual molecule is roughly preserved in the solid state: the absorption bands between 2 and 3 eV approximately correspond to the electronic transition of the monomer at 2.36 eV (cf. Fig. 4.3). In the film, however, the intermolecular interactions lead to alteration of the electronic structure. Consequently, on the finer scale of vibrational excitations, both spectra are quite different.

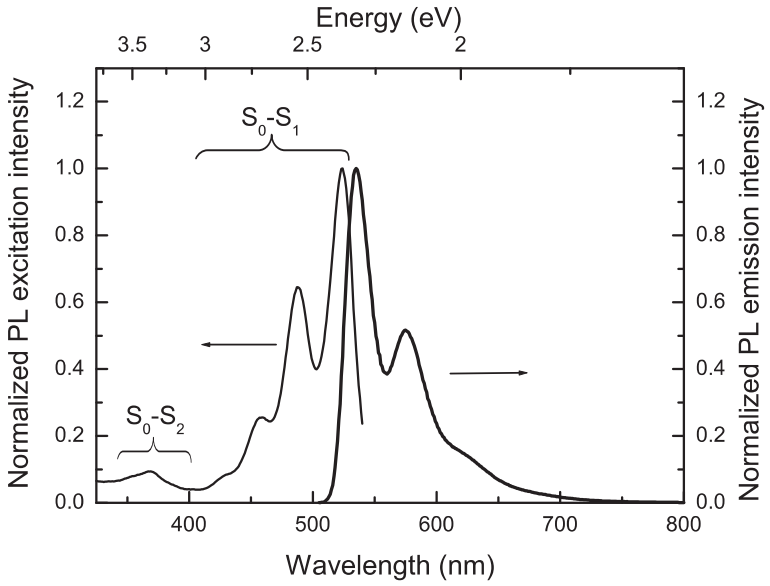

Figure 4.3: Normalized PL excitation and emission spectra of MePTCDI dissolved in DMSO at concentration 10^{-5} mol/l.

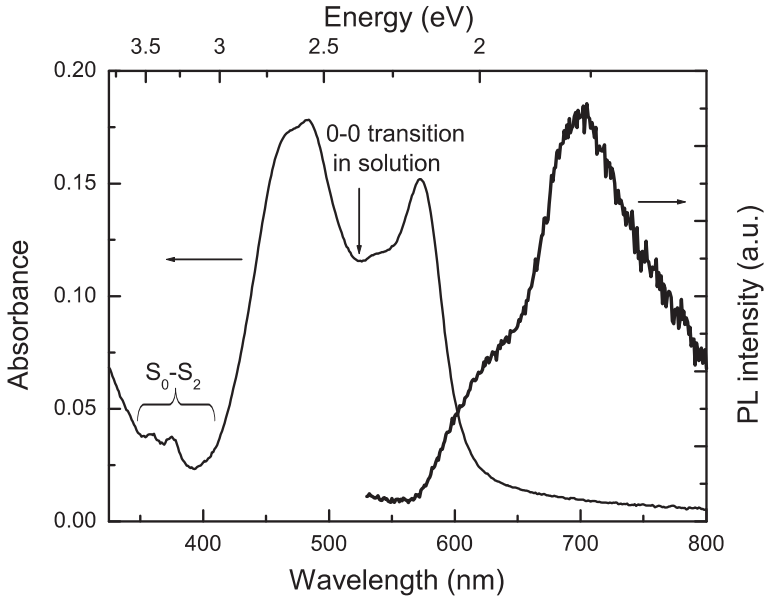

Figure 4.4: Absorption and emission spectra of MePTCDI thin film (20 nm thickness on glass substrate).

The absorption behavior of crystalline MePTCDI has been explained by a band structure model for quasi-1D crystals with strong orbital overlap between neighboring molecules, developed by Hoffmann et al. [103, 104, 105]. The model considers, in addition to the Frenkel exciton with linear coupling to the effective internal vibrational mode, CT excitons that couple to the same vibrational mode. As introduced in Section 3.1.1, the distance between the molecular planes within the one-dimensional stacks of MePTCDI is 3.4 Å, which is small in comparison to the other lattice constants and to the size of the molecules. This causes very strong overlap of the π-electron systems within the stacks. Due to the overlap, the energy of the lowest CT exciton states becomes small. The energies of Frenkel and CT excitons approach each other and a strong mixing occurs. In the crystal, this results in the electronic bands presented in Fig. 4.5c, where any vibronic coupling of the mixed Frenkel-CT states is left out. The electronic Frenkel character at $k = 0$ (Fig. 4.5b) determines the absorption coefficient α, which agrees well with the experimental spectrum, as can be seen from Fig. 4.5a. A detailed description of the model and results from its application to the absorption spectra of MePTCDI and PTCDA are given in [104, 105].

A considerably different exciton band structure model is proposed by Vragovich et al. [163]. It is also based on Frenkel excitons coupled to a single effective vibrational mode, however neglecting any CT contributions. In contrast to the one-dimensional model presented above, it includes the full crystal geometry with two molecules in the unit cell. The model shows good agreement with experimental unpolarized absorption spectra.

The luminescence of the pure MePTCDI film is significantly red-shifted with respect to that of the monomer. This corresponds to a large Stokes shift of around 0.26 eV, compared to 50 meV for the molecules in solution. The emission band is broad with a peak at 1.75 eV and a shoulder at $\sim$ 1.90 eV. The PL emission spectrum is invariant when scanning the excitation wavelength over the absorption maxima. It is thus inferred that the steady-state luminescence of the MePTCDI film has a purely electronic origin (at least at RT). In contrast to absorption, the luminescence behavior of solid MePTCDI is still not clearly understood. According to the band structure model of Hoffmann et al., upon optical excitation into any $k = 0$ state, the free excitons relax down to the bottom of their band at $k = \pi$. The transition from the $k = \pi$ states to the total ground state is strictly dipole-forbidden. Hence, the emission spectrum is explained by phonon-assisted recombination. In Figure 4.5f, the experimental emission spectrum of a single crystal is compared to the calculated peaks of the modeled spectrum from the lowest $k = \pi$ state to the vibrational levels of the ground state [105]. The comparison shows good agreement, especially for the 01 and 02 transitions. However, transient PL measurements have shown that the decay times of the peaks are slightly different, indicating that they are not simply related to one excited state that decays into several vibrational ground state levels. Therefore, for explanation of the luminescence properties, in addition to the emission from free-exciton band states at $k = \pi$, emission from self-trapped states was introduced [106]. After optical excitation, free excitons will interact with phonons. For example, in the dimer-like

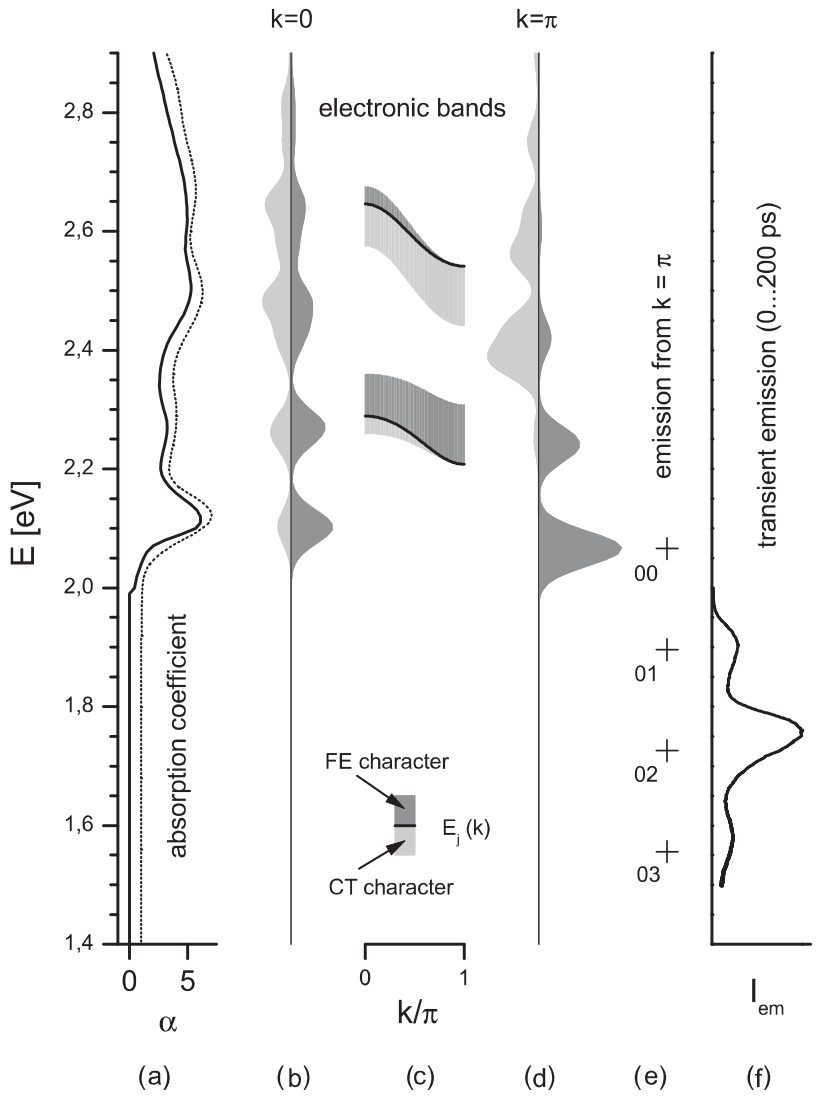

Figure 4.5: Exciton band structure in MePTCDI and experimental spectra (adapted from [105]). (a) Experimental (dashed line) and calculated (solid line) absorption spectra of a poly-crystalline MePTCDI film. The experimental spectrum is measured at 5 K (from [103]). (b) and (d) Vibronic model states at $k = 0$ and $k = \pi$, respectively. Net contributions are summarized by shaded areas, the right side (dark gray) gives the Frenkel character, the left side (light gray) the CT character. (c) Electronic dispersion of the Frenkel-CT mixing bands $E_j(k)$. (e) Calculated emission energies for transition from the $k = \pi$ state to the vibrational levels of the ground state. The 00-transition is strictly dipole forbidden. (f) Transient emission spectrum of a MePTCDI single crystal, measured at 4 K (from [106]).

crystal of α-perylene, strong exciton-phonon coupling is shown to result in a solid state excimer formation [161]. For MePTCDI, a strong exciton-phonon coupling is expected. In contrast to excimer formation (self-trapping) in solution with only one broad emission band, in solids sometimes an additional precursor state arises. Low-temperature luminescence studies, for example in α-perylene or MePTCDI [33, 161] evidence the existence of such self-trapping precursor states. A detailed discussion about the nature of the emitting states in MePTCDI crystalline films can be found in [106].

Simultaneous condensation vs. layer-by-layer film growth

Co-evaporation or simultaneous condensation. As explained in the experimental part of the thesis, the investigated layers were obtained by two different deposition geometries, co-evaporation and layer-by-layer growth. Therefore, we will first present the results concerning films grown by simultaneous condensation of matrix and dye on a static substrate, in order to motivate the necessity of passing over to layer-by-layer film growth.

To highlight the effect of the intermolecular interactions on the luminescence efficiency of the mixed MePTCDI/SiO_2 layers, we followed the evolution of the PL excitation and emission spectra as a function of the MePTCDI concentration. The range of concentrations studied is 0.2 - 6.3 vol%. Figure 4.6 depicts the corresponding normalized PL excitation spectra. A comparison with the absorption spectrum in Fig. 4.3 shows for all samples the presence of single molecules. The spectral features of the lowest S_0 - S_1 transition are clearly manifested: Peak1 at 2.3; Peak2 at 2.47, and a shoulder at around 2.64 eV. Thus, as in solution, the spacing between vibronic levels amounts to 0.17 eV [69]. The positions of the peaks are slightly shifted to the red with respect to the corresponding monomer peaks in DMSO (Peak1: 0.06 eV for the 0.2 vol% sample). This shift to lower energies can be attributed to interactions with the SiO_2 matrix as a solvent environment. Further, there is spectral broadening of the absorption band, which increases from 0.32 up to 0.39 eV with increasing MePTCDI concentration. In addition, a notable change of the ratio of the heights of Peak1 and Peak2 occurs. With increasing dye concentration, Peak2 favorably gains intensity, which denotes enhanced excitation strength of the 0-1 transition and thus evidences dimer formation. For some of the samples, a very weak spectral feature at $\sim$ 3.2 - 3.3 eV, corresponding to absorption from higher excited states, is observed.

Figure 4.7 shows the corresponding luminescence spectra of the samples studied. The intensity values are depicted as recorded in order to follow the alteration in luminescence intensity in dependence on dye concentration. The Stokes shift is relatively small - 0.066 eV for the 0.2 vol% sample. This is expected for a rigid matrix, since in such environment little rearrangement is possible[1]. Two distinct tendencies are observed: (i) in contrast to the absorption spectra, the emission spectra significantly change in spectral shape with increasing dye content (ii) the

[1] In solid solutions, the relaxation time for the solvent molecules τ_R is usually $\gg$ than the lifetime τ_e of the excited state; i.e. emission will occur before any rearrangement of solvent molecules in the solvation cage [37, 38]

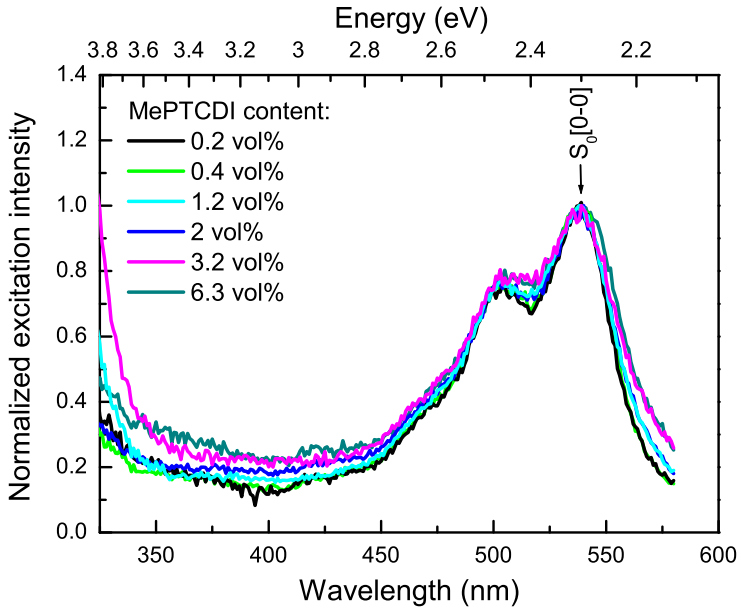

Figure 4.6: Normalized PL excitation spectra of mixed MePTCDI/SiO_2 films on glass at various concentrations of the dye. Detection wavelength is 595 nm. The total thickness of the samples is 1000 Å.

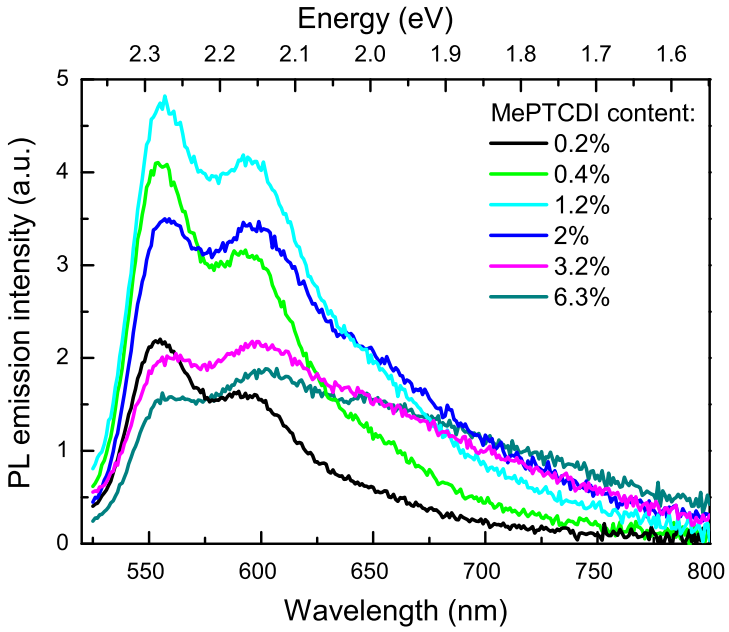

Figure 4.7: PL emission spectra of MePTCDI diluted in SiO_2 matrix at various concentrations. Emission is recorded at excitation of 502 nm. The total thickness of the samples is 1000 Å.

alteration of spectral shape is accompanied by change in luminescence intensity. The samples at low MePTCDI concentrations (up to 1 vol%) show monomer-type emission and increase of the PL intensity at a slight shift to the red of the PL maximum. Above 1 vol%, the shift to lower energies continues (around 0.02 eV for the studied concentration range). The luminescence intensity nearly linearly increases with increasing dye content for the samples at 0.2 and 0.4 %; above 0.4 vol% the linear dependence is violated. Additionally, the second peak (transition S_1[1-0]) becomes considerably broader, and above 2 vol%, more intense with respect to the first peak (transition S_1[0-0]).

This spectral behavior can be explained by aggregation of molecules and resonant energy transfer (Förster transfer), two effects which are substantially influenced by changes in dye quantity. With increasing quantity of dye molecules in the matrix, the probability for aggregate formation increases. Dimer formation, however, results in alteration of the spectral shape and displacement of emission bands relative to the monomer [31]. The deposition technology we use assures rather low-order arrangement of the condensed molecules. Yet, for dimer configuration with nonparallel alignment of the dipole moments both transitions are optically allowed. With a certain probability each dimer state could be excited and could emit upon relaxation to the ground state. Hence, the multiplicity of possible orientations between pairs of MePTCDI molecules, sufficiently close to

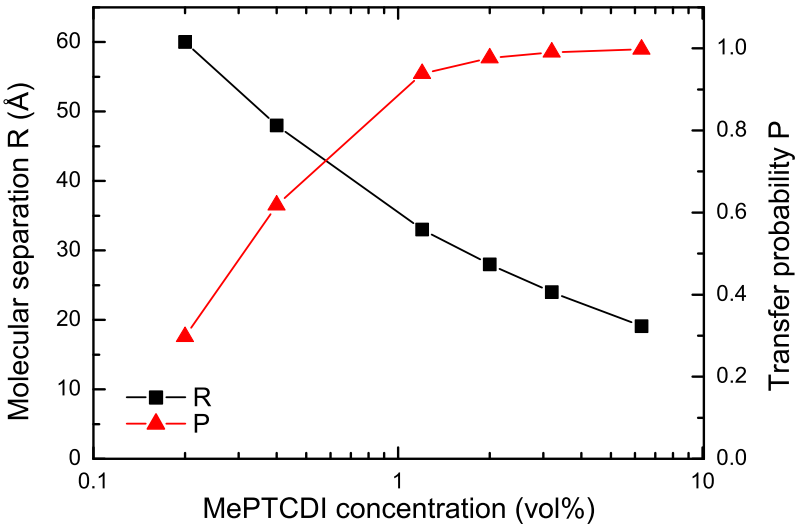

Figure 4.8: Molecular separation R and probability P for Förster energy transfer in dependence on dye concentration for MePTCDI diluted in SiO_2 matrix.

form a dimer, leads to the observed broadening of the emission band. Due to relaxation processes within the dimer complex, emission occurs primarily from the lower energy level. This red shift, along with the induced energy shift of the exciton band splitting, contributes further to the red shift of the emission band. On the other hand, the oscillator strength of the dimers is lower with respect to that of the corresponding monomer states [31]. Therefore, the decrease in luminescence efficiency with increasing dye content can be assigned to predominant emission of dimers or higher-order aggregates within the thin films.

As argued in Section 2.2, the efficiency of the Förster transfer is strongly distance dependent. It is most effective when donor and acceptor are separated by a distance within the Förster radius. Figure 4.8 shows the probability for Förster energy transfer in dependence of the MePTCDI content in the matrix. The probability P is

$$P = \frac{1}{1 + (R/R_0)^6}, \tag{4.1}$$

where R denotes the molecular separation and R_0 is the Förster radius. We calculated R_0 from Eq. (2.32) by determining the spectral overlap for MePTCDI molecules dissolved in Chloroform. It amounts to 52 Å (for the calculation, we used the emission and absorption spectra presented in [107]). The value is consistent with the data in [108], where for perylene derivatives dissolved in various solvents the Förster radii are determined to be $\sim$ 40 - 50 Å. For the studied samples, as evident from Fig. 4.8, 0.4 to 1 vol% dilution corresponds to a mean distance between the MePTCDI molecules in the matrix which lies in the range of the referred critical radius. If the thin film comprises both monomers and dimers,

which are close enough for effective energy transfer to take place, excitation will be transferred with a certain probability from the isolated MePTCDI molecules to the molecular complexes. As a result, the luminescence quantum efficiency of the MePTCDI/SiO_2 system will decrease. For dye contents $\geq$ 1 vol%, the probability for Förster transfer exceeds 90 %, while for 0.1 vol% it is only 9 %. Such an interpretation is consistent with results from luminescence anisotropy measurements on thin films of diluted in SiO_2 PTCDA molecules [14]. The emission anisotropy, *r(t)*, is defined as:

$$r(t) = \frac{I_{\parallel} - I_{\perp}}{I_{\parallel} + 2I_{\perp}}, \tag{4.2}$$

where $I_{\parallel}$ and $I_{\perp}$ are the intensities of light emitted with parallel and perpendicular polarization, respectively, to the direction of the excitation polarization [110]. The anisotropy r is 0 for systems with coupling between luminescence centers with isotropically distributed orientation, and varies between 0.2 and 0.4 for randomly oriented molecules. In PTCDA/SiO_2 thin films, r increases gradually with decreasing dye concentration. For dilution below 0.1 vol%, however, the anisotropy tends to reach the value of 0.4, which corresponds to fully independent luminescent species [14].

On the other hand, the only slight alterations in the absorption spectra upon increasing dye content indicate that the films are mostly composed of isolated molecules. However, due to effective Förster transfer, only a few dimers are needed in order to explain the observed luminescence behavior.

The internal quantum efficiency of evaporated MePTCDI thin films at room temperature was measured using an integrating sphere to be only 0.03 - 0.04 [111]. This confirms the fact that the decay dynamics in pure MePTCDI films are dominated by nonradiative recombination losses. In contrast, the quantum efficiency of isolated MePTCDI molecules in solution is about 0.93 [108]. Accordingly, we have shown that by isolation of dye molecules in the rigid matrix, it is possible to influence the intermolecular interactions. Thus, higher luminescence quantum efficiencies with respect to the MePTCDI crystalline thin film can be reached. Further in this Chapter (see Fig. 4.12), we will present the relative PL quantum efficiency of the MePTCDI/SiO_2 films, grown by simultaneous condensation of dye and matrix, as a function of the dye concentration, along with the data obtained for mixed films grown by layer-by-layer condensation.

However, highly diluted films have the disadvantage of very low absorption which is a substantial drawback for some specific practical applications. Another weak point of the used co-evaporation geometry is the inevitable possibility for energy interactions between the SiO_2 matrix particles and the organic molecules. Since the matrix is obtained by e-beam deposition, it is reasonable to assume that upon condensation of SiO_2 particles, considerable heat is released. During the simultaneous condensation of both materials on the substrate, as a consequence of intermolecular energy transfer, the dye molecules can experience strong local heating. We will refer to this effect as "thermal stress". It could lead to structural changes, or even thermal destruction of the organic molecules, which thus could no more efficiently emit light, but serve as luminescence traps. If this is the case, the

existence of inactive (destructed) molecules could play an important role only in the luminescence response of the samples (due to migration of excitation and effective resonant energy transfer), but could not be detected directly in the absorption spectra. Thus, our assumption is consistent with the only very small variations in the excitation spectra of the samples at various MePTCDI concentrations.

Further, during evaporation the substrate is inevitably heated. We carried out experiments in order to prove that, using a thermocouple fixed on the substrate surface and facing the evaporation source. It has to be noted, though, that the measurement is not necessarily highly accurate, since the substrate is of low thermal conductivity. The results have shown that the substrate temperature rises from RT to a value which depends on the matrix evaporation rate. For example, during the deposition of 2000 Å mixed film ΔT (ΔT = T - RT) was 36 K for 5 Å/s evaporation rate, while for 0.2 Å/s ΔT of 69 K was measured. Similarly, the substrate was heated from RT to 395 K during 120 minutes deposition time at 4 Å/s. These values, however, correspond to an integral substrate temperature while on a local level it is possible that an overheating is reached. Thus, the energy "imposed" on the system could also lead to structural changes in the organic molecules. As we will discuss later, this could be a rather significant effect in particular when the preparation of μm-thick films is concerned. Hence, we carried out most of the spectroscopic measurements exclusively on 1000 Å thick films.

Layer-by-layer growth. Our subsequent studies were devoted to finding the most appropriate evaporation conditions which assure less thermal stress upon the organic molecules during film growth. Additionally, we aimed at influencing the deposition process in a way that permits designing structures with less aggregates and reduced probability for resonance energy transfer to non-luminescent traps, i.e. with increased PL efficiency, at higher dye content.

As a first optimization step, we introduced rotation of the substrate on which the condensation takes place. However, the concurrent condensation of both materials was retained. Technological experience shows that the deposition on rotating substrate has the following advantages:

- the thin films grown are uniform in thickness on large area
- the factors causing an inhomogeneous distribution of material when mixing two or more constituents are reduced, so the deviation from the stoichiometry is lessened
- for materials which show columnar growth morphology, substrate rotation assures upright growth.

Accordingly, thin films with reproducible optical parameters can be prepared.

In order to reduce the thermal stress upon the organic molecules, we further separated the condensation of dye and matrix molecules during the film growth process on the rotating substrate. For this reason, we used an additional disk with 18° - 180° aperture, as described in Section 3.2.6 of the work. This layer-by-layer

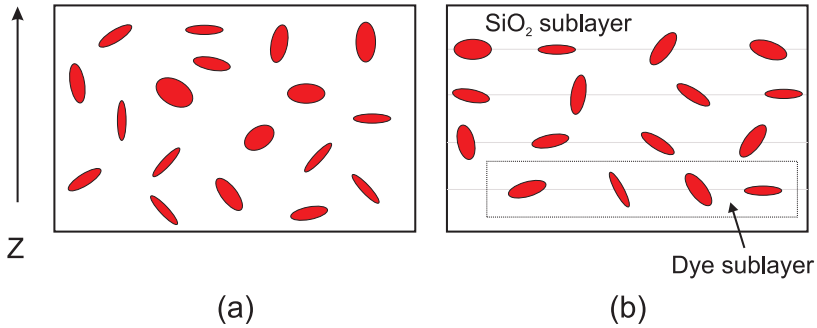

Figure 4.9: Schematic presentation of the dye depth distribution for layers grown by (a) co-evaporation and (b) layer-by-layer.

growth mode (Fig. 4.9b) additionally offers the possibility to control both the amount of dye and matrix in the sublayers. Thereby, we can achieve more or less efficient separation between subsequent dye sublayers. Thus, undesired interactions between matrix and dye molecules, as well as intermolecular interactions leading to luminescence quenching can be prevented.

Using layer-by-layer film growth, molecules of MePTCDI were diluted in SiO_2 matrix at concentrations in the range from 0.5 vol% to 23 vol%, and the optical behavior of the resulting films was investigated. First, Fig. 4.10 presents a comparison of the luminescence of MePTCDI/SiO_2 films for samples grown by simultaneous condensation on static and rotating substrates, and by layer-by-layer growth. The concentration of MePTCDI for all samples is 2 vol%. The corresponding excitation spectra are quite similar (see the inset in Fig. 4.10), while the sample differ in luminescence. All films have an absorption maximum at 2.31 - 2.32 eV, with spectral shape reproducing the main features of the monomer absorption. The band width is almost constant, around 0.34 eV.

In contrast, the luminescence spectra show that the distribution of molecules in the films on rotating substrate is nearly monomer-like. Spectral shapes are similar to the emission of MePTCDI in DMSO solution, indicating weaker intermolecular interactions. However, a comparison of the height ratios of peaks 1 and 2, and the band widths suggests that the emission of the layer-by-layer sample originates mostly from singlet excited states of isolated molecules in the matrix, while the luminescence of the co-deposited film reflects rather dimer-type emission. The assumption is supported by the lower value of the PL integral intensity for the latter sample.

As already discussed, for mixed MePTCDI/SiO_2 films obtained by static co-evaporation geometry, the transition to monomer-type emission occurs at dilution below 1 vol%. In contrast, our experiments with samples on rotating substrate and separate condensation demonstrate that the latter transition is shifted to higher dye quantities, namely 2 vol%. We interpret this result as follows: In case of layer-by-layer growth, the condensation of both materials is separated in time. The film is build up consecutively, i.e. each dye sublayer is followed by a matrix sublayer. Thus, by inserting discrete matrix sublayers, the possibility

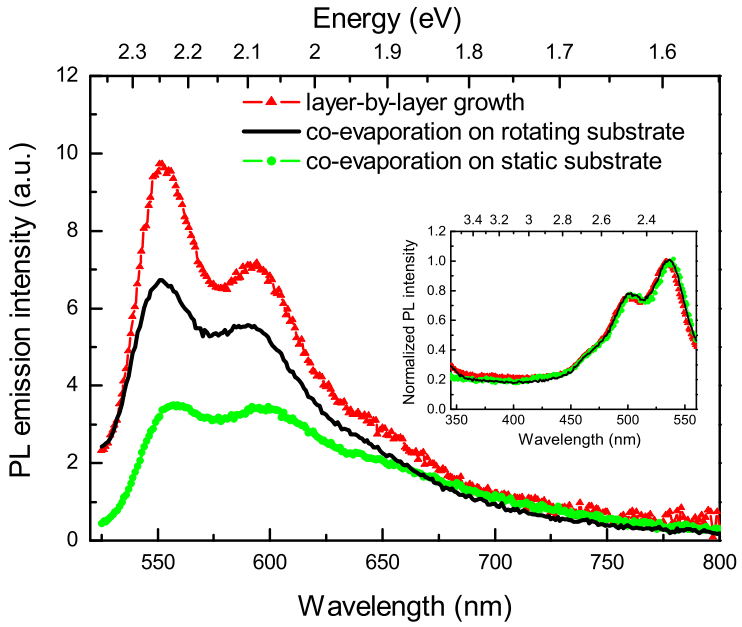

Figure 4.10: Luminescence spectra of composite 2 vol% MePTCDI/SiO_2 films, grown by various deposition conditions. 502 nm is used as excitation wavelength. The inset shows the corresponding normalized excitation spectra; 595 nm is used as detection wavelength. The total sample thickness is 1000 Å.

for interactions between MePTCDI molecules of two neighboring dye sublayers is reduced. Another advantage of the separating SiO_2 sublayer is that it limits the migration of organic molecules in the same dye sublayer. During condensation, some of the molecules of the same sublayer face each other to form dimers, however a substantial part of them remains isolated on the rough matrix sublayer surface, upon excitation emitting from the singlet excited state.

For the samples grown layer-by-layer, we further established that the change in luminescence spectral shape is accompanied by an increase of the integral intensity by a factor of 1.8 - 2.6 with respect to that of the samples at the same dye content, co-deposited on static substrate. The enhanced intensity is assumed to be due to reduced thermal stress for the organic molecules during film growth. By classical co-evaporation, both dye and matrix materials simultaneously condense on the substrate. As a result, the MePTCDI molecules are subjected to energy transfer as a consequence of the heat released by the condensation of SiO_2 particles. However, by evaporation on rotating substrate, first, the condensation of matrix and dye are separated in time. Direct interactions are thus avoided. Second, time for relaxation between the successive layers is gained. As explained in Section 3.2.6, the substrate sees the evaporation sources only for a part of the disk rotation period. This means that by changing the rotational rate, we can prolong the time between the moment of completion of for instance the matrix layer, and the moment when the impinging dye molecules start to form the successive dye sublayer. The MePTCDI molecules hit the already cooled down surface of the SiO_2 sublayer. Thus, the destruction of the initial dye molecules during film growth is limited. The possibility for energy transfer of the excitation to non-luminescent molecules decreases and the channels for luminescence losses are reduced. In general, this assumption can clarify the increased luminescence efficiency of the samples obtained by the layer-by-layer film growth.

We established similar luminescent behavior for the perylene derivatives PTCDA and 01630/021 (a test dye delivered from BASF Farbenlabor, Ludwigshafen), when layer-by-layer film growth was used for their incorporation in the SiO_2 matrix. The composite layers show pronounced monomer emission at higher dye content, combined with increased luminescence intensity compared to the co-deposited samples. However, because the present work is mainly concerned with the MePTCDI dye, these results are not discussed in detail here (a thorough study of mixed PTCDA/SiO_2 films, prepared by simultaneous condensation can be found in [52, 112]). In Figure 4.11, we present as example only results for 1 vol% PTCDA in SiO_2 samples, grown by both deposition modes. A comparison between the PL excitation spectra show that the characteristic spectral features of the dye in liquid solution are visible in the absorption of both samples, yet the peaks are shifted to lower energies by about 0.03 eV (according to [113], in DMSO the 0-0 transition is centered at 2.39 eV, while in SiO_2 Peak1 is positioned at 2.36 eV). Differences in the absorption behavior are expressed in a slightly narrower absorption band for the layer-by-layer sample and a nearly monomer height ratio of peaks 1 and 2 with respect to the co-deposited sample. Both distinct emission peaks of the layer-by-layer sample have almost equal intensity, while for the co-

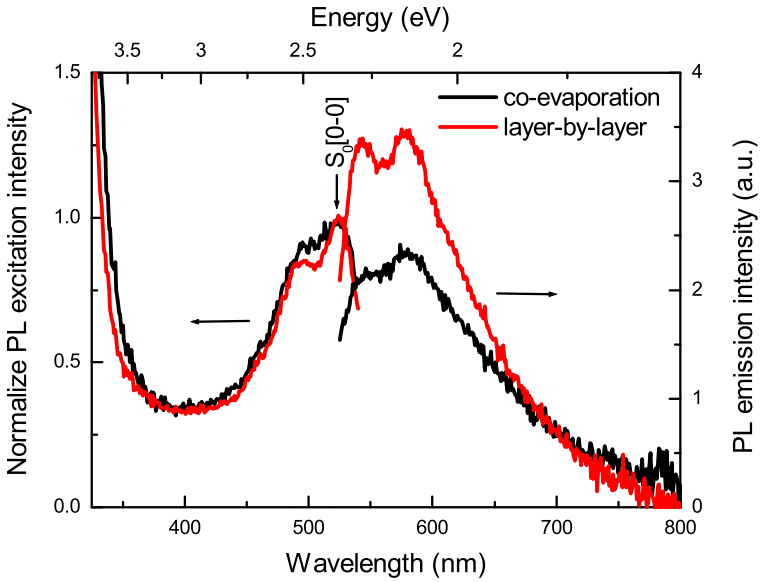

Figure 4.11: PL emission and excitation spectra of mixed 1 vol% PTCDA/SiO_2 films, grown by co-evaporation and layer-by-layer growth. Emission is recorded at an excitation wavelength of 495 nm.

deposited sample, the second emission peak gains intensity with respect to the first one. Additionally, the luminescence low-energy tail of the simultaneously grown PTCDA/SiO_2 film is red-shifted compared to the separately grown film.

On the other hand, differential reflectance spectroscopy (DRS) studies on ultrathin films of PTCDA, grown on mica by organic molecular beam epitaxy (OMBE), reveal that up to 1 ML film coverage, the films show monomer absorption [114]. This behavior is explained by weak electronic coupling between the single molecules at this thickness and stronger aptitude for completion of the first layer than to formation of molecule stacks. In the out-of-plane direction, the molecules are separated only by 3.37 Å. Thus, above 1 ML film coverage the strong interaction of the overlapping π-electron systems prevails and the molecules start to stack in dimers. The transition from monomers to dimers is manifested in the absorption spectra of the films, with enhanced height of Peak2 with respect to Peak1. In contrast, the excitation spectra of the studied samples indicate rather predominantly monomer distribution of PTCDA molecules. The existence of aggregates is revealed only in the emission spectra in modified spectral shape. In this regard, the results are consistent with those presented in [112]. For PTCDA/SiO_2 films grown by simultaneous condensation, it was also established that a transition from monomer to dimer luminescence takes place at a dye content between 0.7 - 1 vol%. However, considering the higher PL intensity and the nearly equal peak intensities of both emission maxima, the number of luminescence traps in

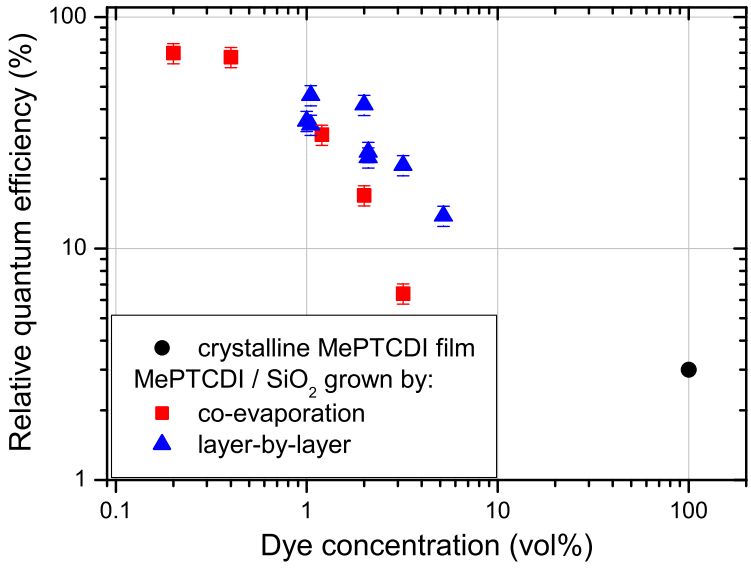

Figure 4.12: Relative PL quantum efficiency of composite MePTCDI/SiO_2 films, grown by simultaneous condensation and layer-by-layer in dependence on MePTCDI concentration.

the layer-by-layer sample is apparently lower with respect to the co-deposited film. This conclusion is supported by results from a comparative study on samples from both deposition geometries and concentration range from 0.3 to 3 vol%, which we did not present here. Thus, the separated condensation in time of both SiO_2 and PTCDA results in enhanced PL efficiency.

In Figure 4.12, the relative PL quantum efficiency of mixed MePTCDI/SiO_2 samples grown layer-by-layer is compared to that of samples grown on static substrate by simultaneous condensation of matrix and dye. Relative refers here to the fact that the efficiency of the samples is defined relative to the internal quantum efficiency of pure MePTCDI layer, assuming equal absorption per molecule for all samples. As a general trend, the graph shows that the PL efficiency increases with decreasing dye content, reaching a value of about 70 % at 0.2 vol%. Moreover, the results suggest the following: At low dye quantities, both film growth modes could be used to produce layers with similar luminescent properties. However, the separation of dye from matrix during film growth results in mainly single molecule distribution, and thus to high PL quantum efficiency even in more concentrated solid solutions of MePTCDI. As a consequence, another important advantage of this technique is that it allows the preparation of mixed films with increased absorption without losing luminescence efficiency.

Another noteworthy observation is that, although the general trend in Fig. 4.12 is easily recognizable, there is considerable deviation of the PL efficiency

values for the various samples at equal total MePTCDI concentrations grown layer-by-layer. The result could stem from a difference in the composition between the investigated films. As already stressed, the layer-by-layer condensation offers the possibility to control the thickness of the constituent sublayers, varying the evaporation rate for the organic and matrix materials via the aperture angle in the disk beneath the substrate holder. In such a way, the distance between the organic molecules in the sublayer and between the organic sublayers themselves could be varied. This leads to a different areal density of MePTCDI molecules in the final film (in-plane and in-depth film direction) and thus to emission from different states. This could easily explain the observed differences.

The above consideration, however, requires a detailed investigation of the luminescence behavior as a function of film composition and the corresponding film structure. The substrate rotation, combined with the temporally separate condensation of dye and matrix, allows the formation of films comprising alternating sublayers of SiO_2 and MePTCDI. In order to clarify the influence of the latter on the luminescence, we prepared samples with various thicknesses of the dye (dye coverage) and matrix sublayers using layer-by-layer growth. Information about the optical quality of the films can be inferred from their PL emission and excitation spectra, since, as pointed out, monomers show different luminescence behavior compared to molecular aggregates. Spectral shape and intensity thus reflect the molecular distribution and accordingly, it is possible to draw conclusions about the optimal film composition for highest PL efficiency.

Figures 4.13 and 4.15 show PL excitation and emission spectra of samples at equal MePTCDI sublayer coverage of 0.1 ML (0.3 Å). They differ in the thickness of the SiO_2 sublayers in-between and total dye concentration, respectively. As in the case of co-deposited films, the emission PL spectral shape changes substantially with increasing matrix sublayer thickness, whereas the excitation spectra at lower total dye content are less influenced by the latter parameter.

In general, in the concentration range between 10 and 2 vol%, the excitation spectra of the VD films are similar to those of dissolved MePTCDI molecules (see Fig. 4.3). In contrast, the film at 23 vol% total dye concentration, and 1 Å SiO_2 sublayer thickness respectively, represents a mixture of monomer and aggregate-type absorption with a broad band and maxima at 2.59, 2.30 and 2.15 eV, the spectrum being quite identical to that of neat MePTCDI film (see Fig. 4.14).

Accordingly, the luminescence of the samples reflects the different composition of the films. With decreasing total concentration, i.e. increasing thickness of the separating matrix layer, the PL maxima shift to higher energies. This phenomenon is accompanied by considerable enhancement of the luminescence intensity. The emission at 1 Å SiO_2 sublayer is identical with that of the crystalline MePTCDI film with a fluorescence peak at 1.77 eV. The sample at 2 Å SiO_2 is characterized by a broad shapeless PL spectrum which corresponds to high degree of aggregation, whereas the emission of the films at 5 and 10 Å originates from low-order aggregates as well as isolated molecules. For the sample at 2 vol% total dye content and 15 Å matrix sublayer thickness, respectively, the luminescence spectrum is dominated by monomeric transitions, with well-resolved vibronic progression

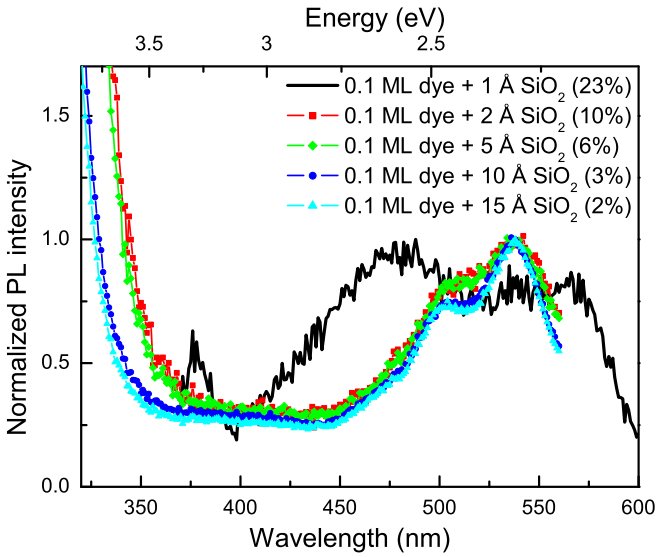

Figure 4.13: Normalized PL excitation spectra of composite MePTCDI/SiO_2 films (layer-by-layer film growth) at 0.1 ML MePTCDI dye coverage, but different total dye concentration. PL excitation is detected at 700 nm for the 23 vol% sample and 590 nm wavelength for all other samples.

and 0-0 peak at 2.27 eV.

As noted earlier, the preparation method we use assures a rather disordered arrangement of the dye molecules within the films. So, again the optical response of the mixed layers is influenced by molecules which are in sufficient proximity to form molecular aggregates, and by energy transfer from isolated molecules to such aggregates. In this regard, the observed spectral changes in the PL excitation and emission spectra can be understood as follows: Although the dye coverage is less than a monolayer (0.1 ML), one can not exclude formation of dimers in the same dye sublayer. However, in the out-of-plane direction, judging by the only slight changes in the excitation spectra of the samples at a total dye content 10 vol% and less, the intermolecular interactions are quite effectively inhibited by a matrix sublayer with thickness > 2 Å. The absorption of these samples indicates the presence of dimers and an additional contribution of isolated molecules. By such a distribution, upon excitation there exists the utmost probability for energy transfer between two neighboring dye sublayers separated by a matrix layer with thickness less than the Förster radius, and also from isolated molecules to aggregates in the same dye sublayer. Yet, following the evolution of the recorded spectra with increasing thickness of the separating SiO_2 sublayer, it is possible to conclude that both Förster transfer in depth of the film and formation of dimers have a decisive effect on the luminescence behavior of the films. At 1 Å matrix sublayer, the organic molecules behave as a quasi-one-dimensional crystal. A further increase

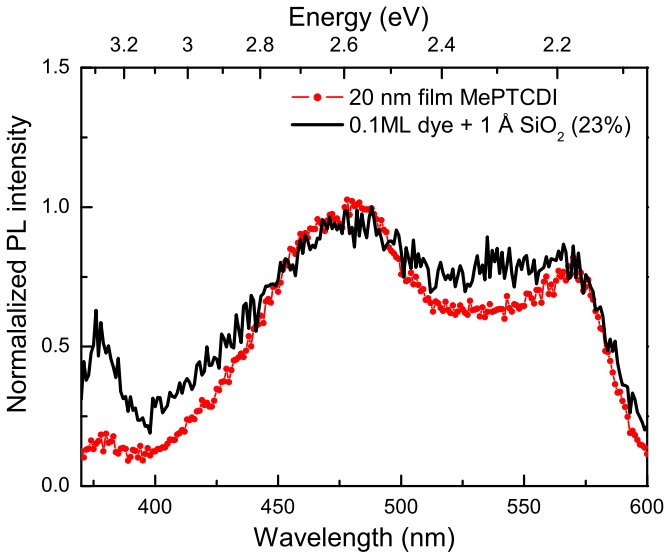

Figure 4.14: Normalized PL excitation spectra of a composite MePTCDI/SiO_2 film (layer-by-layer condensation) at 23 vol% dye concentration and of a 20 nm neat MePTCDI film. The emission wavelength for detection is 700 nm.

of the matrix sublayer thickness results in more effective separation of the neighboring dye layers (the film coverage at which SiO_2 builds a closed layer is known to be around 20 Å) and thus between molecules facing each other. At 2 vol% MePTCDI content, two successive dye layers are isolated by 15 Å matrix layer, which efficiently hinders the formation of aggregates, the result being an increased monomer contribution leading to enhanced luminescence intensity. However, the emission spectral shape suggests that molecule complexes in the same dye sublayer and energy transfer between neighboring MePTCDI sublayers still influence the overall luminescence. The latter could be avoided if one further increases the thickness of the separating matrix sublayer. However, this leads again to a total dye content below 1 vol%.

Another example for the effect of the constituent layers on the luminescence shape and intensity of the final composite film is depicted in Figures 4.16 and 4.17. The graphs present a comparison of the emission of samples at equal total MePTCDI concentration, but at different sublayer composition. Figure 4.16 shows the PL emission spectra of 3 vol% MePTCDI/SiO_2 films with dye coverage of 0.1 ML dye/10 Å SiO_2 and 0.01 ML dye/1 Å SiO_2, while Fig. 4.17 - the respective spectra of 2 vol% MePTCDI/SiO_2 films with compositions 0.1 ML dye/15 Å SiO_2 and 0.01 ML dye/1.5 Å SiO_2.

In contrast to the above samples, not the separating matrix sublayer, but the distribution of organic molecules in the in-plane direction plays here the dominant

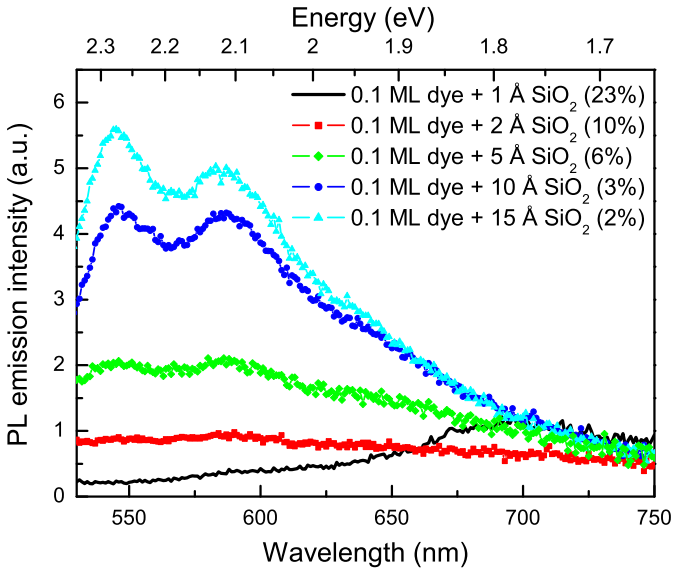

Figure 4.15: PL emission spectra of composite MePTCDI/SiO_2 films (layer-by-layer condensation) at 0.1 ML MePTCDI dye coverage, but different total dye concentration; excitation wavelength 495 nm

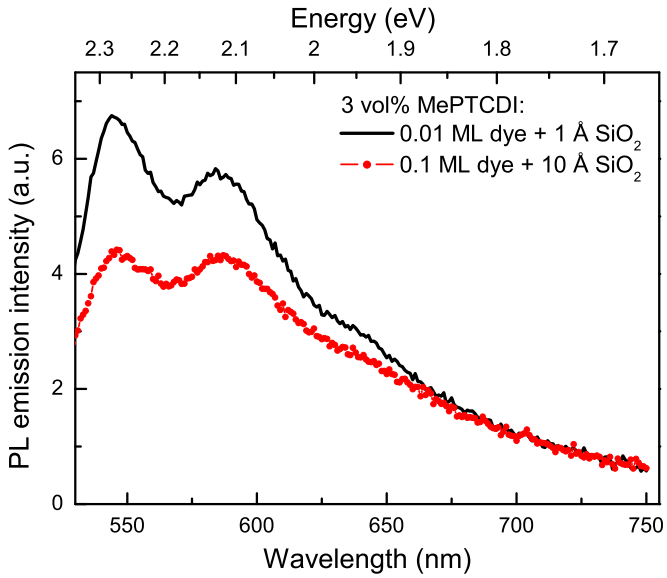

Figure 4.16: PL emission spectra of composite MePTCDI/SiO_2 films at same total MePTCDI concentration of 3 %, but different sublayer composition. For excitation a wavelength of 495 nm is used.

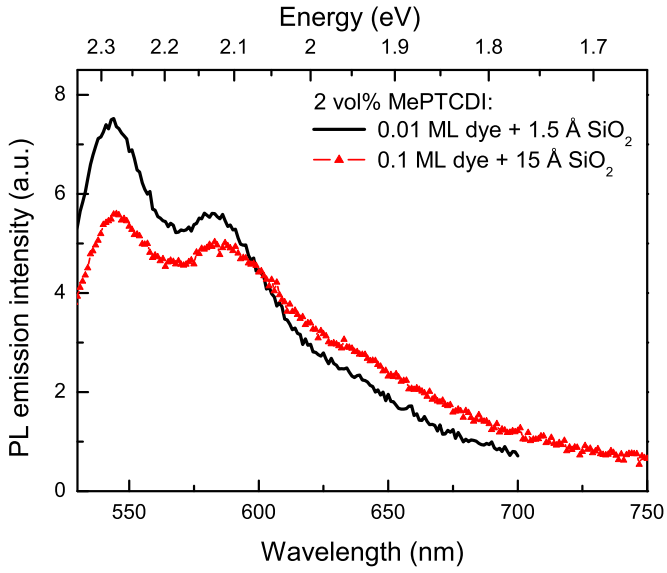

Figure 4.17: PL emission spectra of composite MePTCDI/SiO_2 films at same total MePTCDI concentration of 2 %, but different sublayer composition. Spectra are recorded with 495 nm excitation wavelength.

role. At a dye coverage of 0.01 ML, the distance between MePTCDI molecules in in-plane direction is quite large, the interactions in this direction are therefore very weak and the possibility for Förster transfer of the excitation is very low. The 1 Å SiO_2 sublayer is insufficient for effective separation; nevertheless, at this dilution there is less probability for molecules of two neighboring dye sublayers to interact with each other. As a result, the samples with 0.01 ML dye layers show pronounced monomer emission and the luminescence efficiency increases further.

Photostability. We studied the photobleaching of the mixed samples upon continuous laser light irradiation. The excitation wavelength of 488 nm (Ar^+ laser) fits well into the absorption bands of MePTCDI and PTCDA. The measurements were carried out in air.

Figure 4.18 displays the luminescence behavior of PTCDA molecules incorporated in SiO_2 at 2 vol% upon irradiation with intensity of 2.1 kW/cm^2. The films are grown by co-deposition and layer-by-layer, respectively. The results support the assumption that, compared to simultaneous condensation, layer-by-layer growth assures a more homogeneous dye distribution at relatively high dye quantities. The bleaching profiles unambiguously show that upon irradiation, the 0-0 peak at 540 nm gains intensity for both samples, whereas the intensity of the 1-0 peak around 580 nm decreases. Taking into account that the dye molecules in

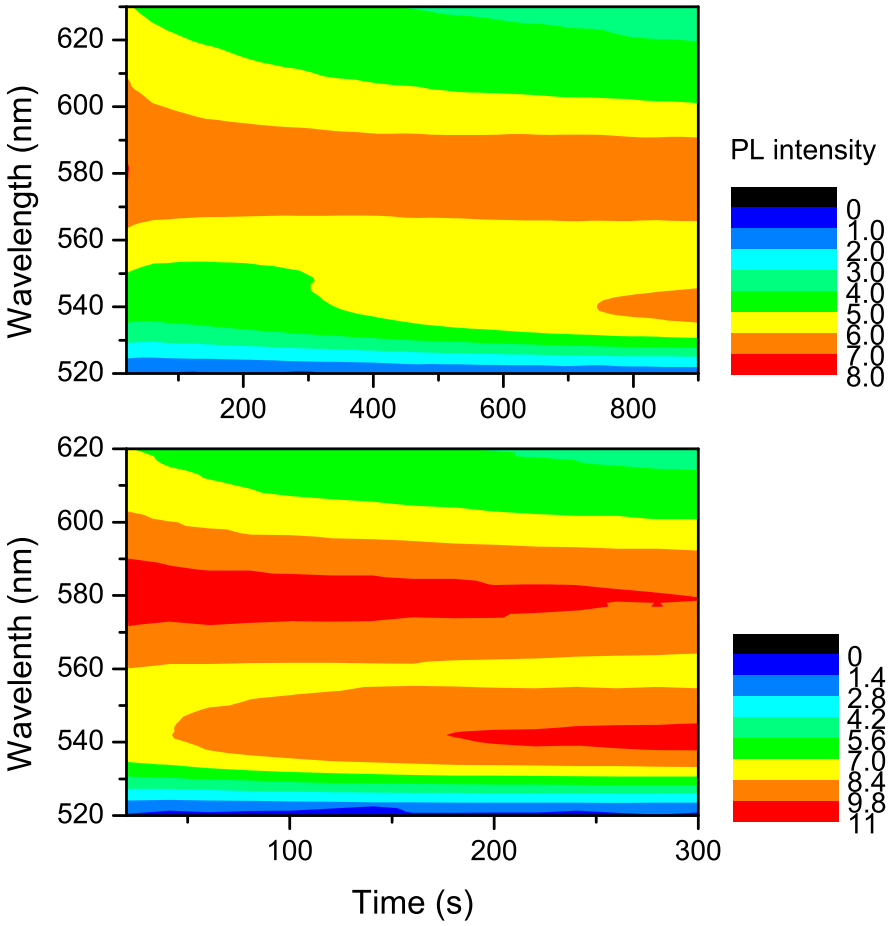

Figure 4.18: Time evolution of the luminescence spectra of mixed 2 vol% PTCDA/SiO_2 films, grown by (above) co-evaporation and (below) layer-by-layer. The total film thickness is 1000 Å. PL is recorded at 488 nm cw-Ar^+ laser excitation (irradiation intensity 2.1 kW/cm^2).

the higher concentrated samples are divided into isolated molecules, dimers, and higher order aggregates (cf. Fig. 4.11), we interpret this result as follows: Upon laser excitation, molecule aggregates are rapidly bleached, while the monomers are more stable and take longer time to degrade. Hence, the luminescence spectral shape changes from a superposition of both species to emission from predominantly monomers. Due to the bleaching, the aggregates are no more available to energy transfer from monomers in close proximity, therefore the PL intensity increases. Similar photobleaching behavior has been observed, for example, for fluorescein distributed in a poly(vinyl alcohol) matrix at a concentration of 1 % [49]. It is further consistent with results obtained from single molecule spectroscopy on layers of terrylene molecules embedded with sub-monolayer thickness in a SiO_2 matrix [155]. The measurements have shown that aggregated molecules are less photostable than the single molecules. Also, the single molecules trapped in the rigid matrix are not easily bleached, even in the presence of oxygen. As shown in Chapter 2, such a behavior is confirmed by various studies on organic fluorescent dyes trapped in thin solid films. The described effects, however, take place on a different time scale for both samples. The alteration in the emission spectrum is faster and more pronounced for the layer-by-layer grown sample. It thus indicates a more homogeneous dye distribution with respect to the co-deposited film.

Figure 4.19 presents results for the luminescence decay of the S_1[1-0] peak ($\sim$ 550 nm) of the mixed layer-by-layer MePTCDI/SiO_2 films in dependence on dye concentration. The photobleaching curves consist of two regions: a fast decrease within the first fifty seconds, followed by region of slower decay. The experimental decay curves for the samples of 0.9 to 3.1 vol% MePTCDI were best fit using a bi-exponential function:

$$I_F(t) = A_1 \exp(-t/\tau_1) + A_2 \exp(-t/\tau_2), \tag{4.3}$$

where $I_F(t)$ is the time-dependent luminescence intensity, proportional to the dye concentration in the electronic ground state, considering absorption governed by Beer's law [49, 115]. An example for such a fit is presented in Fig. 4.20 for the 3.1 vol% sample.

It was thus possible to determine photobleaching rate constants k_1 for the faster process and k_2 for the slower process, respectively ($k_i = 1/\tau_i$). The corresponding results are presented in Fig. 4.21. Accordingly, the photobleaching curves show the presence of at least two decay processes with rate constants dependent on the dye content in the mixed films. The rapid initial decay is more efficient upon increasing dye concentration. Therefore, it is possible to interpret the decay behavior by the average inhomogeneous dye distribution within the mixed layers. The fast decay region can be attributed to interactions between dye molecules in close proximity to each other. In contrast, the slower bleaching mode is likely related to processes involving molecules isolated in the matrix environment. According to studies in literature, e.g. [15], the decay rate in this region is mostly influenced by the mobility of dye molecules in the host and hence to its mechanical and chemical parameters, such as density and composition.

It is noteworthy that the most diluted sample shows a quite high decay rate constant k_2 with respect to the more concentrated samples. On one hand, the

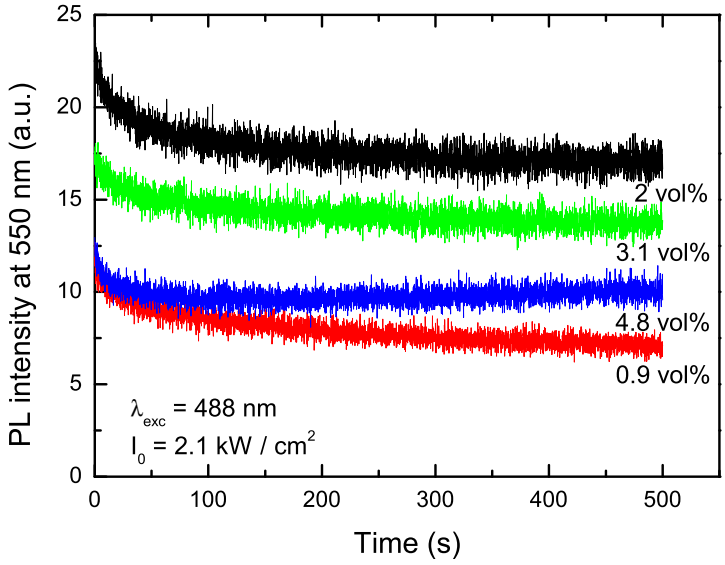

Figure 4.19: Fluorescence decay curves of mixed MePTCDI/SiO_2 films at various MePTCDI concentrations (total film thickness 1000 Å) upon cw-laser excitation at 488 nm, laser intensity 2.1 kW/cm^2. The spectra are recorded at 0.1 s time increment and 0.1 s integration time.

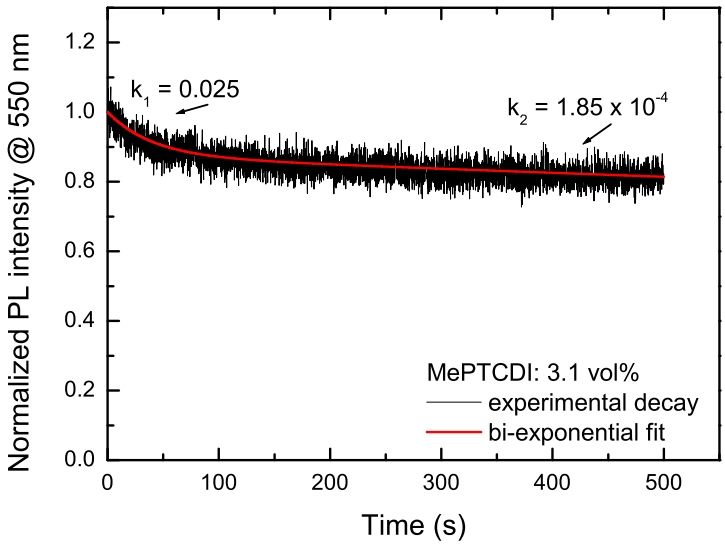

Figure 4.20: Time-dependent PL intensity of mixed 3.1 vol% MePTCDI/SiO_2 film and the corresponding double exponential fit to the data.

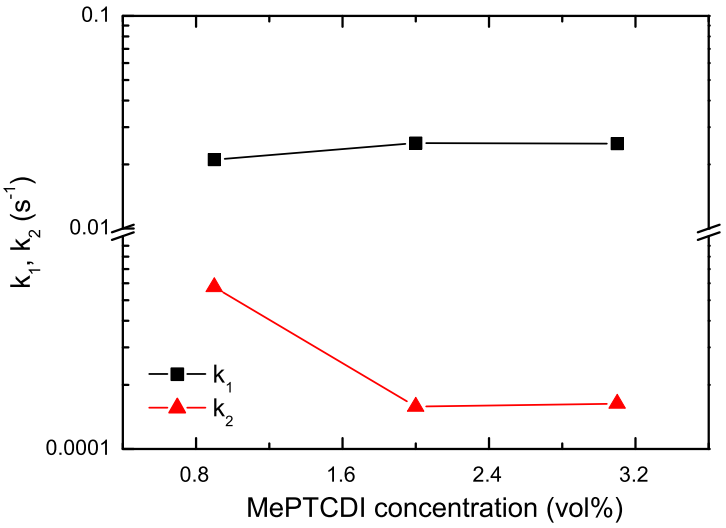

Figure 4.21: Decay rate constants k_1 and k_2 for both decay slopes of the mixed MePTCDI/SiO_2 layers in dependence on dye concentration.

result could be due to slightly different structure of the matrix. In general, the samples are prepared using the same deposition scheme, however in consecutive vacuum cycles. Thus, variations in the matrix structure, and consequently in the dye environment, within the cycles can not be excluded. On the other hand, the experimental data show that an efficient transfer of energy from donor to acceptor decreases the rate of photobleaching [116]. A potential explanation for the faster decay in the case of 0.9 vol% dye content could be the lower probability for Förster transfer, as compared to the more concentrated samples.

In contrast, the decay intensity curve detected at the monomer peak of 550 nm of the 4.8 vol% film (Fig. 4.19) exhibits a special profile, increasing upon continuous irradiation after the initial steep photobleaching. Detection at the lower energy peak at 600 nm, however, shows a time evolution of the PL intensity as in the case of lower dye content (Fig. 4.22). Such a behavior is in accordance with the results presented for mixed co-deposited PTCDA/SiO_2 films upon cw-laser excitation (cf. Fig. 4.18). As discussed, higher dye concentrations result in a variety of molecule configurations inclusively molecule aggregates. These aggregates are less stable upon excitation and diminish as the degradation process develops.

Photoluminescence quantum yield and optical constants. We measured the PL quantum efficiency of the mixed dye/SiO_2 films according to the method presented in the experimental part of the thesis. The main experimental difficulty is the poor absorption of the mixed films at optimal dye content. For example,

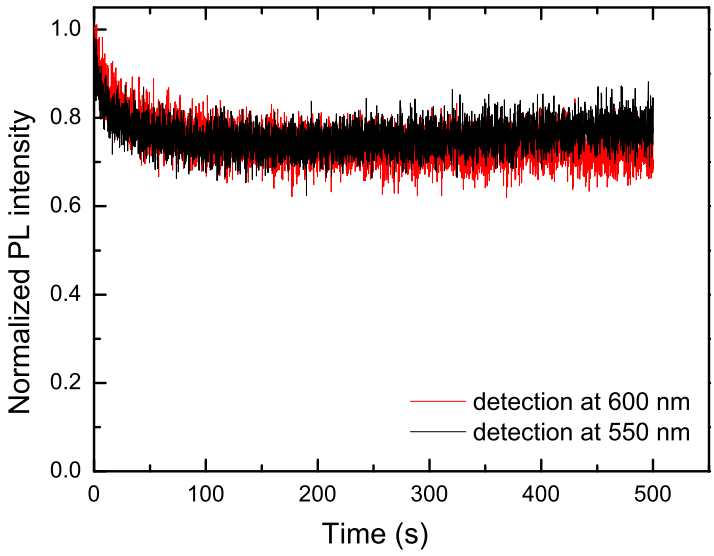

Figure 4.22: Time-dependence of the PL intensity, detected at 550 and 600 nm for 4.8 vol% MePTCDI embedded in SiO_2 matrix upon cw-irradiation at 488 nm, laser intensity 2.1 kW/cm^2. The spectra are recorded at 0.1 s time increment and 0.1 s integration time.

a 1000 Å film at 2 vol% MePTCDI concentration absorbs less than 1% at the excitation laser wavelength of 442 nm. That is, in order to obtain reliable results, it was necessary to grow films of micrometer thickness. Also, the efficiency measured by this method is by a factor 1.6 to 2.4 lower than the internal quantum efficiency of the sample ($\phi_{int} = 2\pi/n^2\phi_{ext}$ [111], with n = 1.7 - 2). This means, that if ϕ_{int} = 0.05, the measured value of ϕ_{ext} will be $\sim$ 0.03. Thus, measurement of samples with low quantum yield, even with sufficient absorption, might be limited by the sensitivity of the detecting system and additionally might require optimization of the integrating sphere design, i.e. sphere diameter, size of port openings, and coating reflectance.

From a technological point of view, it was rather demanding to grow micrometer thick films with good optical quality. Due to the prolonged deposition cycle and the resulting substrate heating, the films tend to crystallize. Also, the films are characterized by poor adhesion to the substrate, and upon increasing film thickness tend to peel off. In addition, although MePTCDI is known to have high thermal stability, such deposition conditions are rather severe for the dye molecules. The films obtained in a single cycle showed alteration in color along with poor luminescence properties, thus arguing for high thermal stress. So, (i) as initial step pure SiO_2 matrix film (100 Å thickness) was grown to increase the adhesion of the real film to the substrate and (ii) the deposition was carried out with breaks, allowing for the sample to cool down. In such a way, we were able to

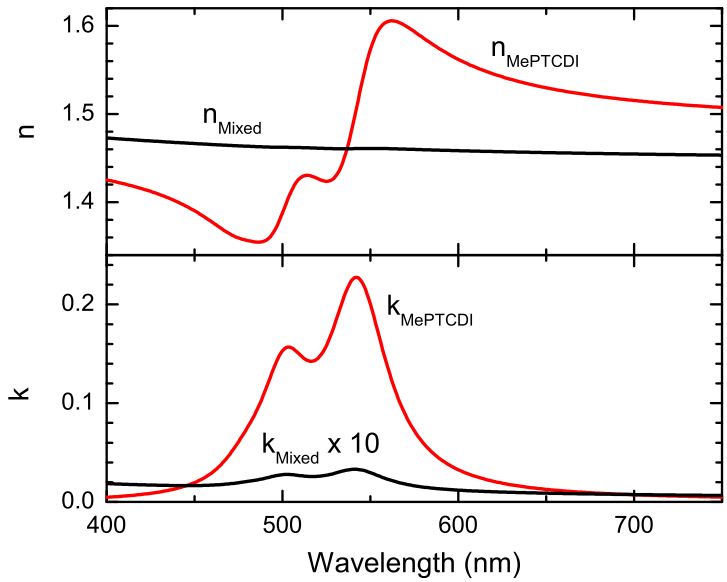

Figure 4.23: Optical constants of MePTCDI embedded in SiO_2 and a 1 vol% MePTCDI/SiO_2 film, defined using Lorentz Oscillator and EMA models, respectively. The SiO_2 matrix is modelled as a Cauchy material.

grow mixed MePTCDA/SiO_2 films of good quality with a thickness in the range 0.6 - 4 μm.

In contrast to the 1000 Å thick films, these "thick" layers gave the opportunity to record reliable transmittance and reflectance spectra. On their basis, as described in Section 3.3.1, it was possible to define the optical constants of the films. As example, Fig. 4.23 shows the determined real and imaginary part of the index of refraction, n and k, of MePTCDI and 1 vol% MePTCDA/SiO_2 film as a function of wavelength. The n and k of MePTCDI were modelled by employing a 3 oscillator LOM. The optical constants thus determined were further substituted in the EMA Bruggeman model with SiO_2 as a Cauchy host material and shape factor q=1/3. In the absorbing range of MePTCDI (330 - 550 nm), a comparison between the experimental spectra and those simulated with Film Wizard shows good correspondence, with maximal difference of 1.6 % in both T and R (Fig. 4.24).

The measurements of the luminescence quantum efficiency have shown that it is strongly influenced by several parameters such as film thickness, preparation time, and deposition procedure. Accordingly, ϕ_{ext} varies between 0.08 - 0.19. The highest efficiency was measured for 6300 Å thick sample at 0.6 vol% MePTCDI. With increasing film thickness, the reproducibility of the luminescence properties drops; the emission spectra of the samples change drastically, indicating enhanced aggregation. Since the samples are characterized by a relatively small Stokes shift,

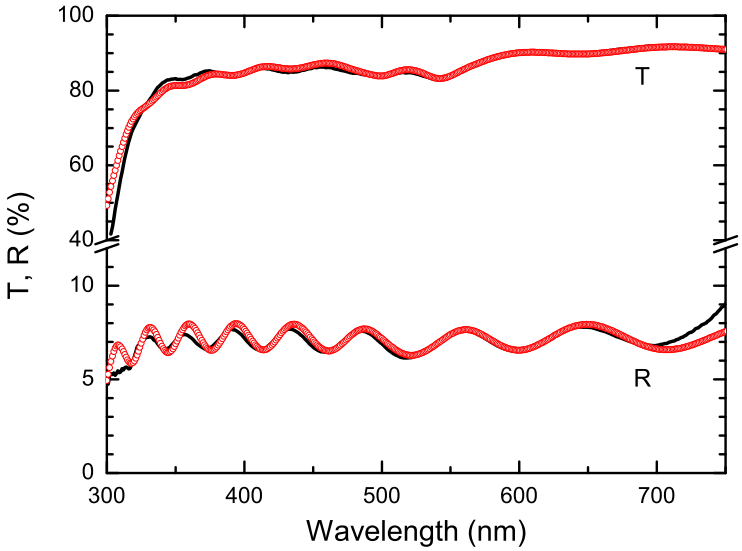

Figure 4.24: Transmittance and reflectance spectra of 1 vol% MePTCDI/SiO_2 film, total film thickness 1.34 μm. Solid lines display the measured spectra, while open circles show the calculated spectra using n and k from EMA model.

at higher film thickness, reabsorption could additionally contribute to the efficiency decrease. However, due to the low absorption coefficients, such an influence seems to be rather insignificant.

Summary

To summarize, examination of the PL emission and excitation spectra of samples grown layer-by-layer confirm that by varying the thickness of the MePTCDI and SiO_2 sublayers, the optical response of the composite films can be varied. The technique allows to control the molecular distribution in both horizontal and vertical direction of the film, and assures better conditions for creation of single molecules - one of the well known prerequisites for high quantum efficiency. Furthermore, the proposed preparation method has some additional advantages. Dye and matrix materials condense separately in time. Hence, the possible ways for degradation of the initial organic molecules are limited and the channels for luminescence losses are reduced. Consequently, the layer-by-layer condensation leads to increased PL quantum efficiency in more concentrated mixed films, compared to the conventional co-evaporation. From the results presented above, we derive 2 vol% to 3 vol% MePTCDI as the optimal dye quantity for preparation of highly luminescent films at higher absorption.

In addition, the results from photobleaching experiments show that the photostability curves of the samples are characterized by a bi-exponential decay, with

decay rate constants which depend on dye concentration. Therefore, two different types of bleaching mechanisms, one for isolated molecules and another for molecular aggregates, have to be taken into account.

4.1.3 Alq_3

Motivation

In the previous Section, we emphasized that due to the SiO_2 deposition method, the organic molecules are subjected to thermal stress during the simultaneous condensation of dye and matrix. It could cause a degradation, thus transforming the molecules into potential traps for the created excitons. Yet, the stress could also induce modifications in the initial structure of the molecules, leading to a different spectral response. Therefore, the aim of the following investigation was to support the above assumptions by experimental findings.

As a "sensor" dye for the changes the molecules undergo during the evaporation, we chose Alq_3. The idea behind is to take advantage of the possibility for thermal conversion between the two geometrical isomers of Alq_3 at high temperatures [83] and their distinctive luminescence behavior.

The coexistence of the meridional and the facial isomers in the thin film was stated by Curioni et al. [28, 29] on the basis of ab initio calculations of the ground-state properties of isolated Alq_3 molecules. In the facial isomer, the oxygen and nitrogen atoms of the coordinating quinolate ligands share opposite faces of the octahedral complex, while in the meridional isomer the latter atoms lie along opposite edges of the octahedron (Fig. 4.25).

According to the theoretical results, the meridional isomer, observed in the α- and β-phases of Alq_3, is slightly lower in energy (by $\sim$ 4 - 5 kcal/mol, as reported in [28, 78]). Hence, the facial isomer is the less stable one, but has a larger dipole moment (7.9 D vs. 4.1 D for the *mer*-isomer [117]). Several studies argue for the coexistence of these isomers in amorphous Alq_3 thin films [79, 118]. Moreover, such a coexistence is seen as a factor favoring the stability of the amorphous state itself, which appears to be a prerequisite for good performance and thermal stability of Alq_3-based devices.

Recently Braun et al. [81] reported the existence of a crystalline phase of Alq_3, the δ-phase, showing blueshifted luminescence upon UV excitation. Later, a series of experimental and theoretical results proving that the phase consists of facial Alq_3 molecules has been published [82, 119]. Along with the blueshifted luminescence band, the δ-phase is characterized by a blueshifted excitation edge in the PL absorption spectra, smaller Stokes shift between excitation and emission spectra compared to the *mer*-Alq_3, a simpler Raman IR spectrum (suggesting the higher symmetry of *fac*-Alq_3) [122], and a much lower triplet-state population during luminescence [81].

The δ-phase was observed only in sublimed powders or in films prepared from solutions of these powders. However, up to now no reports of blueshifted luminescence in amorphous Alq_3 films prepared by direct condensation on substrates at room temperature are available.

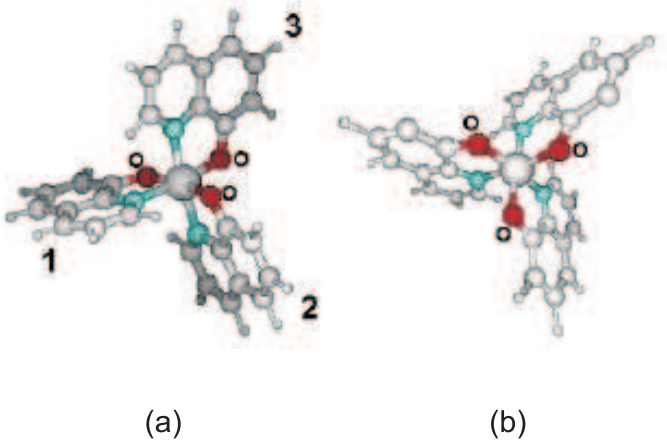

Figure 4.25: (a) Meridional and (b) facial Alq_3 isomers. In the *mer*-Alq_3 1, 2 and 3 denote the three ligands (from [117]).

On the other hand, our previous investigations on VD films of Alq_3 embedded in SiO_2 by co-evaporation [120] and confirmed by Gehlhaar [112], have established that the luminescence maximum shifts to higher energies (see Fig. 4.26). The magnitude of the resulting shift strongly depends on the Alq_3 concentration. We attribute this behavior to the rigid matrix environment of the dye molecules and thermal effects upon matrix condensation. On the basis of the spectral data, we assume that during film growth, a transformation from *mer*- to *fac*-isomer Alq_3 molecules occurs. Therefore, samples at equal Alq_3 concentration, corresponding to single-molecule distribution, but at various matrix evaporation rates and evaporation modes were prepared. Then, the luminescence peak position and intensity as a function of the preparation conditions were studied in order to clarify the origin of the luminescence blue shift, as well as to find technological ways to prevent undesired effects of the matrix on the organic molecules.

Results and discussion

Figure 4.26 depicts the normalized PL emission spectra of mixed films at different Alq_3 concentrations, recorded upon 370 nm UV excitation. The samples are prepared via simultaneous deposition of e-beam SiO_2 and thermally evaporated Alq_3. As a general trend, the PL maximum shifts to higher energies with dilution of Alq_3 in the SiO_2 matrix. For the 0.01 vol% sample, the corresponding shift is 0.28 eV with respect to the pure Alq_3 thin film.

This behavior implies the following possibilities: If one considers the influence of the SiO_2 environment as a dielectric medium, it is reasonable to expect a shift of the PL emission maximum of the mixed layers with respect to the pure Alq_3 film. Amorphous SiO_2 has a static dielectric constant ε of 2.14 [92] and can thus be regarded as a non-polar solvent. In Table 4.1 experimental results about the spectral behavior of Alq_3, dissolved in both polar and non-polar solvents are presented. Accordingly, no obvious relation in band shifts is observed with increasing

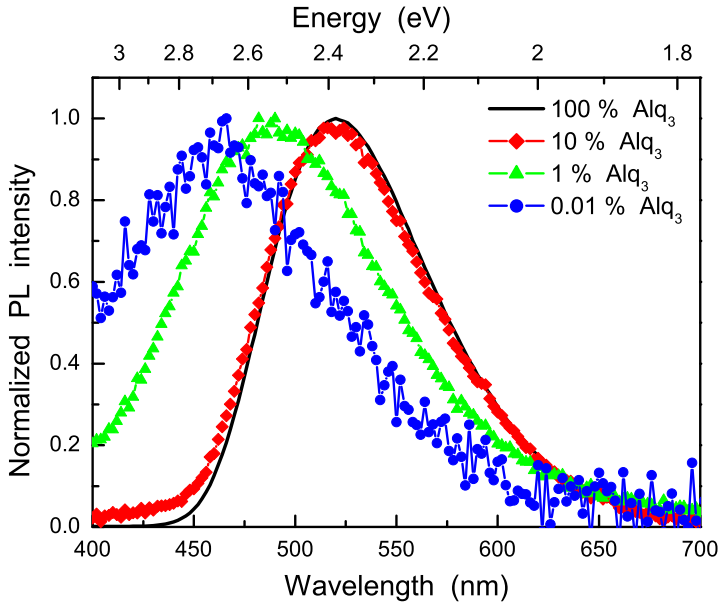

Figure 4.26: Normalized photoluminescence emission spectra of Alq_3 diluted in SiO_2 films at various concentrations for 370 nm excitation.

concentration, but solvents with different polarity lead to changes in both absorption and emission maxima (consistent with results in reference [27]). Depending on the deposition conditions, the reported PL maximum of VD Alq_3 films varies from 520 to 536 nm, thus in solution the emission shifts to the blue by up to 0.1 eV with respect to the Alq_3 film. On the other hand, data reported for a shift of the PL maximum of Alq_3 due to solid state solvent effect have similar magnitude (0.11 eV in [30]). Yet, this is far less than the spectral shift of ~ 0.3 eV which we observed in SiO_2.

Conversely, Cölle and co-workers [82] have shown convincingly that such extremely blueshifted photoluminescence (about 0.2 eV) is characteristic for the high temperature δ-Alq_3 phase, containing facial isomer molecules. For Alq_3 polycrystalline powder, it has also been proven that thermal interconversion between the known Alq_3 phases, respectively between the *mer*- and *fac*-isomers, is possible [83].

Hence, we assume that during the process of co-evaporation, the Alq_3 molecules interact with the SiO_2 particles upon condensation on the substrate, causing an energy transfer. As a consequence, the Alq_3 molecules can experience strong local overheating (thermal stress) leading to formation of *fac*-isomer molecules, i.e. isomer transformation of some of the molecules from *mer*- to *fac*-Alq_3. Further, the SiO_2 matrix as rigid environment supports the conservation of the already condensed *fac*-Alq_3 molecules.

Solvent	polarity	dye concentration mol/l	λ_{abs} (nm)	λ_{exc} (nm)	λ_{emis} (nm)
Chloroform	4.8	10^{-5}	385	380	516
		10^{-4}	386	376	514
THF	7.6	10^{-5}	392	390	528
		10^{-4}	393	388	528
CH_2Cl_2	8.9	10^{-5}	387	386	531
		10^{-4}	387	381	534
DMSO	46.7	10^{-5}		370	516
		$5x10^{-5}$		369	520
		$5x10^{-4}$		370	520

Table 4.1: Positions of the absorption, PL excitation and emission maxima for Alq_3 in various solvents, arranged according to increasing polarity (according to [121]).

As argued in the beginning of this Chapter, in mixed films at guest concentrations around 1 vol% and below, predominantly ensembles of single molecules are formed. Therefore, we interpret the luminescence shift as originating from a mixture of both *mer*- (green luminescent) and *fac*-Alq_3 (blue luminescent) molecules, incorporated in the matrix during film growth. At low dye concentrations, there are two effects: (i) the transferred energy per Alq_3 molecule is higher, thus the probability for *fac*-transformation increases (ii) the matrix becomes denser, which is a prerequisite for conservation of the *fac*-Alq_3 molecules. Hence, the resulting PL shift is more pronounced.

On the basis of these considerations, we examined Alq_3/SiO_2 films at 0.5 vol% Alq_3, embedded in the matrix by different preparation conditions. Figure 4.27 shows the PL emission spectra of mixed films prepared at various SiO_2 effective evaporation rates. These rates correspond to different thermal power of the matrix particles. Thus, the released energy during the condensation of SiO_2 is influenced.

The results show that with decreasing rate, the PL maximum shifts to higher energies, from 2.58 eV to 2.71 eV, and the band broadens significantly. The observed blue shift is associated with a change in the spectral shape, which is less symmetric for the lower evaporation rates. Also, the integral PL intensity increases at the same Alq_3 concentration. This means that, although the samples have equal Alq_3 content, alterations in the preparation conditions strongly influence the optical response of the films.

The changes the organic molecules undergo during co-evaporation can be evaluated by separating the contribution of both Alq_3 isomers on the overall luminescence. For this purpose, we compared the emission of a neat Alq_3 film with that of Alq_3 molecules diluted in the matrix at the above concentration of 0.5 vol%. The thickness of the pure film is 500 Å and the total thickness of the mixed film is 10 μm, respectively. This corresponds to an equal dye quantity in both layers. For the δ-phase of Alq_3, containing the facial isomer, the PL excitation spectra show a

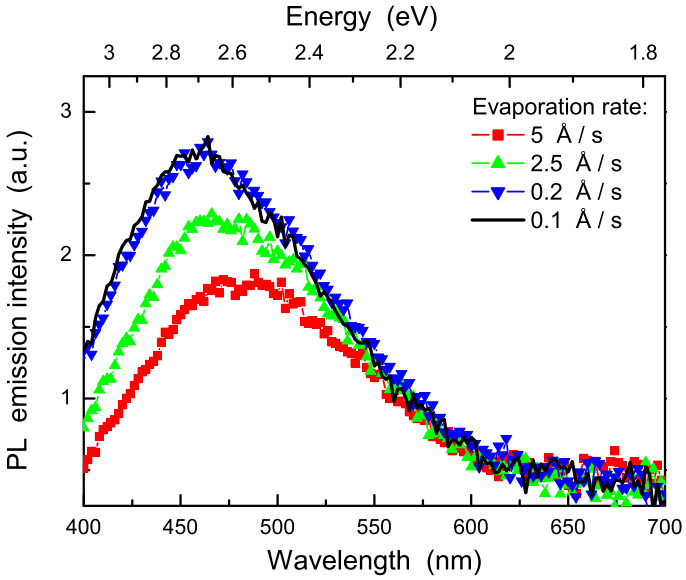

Figure 4.27: PL emission spectra of 0.5 vol% Alq_3 in SiO_2 thin films at various matrix evaporation rates; excitation wavelength 370 nm. The total thickness of the samples is 2000 Å.

sharp excitation edge at 426 nm [81]. Thus, the PL emission spectra are recorded using excitation at 370 nm and 440 nm (above the referred excitation edge). The excitation spectra were recorded at detection wavelengths 530 nm and 470 nm, which are the characteristic peak positions of the blue and green luminescent Alq_3. The corresponding results are presented in Fig. 4.28.

The absorption bands of the pure Alq_3 film are located at 3.69 eV (336 nm) and 3.15 eV (393 nm). For comparison, in solution (i.e. *mer*-Alq_3) a broad and intense absorption band of Alq_3 has maximum between 370 and 390 nm (cf. Table 4.1). Additionally, as in thin film, there is a weak absorption band located at 333 nm. In this respect, a theoretical evaluation [119] predicts for both Alq_3 isomers nine low energy bands, overlapped to produce a rather broad feature. The excitation values for the meridional isomer are computed to be between 379 and 417 nm, those having greater oscillator strength are positioned at 394, 417 and 427 nm. In contrast, for the *fac*-isomer, the most intense computed excitation is located at 429 nm (oscillator strength $f = 0.0588$; for details see [119]). On the other hand, the PL excitation spectra of the mixed film show no distinctive bands. A peak analysis gives 3.69 eV as a possible center of absorption band. However, this has to be assumed only as a tentative figure, related to the mixed system as such. Although the matrix absorbs only slightly in the spectral range of the dye, to resolve the contribution of both species is not trivial, since the exact position of the base line is not known.

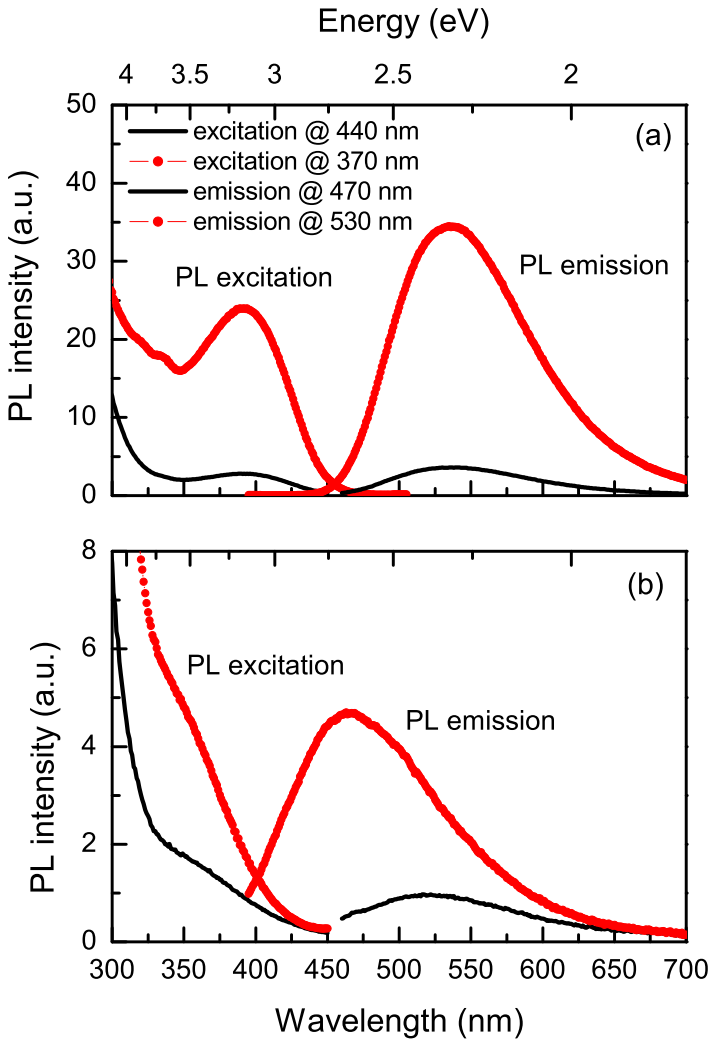

Figure 4.28: Photoluminescence excitation and emission spectra of (a) pure Alq_3 and (b) mixed 0.5 vol% Alq_3/SiO_2 films. Emission spectra are recorded by using excitation at 370 nm and 440 nm. Excitation spectra are recorded at detection wavelengths of 470 nm and 530 nm. All measurements are carried out at RT.

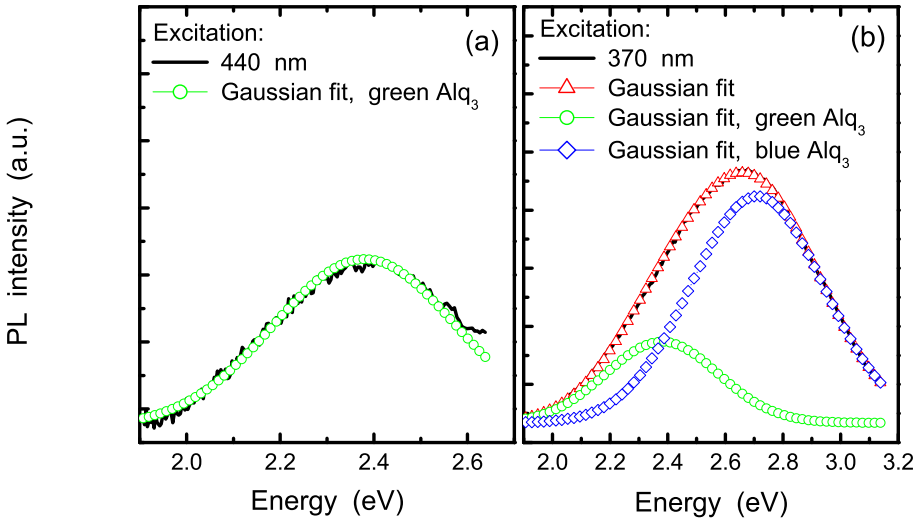

Figure 4.29: Gaussian fits of the PL emission spectra of 0.5 vol% Alq_3/SiO_2 film for (a) 440 nm and (b) 370 nm excitation.

The PL emission spectra of the pure Alq_3 sample are characterized by a broad band, with maximum at 536 nm (2.31 eV). While the spectral position of the PL maximum of the pure film is independent of the excitation wavelength, the peak position of the Alq_3/SiO_2 film significantly depends on the excitation wavelength: There is a shift of the PL maximum between 465 nm (2.67 eV) at 370 nm excitation and 520 nm (2.38 eV) at 440 nm excitation, respectively. Thereby, the emission spectra obtained at different excitation wavelengths denote the existence of two different species. Consequently, the luminescence of the mixed film could be described as consisting of green and blue luminescent components. The shift of the PL maximum of the mixed Alq_3/SiO_2 film in dependence on the excitation wavelength is used to evaluate the contribution of these components on the overall luminescence. A peak position of 2.377 eV and a FWHM of 0.389 eV corresponding to green luminescent Alq_3 molecules are obtained by fitting the emission spectrum for excitation at 440 nm with a Gaussian centered at the most apparent spectral feature (Fig. 4.29a). These data are substituted in another fitting procedure to which the emission spectrum at excitation 370 nm was subjected. Thus, a peak position of 2.715 eV and a FWHM of 0.458 eV for the blue luminescent Alq_3 are defined (Fig. 4.29b).

The described approach is applied to the emission spectra of the samples prepared at different evaporation rates of the SiO_2 matrix. From the fits, the PL integral intensities I_{gr} (green) and I_{bl} (blue), corresponding to both components were inferred. The results for the peak positions, band widths (FWHM) derived from the fitting are listed in Table 4.2 and presented in Fig. 4.30.

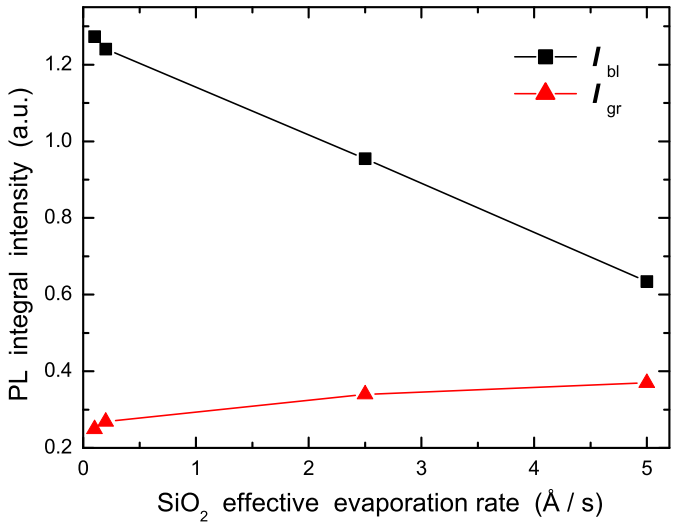

Figure 4.30: Relative intensities of the blue I_{bl} and green I_{gr} luminescent components of 0.5 vol% Alq_3/SiO_2 films in dependence on the matrix evaporation rate.

v_d (Å/s)	5	2.5	0.2	0.1
E_{gmax} (eV)	2.377	2.369	2.372	2.370
$FWHM_g$ (eV)	0.386	0.376	0.401	0.380
E_{blmax} (eV)	2.716	2.721	2.718	2.720
$FWHM_{bl}$ (eV)	0.459	0.463	0.463	0.461

Table 4.2: Spectral positions and band widths of the blue and green luminescent Alq_3 components in the fluorescence spectra of mixed 0.5 vol% Alq_3/SiO_2 samples in dependence on the matrix evaporation rate.

Accordingly, by decreasing the matrix evaporation rate, it is possible to obtain mixed films with enhanced contribution of blue luminescent Alq_3 species. The increased overall PL efficiency further confirms the presence of more blue luminescent molecules, since, as referred in [83], the blue-luminescent Alq_3 has higher PL quantum efficiency.

We explain the increased blue luminescence at low SiO_2 evaporation rates by the influence of the matrix structural properties on the organic molecules. The inorganic matrix in composite films represents a rigid environment for the dye molecules. Structural investigations of pure SiO_2 films have shown that their quality strongly depends on the energy of the impinging particles. When the latter have low energy (i.e. at low evaporation rates), fewer nuclei are produced, but they have limited mobility. The probability for the film to preserve its initial structure is higher. Thus, the obtained film is denser and has less structural defects in comparison to layers at higher energy of the matrix particles. A rigid matrix with such properties could easily assist the preservation of the already condensed facial Alq_3 molecules, restricting the possibility for their conversion in the energetically more stable meridional isomer.

In Ref. [122], Cölle et al. have reported results from a vibrational analysis of the two crystalline phases of Alq_3 - α-Alq_3 and δ-Alq_3. They have found significant differences in the IR spectra of the two phases, explaining them in terms of the different symmetries of the facial and meridional isomer. The δ-phase IR spectrum shows less features, thus indicating the higher symmetry of the facial isomer. So, in order to prove the presence of *fac*-isomer Alq_3, mixed layers were subjected to FTIR spectroscopy. For that reason, samples of 0.5 vol% Alq_3 diluted in 10 μm SiO_2 on KBr pellets were prepared. The thicknesses of the pure Alq_3 reference layer were 500 Å. Unfortunately, at this low dye content it was impossible to obtain significant IR signal from the mixed layers and to obtain information about the isomerism of Alq_3 in the SiO_2 matrix.

As a way to reduce thermal energy interactions between matrix and dye molecules, we further applied a layer-by-layer approach. Experiments with separate condensation of SiO_2 and Alq_3 were carried out. This was achieved by varying the aperture in the rotating disk for the layer-by-layer evaporation, starting from 360° (equal to co-evaporation) through 36° to 18°. It corresponds to alteration of the time for condensation between the successive dye and matrix sublayers on the substrate from 0 up to 0.45 seconds. The recorded photoluminescence of two samples at 0.5 vol% Alq_3 in SiO_2, obtained by separate (18° disk aperture) and co-evaporation are presented in Fig. 4.31. A comparison shows that the PL maximum is still shifted to higher energies and the PL intensity is higher, even when both materials condense separately in time. Thus, although the time between the encounter of molecules of two successive dye and matrix sublayers can be affected, for the experimental set-up used, layer-by-layer mode could not inhibit energy interactions between matrix and Alq_3 molecules. Additionally, the results demonstrate that the improved matrix rigidity and isolation of monomers in the initial state, ensured by the layer-by-layer mode, are the more important effects for obtaining *fac*-Alq_3 molecules.

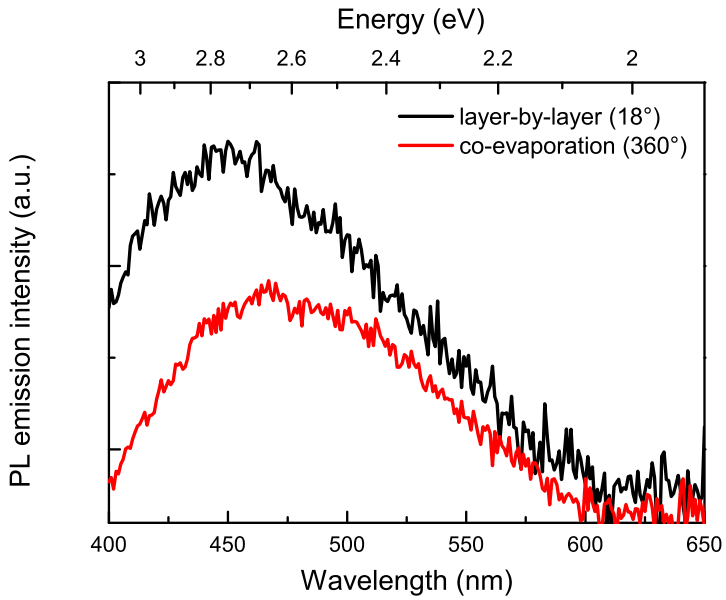

Figure 4.31: PL emission spectra of 0.5 vol% Alq_3 in SiO_2 films (1000 Å total film thickness) deposited by co- and layer-by-layer evaporation modes. The evaporation rate of the SiO_2 is 1 Å/s. Spectra are recorded at 370 nm excitation wavelength.

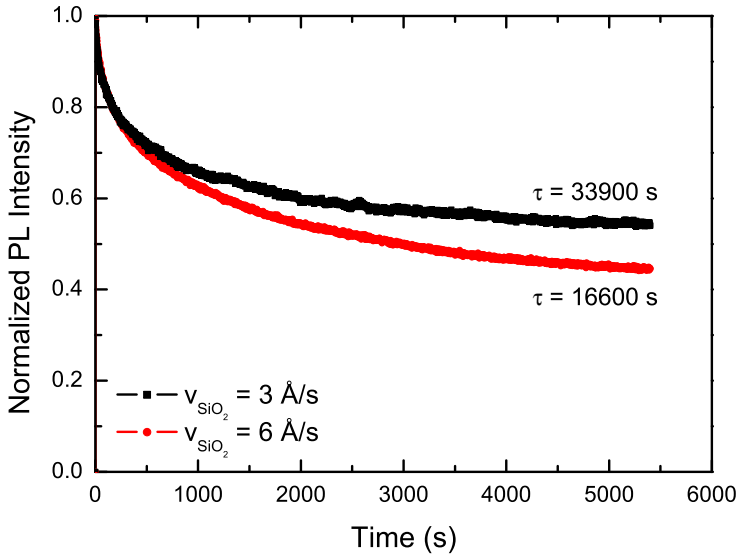

Figure 4.32: Time dependence of the peak luminescence intensity for mixed Alq_3/SiO_2 samples at 0.5 vol% dye concentration, grown at different matrix deposition rate.

We performed photostability measurements which indirectly confirm the above considerations about the growth morphology of the SiO_2 matrix. Figure 4.32 presents the evolution of the peak luminescence intensity of Alq_3/SiO_2 samples in time upon photoexcitation by cw-HeCd laser light at 442 nm. The irradiation intensity is 3.82 W/cm^2. Both samples have equal dye concentration, but are grown at low and high matrix evaporation rate. The decay behavior of the PL intensity is similar to the one observed for mixed $MePTCDI/SiO_2$ or $PTCDA/SiO_2$ layers, characterized by a steep initial region, followed by a slower decay. The evolution of the curves can be associated with the heterogeneous environment of Alq_3 molecules within the SiO_2 matrix. Molecules can be located in open pores or defects, or trapped in a dense matrix environment. Dye molecules located in open pores degrade fast, while Alq_3 molecules immobilized in the matrix take much longer to be bleached. For the region after the fast decay in the beginning, an exponential decay law can be used:

$$I_F(t) = A \exp(-t/\tau). \tag{4.4}$$

The defined time constants differ by a factor 2 in favor of the sample grown at lower matrix evaporation rate (3.4 x 10^4 s vs. 1.7 x 10^4 s). The relative decrease in the PL integral intensity due to the irradiation is 24 % for the sample grown at 3 Å/s, compared to 46 % for the sample grown at 6 Å/s SiO_2 evaporation rate. Hence, the microstructure of the host has to be considered as a crucial factor for the photostability of the system. A dense and homogeneous matrix represents

a favorable environment, since dye molecules located within matrix pores or in regions with structural defects are more accessible for the influence of oxygen. In contrast, molecules trapped in a dense host environment have less vibrational and translational modes of excitation, and therefore should be less susceptible to photodegradation.

Summary

To summarize, we established a blue shift of the PL maximum corresponding to isolated Alq_3 molecules in a SiO_2 matrix. At a given guest to host volume ratio, the PL intensity depends strongly on the matrix evaporation rate. Increased PL efficiency is obtained at lower evaporation rates. We explain these effects as a result of the formation of *fac*-Alq_3 molecules. Two parameters influence the presence of facial molecules: First, local heating of Alq_3 molecules during film growth causes meridional to facial isomer transformation. Second, the rigid matrix supports the conservation of the already transformed *fac*-Alq_3 molecules.

Furthermore, we demonstrated that the variation of the deposition conditions can be used as an effective way to obtain mixed layers with increased contribution of blue compared to green luminescence, if films with this quality are beneficial for practical applications. The increased contribution of facial Alq_3 molecules in the layer-by-layer grown films is explained by the improved rigidity of the matrix environment and the more homogeneous isolation of monomers. The result is thus in accordance with the established findings for the perylene derivatives MePTCDI and PTCDA embedded in SiO_2.

We have shown that at lower evaporation rates, the matrix grows with reduced porosity, consequently favoring the photostability of embedded organic molecules.

Again, the results of films of Alq_3 diluted in SiO_2 back the assumption of thermal stress upon the organic molecules during their incorporation in the inorganic matrix. As noted in the beginning, such an effect could lead in general to unwelcome modifications of the initial molecules, manifesting themselves in decreased PL efficiency or even in loss of luminescence properties.

4.1.4 2,2-Difluoro-1,3,2-dioxaborine derivatives

Until now, comprehensive studies on the luminescence of liquid solutions or crystals of 2,2-difluoro-1,3,2-dioxaborine derivatives have been reported. In this Section, we present first results on the optical response of solid solutions of these compounds. They are known to build crystalline structures in the solid state, hence it is reasonable to expect an alteration in spectral behavior upon incorporation of the molecules in the rigid SiO_2 matrix. On the other hand, in solution, the 2,2-difluoro-1,3,2-dioxaborines absorb in the blue-green spectral region and exhibit relatively large Stokes shift. So, the latter properties in combination with the mechanical and chemical stability of the matrix could be in addition favorable for application of the mixed layers in luminescence conversion devices (more details about the LUCO principle will be presented in Chapter 6).

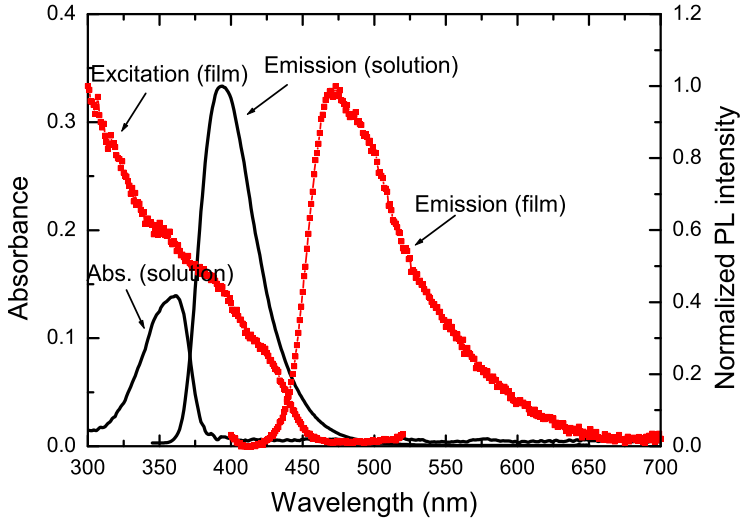

Figure 4.33: Absorption, PL excitation and emission spectra of GG277 in solution and in thin film. Emission spectra are recorded at 325 nm (solution) and 350 nm (film) excitation wavelength. PL excitation spectrum of the thin film is recorded at 540 nm detection wavelength.

The 2,2-difluoro-1,3,2-dioxaborine dyes GG277, GG274, and GG142B were embedded in the SiO_2 matrix at concentrations from 0.5 to 3 vol%. The absorption and luminescence properties of the dyes in the mixed films were compared with the corresponding in solution and of neat dye film. Figures 4.33, 4.34, and 4.35 present the absorption and emission spectra of the dyes, dissolved in chlorobenzene, and of the VD thin films. The results for the absorption and emission maxima for all GG-dyes in both systems are summarized in Table 4.3.

In general, the absorption and luminescence spectra display mirror symmetry. As chlorobenzene is a solvent with a relatively low polarity, the absorption and emission peak positions of GG277 in solution are similar to the reported for the dye, dissolved in CH_2Cl_2 [86]. The GG274 dye in solution, where the rotation of the phenyl ring is blocked, absorbs in the same spectral range as GG277, however the absorption band is much broader and is more structured, with separate absorption band located at 323 nm. The emission maximum is red-shifted by about 28 nm. On the other hand, the GG142B solution is characterized by the smallest Stokes shift - only 21 nm compared to 31 nm for GG277 and 60 nm for GG274. However, these values are quite large compared to the Stokes shift for the perylene derivatives MePTCDI and PTCDA already presented, where the shift amounts to $\sim$ 11 nm.

Measurements of the PL quantum yield of the molecules in solution [86, 89] show that GG274 is most efficient with ϕ_{PL} between 0.74 - 0.84, whereas for the unbridged molecules, ϕ_{PL} amounts up to 0.39 in slightly polar solvents. The

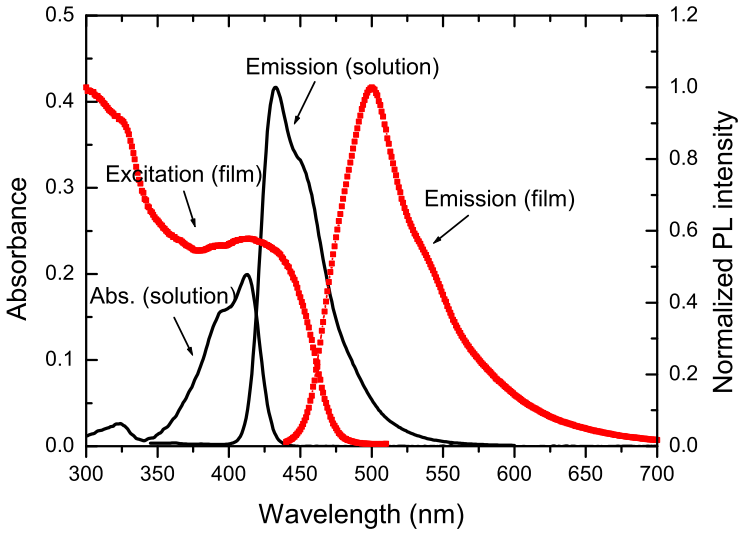

Figure 4.34: Absorption, PL excitation and emission spectra of GG142b in solution and in thin film. Emission spectra are recorded at 325 nm (solution) and 410 nm (film) excitation wavelength. PL excitation spectrum of the thin film is recorded at 530 nm detection wavelength.

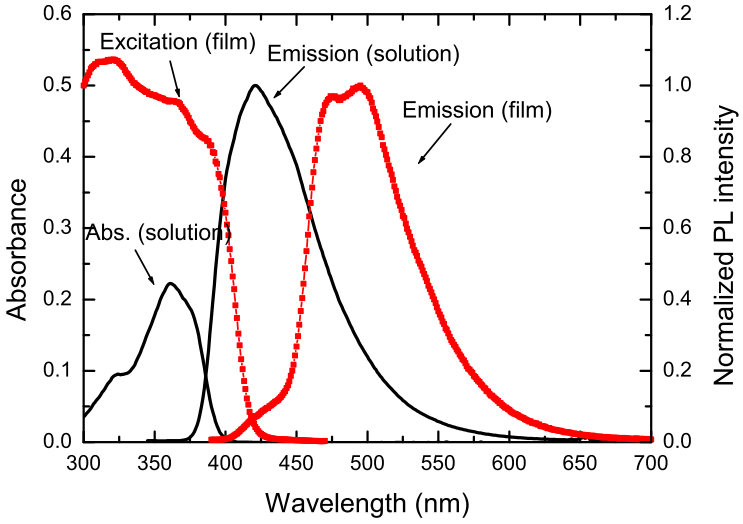

Figure 4.35: Absorption, PL excitation and emission spectra of GG274 in solution and in thin film. Emission spectra are recorded at 325 nm (solution) and 370 nm (film) excitation wavelength. PL excitation spectrum of the thin film is recorded at 500 nm detection wavelength.

Dye	λ_{max} (nm)	chlorobenzene	solid state
GG277	λ_{abs}	362	352, 385, 417
	λ_{emis}	393	473, 497^s, 529^s
GG142B	λ_{abs}	323, 394, 412	324, 388, 412
	λ_{emis}	433, 449	500, 531^s
GG274	λ_{abs}	323, 361, 376^s	321, 367, 388
	λ_{emis}	421	440^s, 475, 494

Table 4.3: Positions of the absorption, PL excitation, and PL emission maxima for the GG-dyes in solution and in thin film (s denotes shoulder).

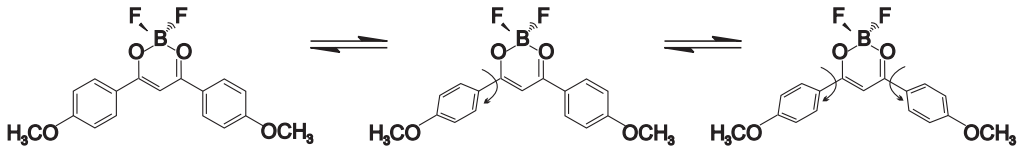

Figure 4.36: Formation of rotamers in GG142B.

increased efficiency of the bridged molecule is attributed to the fixed position of the substituent. The internal rotation around a single bond, as in GG277 and GG142B, leads to dissipation of the excited-state energy. Thus, the formation of rotamers with different position of the phenyl rings relatively to the plane of the diketonate cycle (see Figure 4.36), is established to represent a significant non-radiative deactivation channel [123, 124].

At first glance, the VD GG-dyes thin films are rather crystalline, characterized by strong opalescence. AFM studies confirm that the films have micro-crystalline structure (Fig. 4.37). The lateral crystallite dimensions are of the order of 500 - 1000 nm. There is no preferential orientation of the crystallites visible in the AFM images.

In contrast to the dissolved molecules, the absorption of the thin solid films of GG-dyes is characterized by broad bands, the most structured one being that of GG142B. At the same time, a close comparison with the solution spectra shows that the monomer absorption peaks can be distinguished in the thin film spectra. In addition, the band edges are shifted to longer wavelengths, compared to the dissolved molecules. The thin film luminescence is red shifted by 67 to 80 nm with respect to the monomer emission, and is quite intense. Still, on the low-energy side of the GG274 thin film emission, the contribution of the monomers can be identified. As presented in the experimental section of the thesis, in the crystal lattice of GG277 and GG142B the molecules are planar and stacked in parallel planes, separated in out-of-plane direction by only $\sim$ 3.5 Å [87]. Also, two close molecules are oriented along opposite directions. Thus, the bathochromic shift is attributed to transitions with a charge transfer character, involving two molecules lying in neighboring parallel planes. Here, the aryl group of each molecule acts as an electron donor to the dioxaborine moiety of the other molecule. On the other

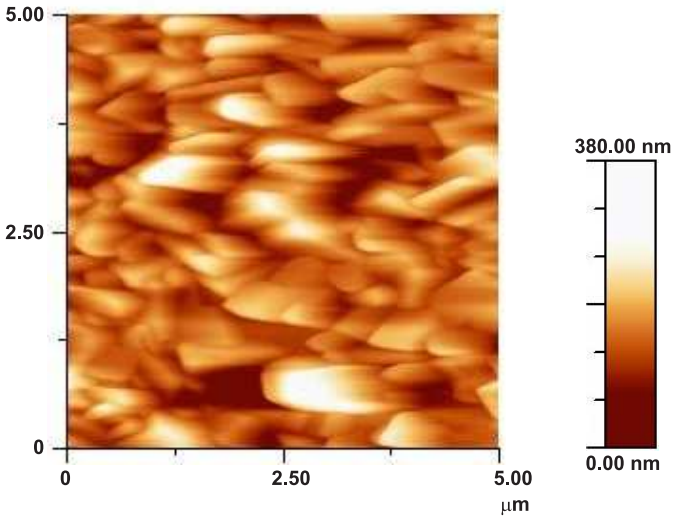

Figure 4.37: AFM image of vacuum deposited pure GG142B film on glass substrate (image section: 5.00 x 5.00 μm). The film thickness is 4000 Å.

hand, there is no thorough information about the crystal structure of GG274. However, taking into account the nearly planar structure of the molecule and the resemblances to the arrangement of the molecules in the crystal lattice of ABMBF and DBMBF and their derivatives [89, 125], one cannot exclude the formation of charge-transfer states as well. Figures 4.38, 4.39, and 4.40 display results from PL excitation and emission measurements of GG-dyes distributed in SiO_2 matrix. At this film thickness and dilution range, it was possible to obtain reliable optical absorption spectra only of the mixed layers at the highest dye concentration. However, as argued in the experimental section, both spectra are quite identical as can be seen from the spectra in Fig. 4.41.

The luminescence spectra of the mixed layers follow the tendencies established for the embedded perylene derivatives. Spectral shape and peak positions of the excitation spectra only insignificantly depend on dye concentration, showing a slight broadening and red shift by a few nanometers. In comparison to solutions, the absorption maxima of the deposited films are located at similar wavelengths, however shifted to lower energies by up to 4 nm. The peakwidths for GG277 and GG274 are only somewhat larger with respect to the monomer absorptions, while for GG142B the broadening is more pronounced and individual features can not be resolved. The latter can be indicative for a higher degree of interaction between matrix and dye. The GG142B molecule comprises two phenyl rings attached to the diketonate ring. If one considers the rigidity of the host and the smaller dimensions of the host particles with respect to the incorporated dye molecules, the SiO_2 particles could effectively fill the spaces around the ligands during the condensation process. Hence, the altered environment could lead to an energetic modification of the excited state. Additionally, the PL excitation spectra of the mixed samples at concentrations 2 vol% and below exhibit only weak dependence

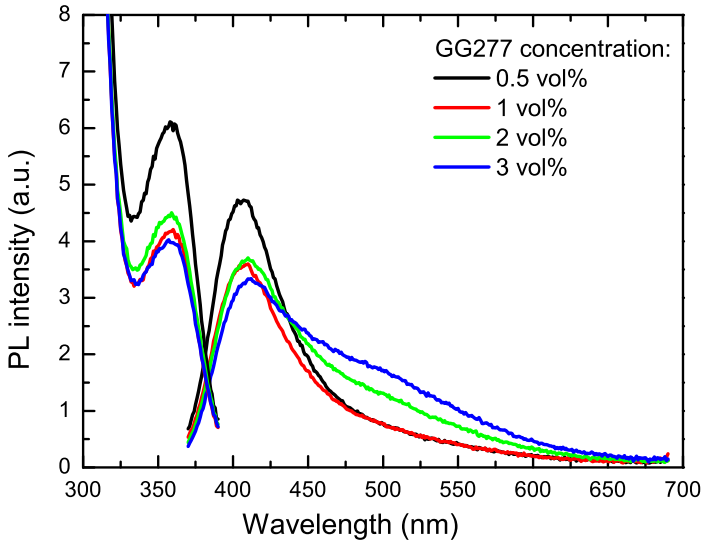

Figure 4.38: PL excitation and emission spectra of GG277 dye diluted in SiO_2 matrix. Emission is recorded for 350 nm excitation, whereas PL excitation spectra are recorded at 415 nm detection wavelength. The total film thickness is 1000 Å.

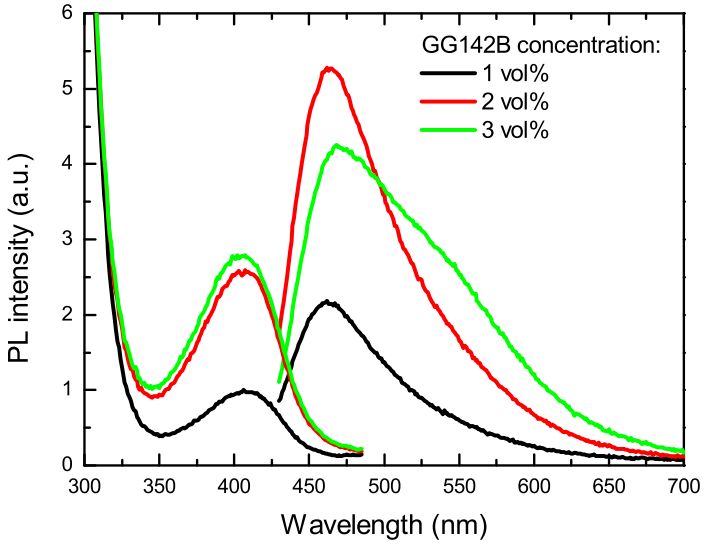

Figure 4.39: PL excitation and emission spectra of GG142B dye incorporated in SiO_2 matrix. Emission is recorded for 410 nm excitation wavelength. PL excitation spectra are recorded at 505 nm detection wavelength. The total film thickness is 1000 Å.

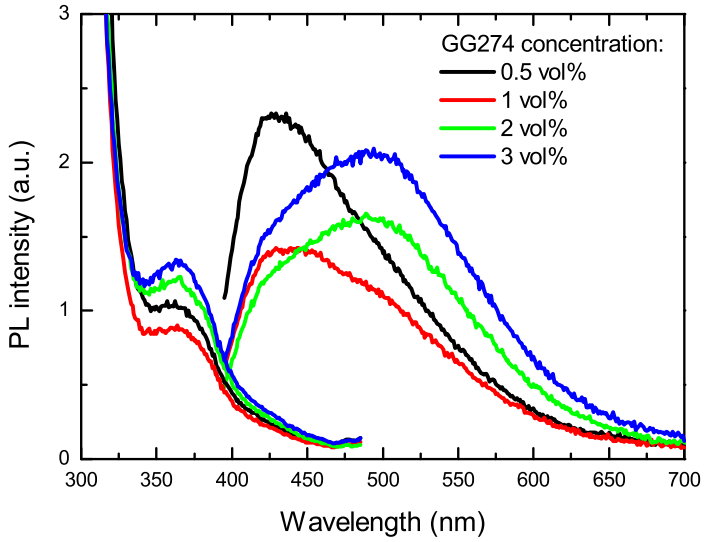

Figure 4.40: PL excitation and emission spectra of GG274 dye diluted in SiO_2 matrix. The films are excited by 370 nm wavelength, the emission detection wavelength for the PL excitation spectra is 505 nm. The total film thickness is 1000 Å.

on the emission detection wavelength, revealed again in minor spectral broadening upon detection at longer emission wavelengths (see Fig. 4.42). This observation suggests a low degree of intermolecular interactions.

Upon increasing dye quantity, the emission spectra undergo significant changes in both shape and intensity. The peak positions are located at higher wavelengths than in solution. In general, the Stokes shift between absorption and emission is dye dependent, the largest one is obtained for mixed GG274/SiO_2 layers (e.g., 64 nm at 0.5 vol%). Comparison between the luminescence of the dye molecules dissolved and incorporated within the matrix indicates that the emission of the most diluted samples originates from excited states with similar geometry as the ground state. However, upon increasing concentration, additional bands at longer wavelengths appear and gain intensity. The spectral shape of the mixed GG274/SiO_2 layers changes most dramatically. Since the absorption of the embedded dyes is similar to that of the dissolved dyes, we assign the low energy bands in the emission spectra to excited dimers, formed by the association of ground-state and excited molecules.

Figure 4.43 presents the integral luminescence intensity of the mixed layers as a function of dye concentration. Because the spectra are normalized for equal dye quantity, they could be regarded as a measure of the luminescence efficiency. Accordingly, for all dyes dilution in the SiO_2 matrix leads to increased efficiency. The lowest efficiency of the mixed GG274/SiO_2 films is easy to comprehend according

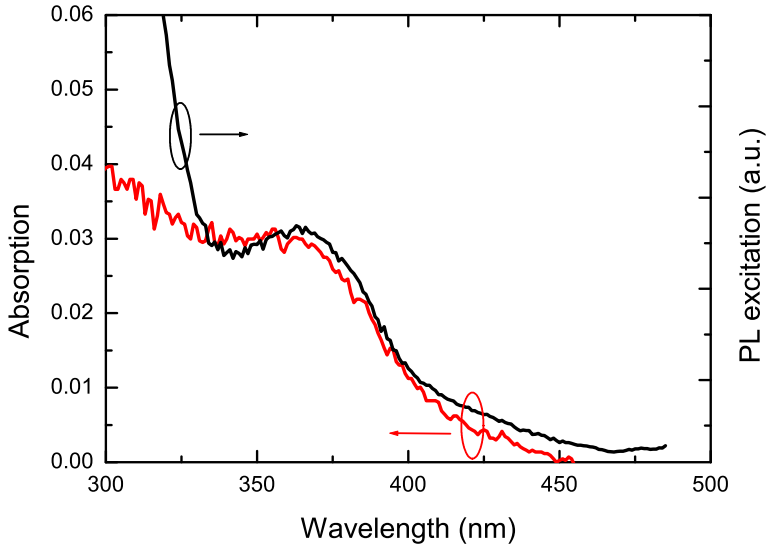

Figure 4.41: Comparison between the absorption and PL excitation spectra of GG274 dye diluted at 3 vol% in SiO_2 matrix.

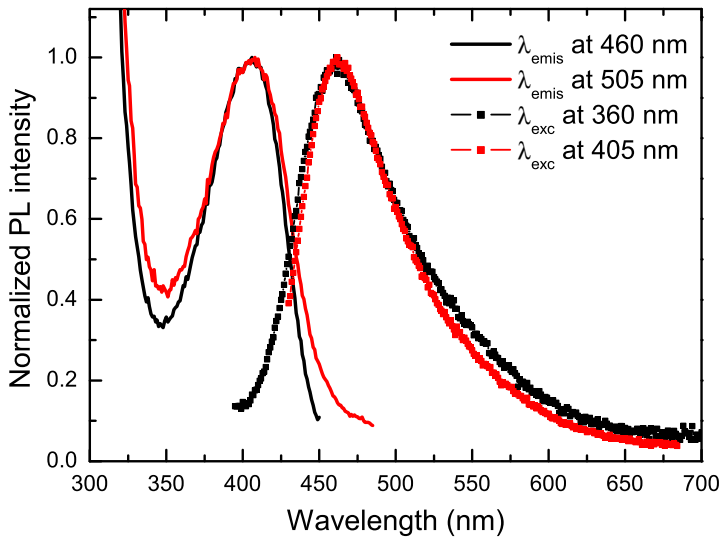

Figure 4.42: Normalized PL excitation and emission spectra of GG142B dye diluted at 2 vol% in SiO_2 matrix in dependence on the detection excitation and emission wavelengths.

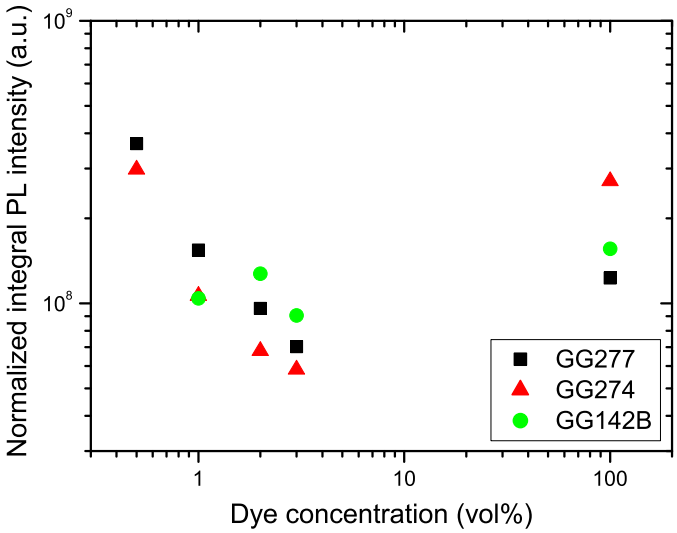

Figure 4.43: Normalized to equal dye quantity integral luminescence intensity of the GG-dye diluted in SiO_2 matrix as function of concentration.

to the observed emission spectra. This behavior is expected, considering the polycrystalline character of the pure GG-films, and is in agreement with the established one for embedded MePTCDI molecules. In contrast, however, the incorporation of GG-molecules in the matrix results in higher luminescence efficiencies with respect to the pure VD dye films only for concentrations $\leq$ 1 vol%. Following the deposition procedure described in Section 4.1.2, it was possible to obtain mixed GG-dye/SiO_2 films of micrometer thickness and to define absolute values of the luminescence quantum yield. ϕ_{ext} is in the range 0.05 to 0.13 depending on the dye, the highest efficiency showing GG142B/SiO_2 films.

Such results could be partly due to the low thermal stability of the studied GG-dyes. For GG277 and GG274, typical evaporation rates of 0.2 - 0.4 Å/s are obtained at relatively low temperatures in the range 90°C - 110°C. The GG142B dye makes an exception with 190°C - 200°C sublimation temperature. If we consider the influence of the thermal stress upon condensation, the presence of only a small number of destroyed dye molecules will lead to luminescence losses, even at low concentrations, where the intermolecular energy transfer is inhibited. On the other hand, in comparison to the perylene derivatives, the overlap between molecules of neighboring layers in the stack is smaller. Hence, the intermolecular interactions should have less influence on the efficiency of the pure layers and the transition to monomers should not lead to as considerable alterations in the luminescence efficiency as in the case of, e.g., MePTCDI.

4.2 Organic dyes dispersed in polyimide matrix

4.2.1 Neat polyimide films

A suitable candidate for a matrix material allowing softer condensation conditions for the dye molecules during their incorporation is polyimide. In recent years, aromatic polyimides have attracted enormous interest for optoelectronic applications. There are various studies demonstrating that PI could be quite successfully used as a hole transport or light emitting material [126]. The synthesized PI light emitting materials can contain perylene or fluorine moieties [54, 93, 127, 128, 129, 139]. Investigations of PI films doped with dyes, metal-organic compounds, or metal oxides show that they are a feasible matrix for organic electroluminescence devices [53], active layers in microcavities [130], etc.

Concerning the present study, PI is also an organic material, which makes it compatible with the organic dyes to be embedded. The evaporation temperature of the initial monomers PMDA and ODA is between 140°C and 180°C. The necessary thermal treatment of the monomer mixture in order to obtain the final PI matrix is usually carried out at temperatures in the range 170°C - 300°C. This temperature interval is considerably lower or of identical magnitude compared to the mean evaporation temperatures of the used dyes (e.g. 300°C - 350°C for MePTCDI, 200°C - 250°C for Alq_3 depending on the evaporation rate).

Before going into a more detailed discussion about the luminescent properties of dye-doped PI films, we first present results regarding the structural and optical features of the neat matrix layers.

All films obtained by VDP exhibit good adhesion over the whole area of the substrate. The as-grown layers are optically transparent and homogeneous. The thermally treated PI films are also transparent, however slightly yellowish-brown. This additional coloration usually accompanies the transformation of the initial monomers to polyimide. No opalescence, typical for the excess of ODA in the cured films, is observed. The latter indicates the stoichiometric composition (ODA:PMDA = 1:1) of the PI films.

An overview of literature shows that the degree of imidization is a decisive factor for the quality of the obtained PI films. This parameter is connected to the percentage of the participated in the chemical reaction initial monomers and is determined from FTIR measurements. Generally, the imidization is followed by disappearance of the anhydride peaks, positioned at 1860, 1806 or 1770 cm^{-1} for PMDA, in the IR spectra [132]. Additionally, the imidization degree is determined by comparing the absorption of the imide groups at 1380 cm^{-1} or 1776 cm^{-1} with that of phenyl groups at 1500 cm^{-1} as a standard [133], or by normalizing the ratio of the imide band area at 1776 cm^{-1} to a reference band area at 1012 cm^{-1}, which originates from invariant aromatic vibration [134].

However, the degree of imidization depends strongly on the thermal treatment conditions, as evident from the summarized results in Table 4.4 (for additional data see also [134]). The PI films subjected to prolonged thermal treatment at lower temperatures contain more unreacted material and are characterized by lower micro hardness values, while a higher temperature at the second stage of

Film thickness (μm)	Thermal treatment	Degree of imidization (%)
1	30min/175°C + 30min/300°C (dry N_2)	> 30 - 50[131]
1	6h/170°C (air)	36.8[26]
1	1h/170°C + 1h/250°C (air)	40.2[26]
1	1h/170°C + 1h/350°C (air)	63.4[26]

Table 4.4: Imidization degree of PI films as function of thermal treatment conditions. Data are taken from Refs. [26, 131].

IR band (cm^{-1})	Absorption band
1116	Imide III $(OC)_2NC$
1378	Imide II C-N stretch
1500	Aromatic C=C stretch
1660	Amide I C=O stretch
1722	Imide I asym. C=O stretch
1775	Imide I sym. C=O stretch
1860	Asym. C=O stretch (anhydride)

Table 4.5: Assignment of the major peaks in the FTIR spectrum of the thermally treated 5000 Å PI film (data from [136]).

the curing process determines lower values of the relative dielectric constant ε_r of the films [135].

For the FTIR spectroscopy study, we prepared neat matrix samples at 5000 Å thickness on KBr pellets. The as-grown films were thermally treated in order to follow the behavior of the initial monomers upon heating. Figure 4.44 presents the corresponding FTIR spectra of an as-grown film and a film, cured for one hour at 180°C, followed by 1 hour at 250°C. The major spectral features are summarized in Table 4.5. The assignment of the peaks is based on Ref. [136]. It can be seen that the thermally treated film shows pure imide peaks (at 1775.13; 1722.06 and 1378.68 cm^{-1}) and no anhydride peaks. This result further evinces the stoichiometric composition of the samples. On the other hand, the absence of absorption bands around 1660 and 1550 cm^{-1}, which are indicative for the presence of secondary amide of the polyamic acid (-CO-NHR-) reveals that the polyamic acid has disappeared upon curing. The imide band at 1380 cm^{-1} has been used to determine the degree of imidization. Peak height and area were normalized to those of the band at 1500 cm^{-1}, which is assumed to remain unchanged during the polycondensation reaction [137]. Thus, the evaluated imidization degree for the studied neat sample is 38.2 %. The value agrees well with the corresponding data in Table 4.4 and points at a good quality of our PI films.

Absorption spectra of PI films in dependence on the curing temperature are presented in Fig. 4.45. The absorbance of the as-deposited film, which represents

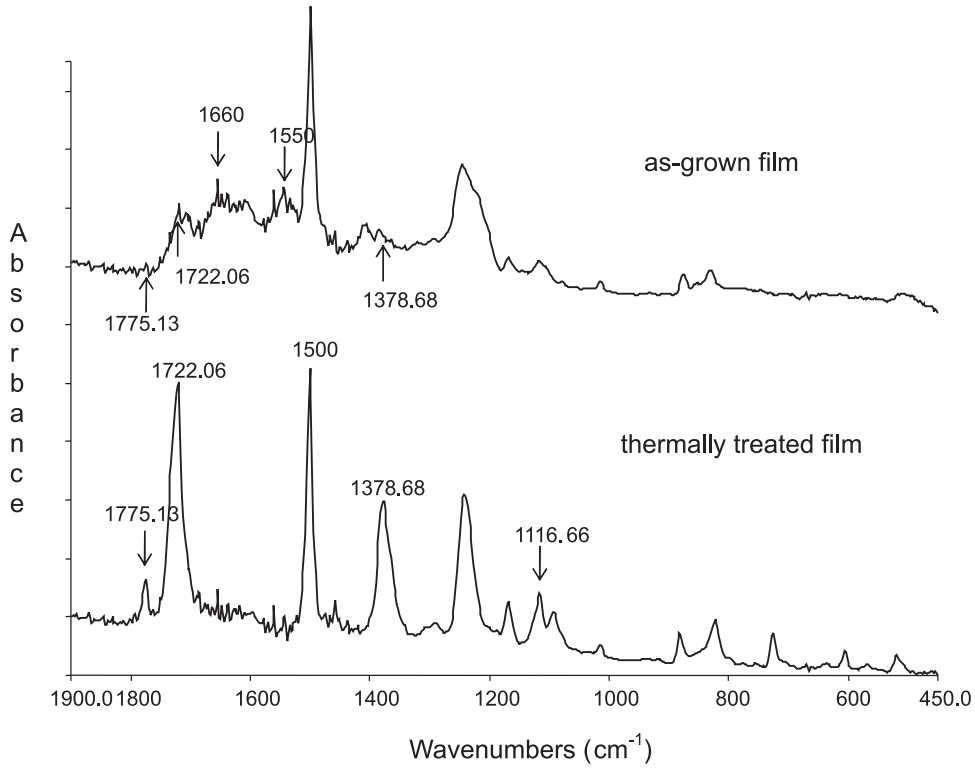

Figure 4.44: FTIR spectra of PI films: as-grown and thermally treated (1 h at 180°C, followed by 1 h at 250°C); film thickness 5000 Å. An assignment of the peaks is given in Table 4.5.

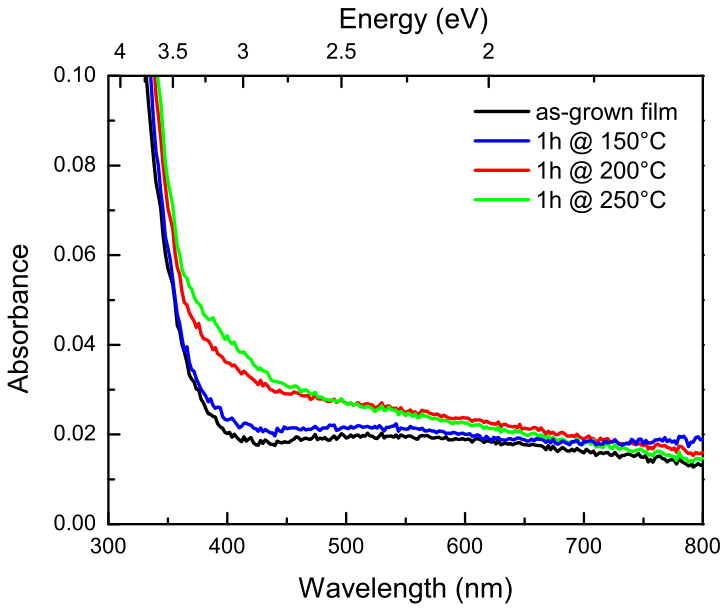

Figure 4.45: Absorption spectra of neat PI films cured at different temperatures.

a mixture of the initial monomers PMDA and ODA, is given for comparison. It is evident from the spectra that there is no absorption feature in the spectral range from 400 to 800 nm. Upon curing, substantial changes in absorption do not appear until temperatures above 150°C. The broad absorption band at 360 nm of the films cured at 200°C and 250°C is indicative for the formation of polyimide. Published data confirm that the imidization process starts at temperatures of about 150°C - 175°C [134, 138].

Upon heating above 200°C - 210°C, the polycondensation reaction between PMDA and ODA is accompanied by shrinkage of the film thickness [26, 134, 138]. The effect is due to dehydration process, and exists for films cast from solution to solvent evaporation as well [153]. For the PI films used in this study, we defined the contraction comparing the transmittance and reflectance spectra of cured and as-grown films. Due to curing, the films contract by about 15 % to 20 %, which corresponds to values reported for vacuum deposited PI films [26, 134].

The optical spectra of all investigated samples were recorded with unpolarized light, as introduced in the experimental Chapter of the work. For PI films, though, it is known that they are characterized by intrinsic birefringence. This holds true for both films cast from solution and vacuum deposited films. Extensive optical studies have shown that the aromatic rings within the PI backbone contribute essentially to the refractive index, thus the anisotropy in polymer chain orientation is dominant factor for the appearance of the birefringence [131]. In literature, the obtained birefringence for PMDA - ODA polyimide varies from 0.34 [94] to 0.078

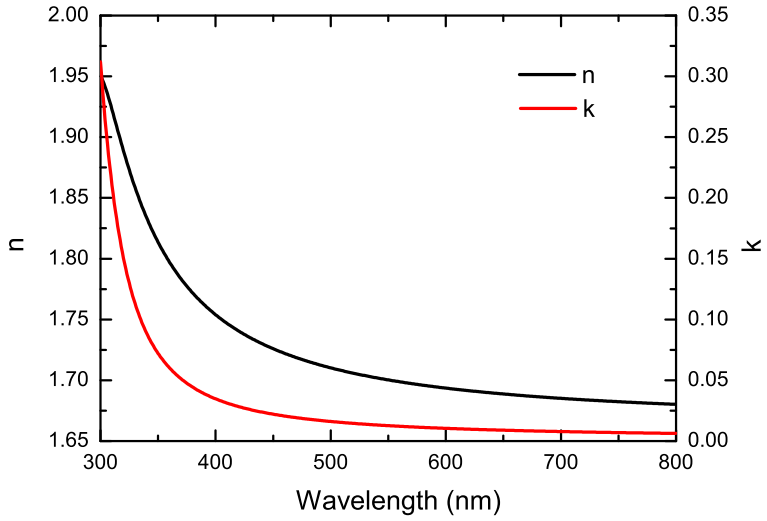

Figure 4.46: Optical constants of a neat PI film, treated thermally for 1 hour at 200°C.

(Dupont RC5878) - 0.042 [131]. Yet, our interest in PI being as a host material only in linear optical applications, it was quite sufficient to define the mean value of the refractive index. The n and k values of neat PI films have been determined by fitting the experimentally recorded spectra using Film Wizard and a one oscillator LOM. Results from the fit for a PI film, cured 1h at 200°C, are presented in Fig. 4.46. The obtained n at 633 nm is 1.69, which is close to the values for VD PI films referred in [131].

We further recorded PL emission spectra of neat 1000 Å PI films at wavelengths corresponding to those used for characterization of the luminescent properties of the dye molecules embedded in the matrix. They show only a weak featureless signal. Also, no visible dependence of the signal on the thermal treatment conditions was detected.

Hence, the accumulated results concerning the optical characterization of the obtained VD PI films, along with the possibility to chose the curing temperature range with respect to the embedded dye without influencing strongly the PI properties, demonstrate the suitability of polyimide as opically inert matrix.

4.2.2 Mixed MePTCDI/PI thin films

We investigated the optical response of MePTCDI molecules embedded in the PI matrix in order to clarify the influence of the matrix environment and to contrast both types of inactive matrices - organic and inorganic.

The concentration range of dispersed MePTCDI molecules studied is 0.2 - 3 vol%. Samples were grown by simultaneous condensation of both precursors ODA and PMDA, and dye on rotating substrates.

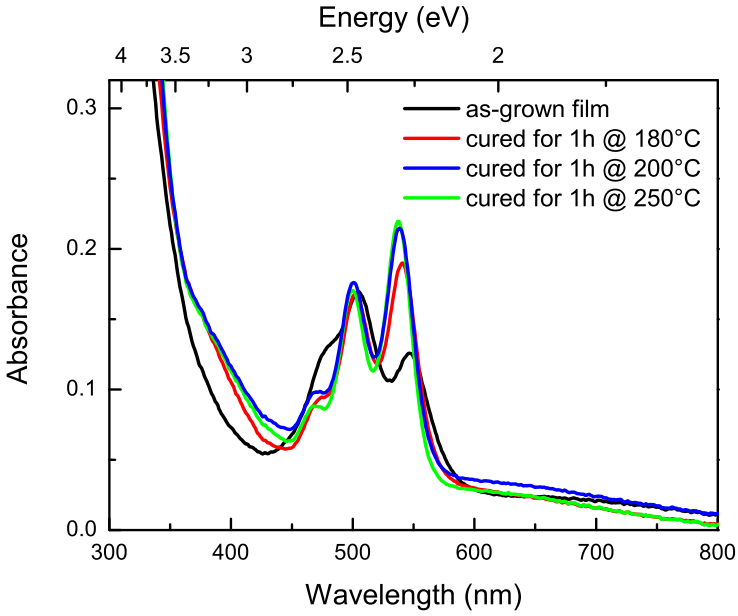

Figure 4.47: Absorption spectra of 2 vol% MePTCDI in PI films cured at different temperatures. The total thickness of the layers is 5000 Å.

We already discussed the importance of thermal treatment for the physical properties of the PI matrix. Therefore, it is reasonable to expect that the absorption and luminescence of the MePTCDI/PI layers would also be influenced by the curing process. On the other hand, spectral features depend on the molecular packing [84]. Thus, visible absorption spectroscopy can be used for drawing conclusions about the film microstructure. Figure 4.47 shows the room-temperature absorption spectra of 2 vol% MePTCDI embedded in a PI matrix in dependence on thermal treatment conditions. The as-grown film has a prominent absorption band at 546 nm and a broader one, centered at 504 nm, with a pronounced shoulder at 481 nm. Comparison with the absorption spectrum of pure crystalline MePTCDI film (cf. Fig. 4.4) shows that at this dye quantity (100 Å dye total thickness), the untreated mixed film consists basically of molecular aggregates. Upon increasing curing temperature, several effects are observed. First, an absorption band centered at around 360 nm appears. It is common for all investigated samples cured at temperatures above 170°C and is, as already noted, typical for the formation of polyimide from the initial monomers PMDA and ODA. The appearance of this band confirms literature results that the imidization of doped polyamic acid occurs despite the presence of dopant molecules [53, 54, 138].

Second, as a general trend, with increasing temperature there is a shift of the absorption band to higher energies ($\sim$ 38 meV for the film cured at 250°C with respect to the as-grown film), accompanied by bandwidth narrowing. In addition,

the ratio between the relative heights of the peaks centered around 538 nm and 500 nm changes in favor of the first peak. The shoulder at 480 nm grows to a discrete peak. Judging from the positions of the peaks and their relative intensities (see for comparison the absorption spectrum of the monomer in Fig. 4.3), the absorption could be interpreted as originating from both isolated MePTCDI molecules and a small portion of low-order aggregates.

These observations imply that during the heat treatment, a considerable part of the molecular aggregates transforms into monomers. Upon curing above 180°C, the spectral changes in the recorded absorption spectra are induced mainly by alternating contribution of monomers with respect to dimers. The increment of the height ratio of the peaks at 538 nm and 500 nm with increasing curing temperature clearly indicates that the quantity of absorbing monomers increases. The contribution of isolated MePTCDI molecules in the spectrum at 250°C is predominant, resulting in an intensified vibronic band at 538 nm, corresponding to the 0-0 peak of the S_0 - S_1 transition. The narrowing of the absorption band with growing curing temperature can thus be due to reduced intermolecular interactions.

At a first glance, the effect is rather surprising, based on the assumption for increased mobility of the dye molecules upon increasing temperature and hence enhanced aggregate formation. In fact, annealing of polymer/fullerene blend films generally results in larger fullerene crystals, as in e.g MDMO-PPV:PCBM or P3HT:PCBM (for details see e.g. [166]). However, the data reported concern mostly films prepared by spin coating. Thus, the mobility of the components, and accordingly the changes in blend morphology upon thermal treatment, have to be considered as affected by complex parameters, such as type of solvent, composition between polymer and fullerene, chemical structure and solubility of the materials, etc. On the other hand, in the present study we examine films grown by VDP, therefore solvent influence is excluded. We consider the following possibilities for explanation of these findings. First, the MePTCDI molecules can react chemically with the PI precursors or with products of the chemical reaction during their transformation to polyimide. Second, Salem et al. [131] reported more random chain orientation in VDP polyimide films than in solution cast films. Hence, the formation of polymer chains could lead to separation of dye molecules and their encapsulation within the polymer net. Taking into consideration the appearance of absorption features typical for PI upon increasing temperature, the latter explanation is the more plausible, although the first could not be excluded.

The established changes in the absorption of cured MePTCDI/PI films as well as the above reasoning are consistent with results published by Sakikabara et al. [138]. They describe a similar behavior when CuPc or metal-free phthalocyanine (H_2Pc) molecules are embedded in polyimide matrix. Upon heating, the absorption of Pc changes from basically crystalline to enhanced monomer. The effect is explained by breaking of the α-form micro crystals into smaller pieces, the driving force for this effect being the morphological changes of the matrix. In contrast, in polyurea matrix, also prepared by VDP, CuPc microcrystalline structure changes only slightly after heating [138]. As argued above, the chemical transformation of polyamic acid into polyimide upon thermal treatment is accompanied by a con-

traction of film volume. Thus, the polymer environment exerts stress upon the embedded dye molecules, resulting in break up of micro crystals and unstable aggregates into isolated molecules. The minimum temperature for the occurrence of such transformations is defined to correspond to the imidization temperature of the studied polymer, which is in agreement with the results presented here. Thermal treatment of polyurea, however, does not induce any chemical reaction between the initial monomers, but only thermal motion of polymer chains. Thus, the polycondensation reaction plays a significant role for the observed modifications in absorption.

The absorption spectra of mixed MePTCDI/PI films at concentrations in the range between 1 and 3 vol% confirm the behavior discussed above. Thermal treatment causes alteration in matrix structure, influencing the molecular distribution towards size reduction and separation. As expected, the effect is less significant for more diluted samples, 0.2 - 0.8 vol%, where the low dye coverage with mean distance between the molecules > 50 Å predetermines nearly monomer distribution.

Figure 4.48 depicts the corresponding luminescence emission spectra of the 2 vol% MePTCDI/PI sample. In general, compared to that in SiO_2 matrix at the same dye quantity, the luminescence response in the case of PI matrix is quite difficult to interpret. Similar to the absorption, the luminescence of the as-grown film is easily comparable with the PL spectrum of a neat MePTCDI layer (cf. Fig. 4.49). The emission is an excimer-type, characterized by a broad, structureless band, centered at longer wavelengths. It is thus consistent with the assumption for significant dye aggregation in the uncured mixed film. Another spectral feature is the slight indication for a peak centered at 554 nm. With increasing curing temperature, the luminescence shifts to the blue and the PL intensity increases. In addition, from the spectra of the samples treated at 200°C and 250°C, a shoulder centered at 600 nm can be extracted. The weak feature at 554 nm grows to a pronounced peak. However, its intensity and the overall spectral shape do not argue for monomer emission as in the case of MePTCDI in SiO_2 at the same dye content. In fact, comparison with the luminescence of isolated MePTCDI molecules in DMSO allows to assign the S_1 [0-0] vibronic transition to a peak at 547 nm (see the PL spectrum of 0.2 vol% MePTCDI/PI in Fig. 4.51).

Although the absorption spectra indicate a prevailing presence of single dye molecules, we interpret the overall luminescence as superposition of emission from monomers and molecular aggregates with different orientations of the participating MePTCDI molecules, formed during the optical excitation. The contribution of the individual components could be inferred by recording the excitation spectra, changing the detection emission wavelength. Results from such measurements for the sample treated at 250°C are presented in Fig. 4.50. As detection wavelengths we selected 570, 600, and 650 nm at distinctive features in the PL emission spectra. In principle, all three excitation spectra are similar to the absorption spectrum, although the graphs reveal that the heights of the absorption peaks at 504 and 538 nm vary by scanning the detection wavelength over the luminescence spectrum. The I_{538}/I_{504} ratio starts at a value of 1.23 (detection at 575 nm), decreases to

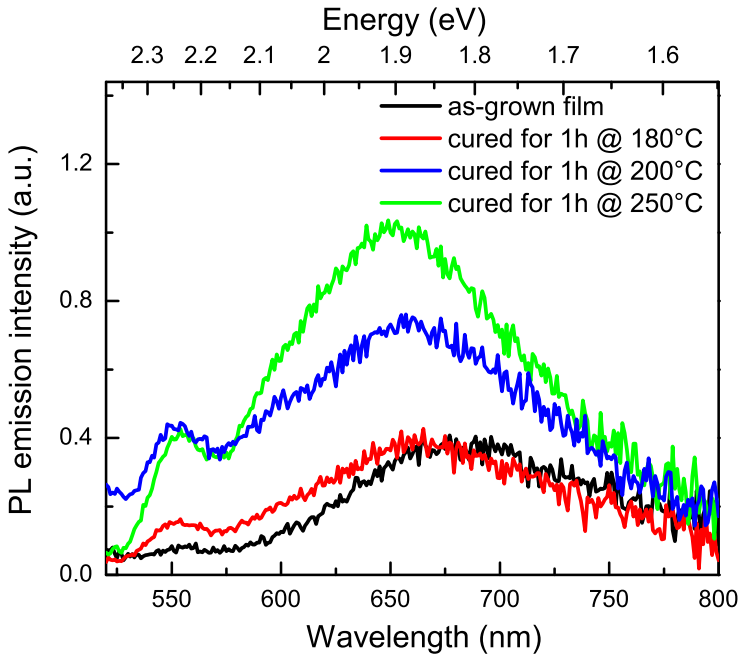

Figure 4.48: PL emission spectra of 2 vol% MePTCDI diluted in PI matrix; excitation wavelength 500 nm. The curing temperatures are shown in the graph. The total thickness of the layers is 5000 Å.

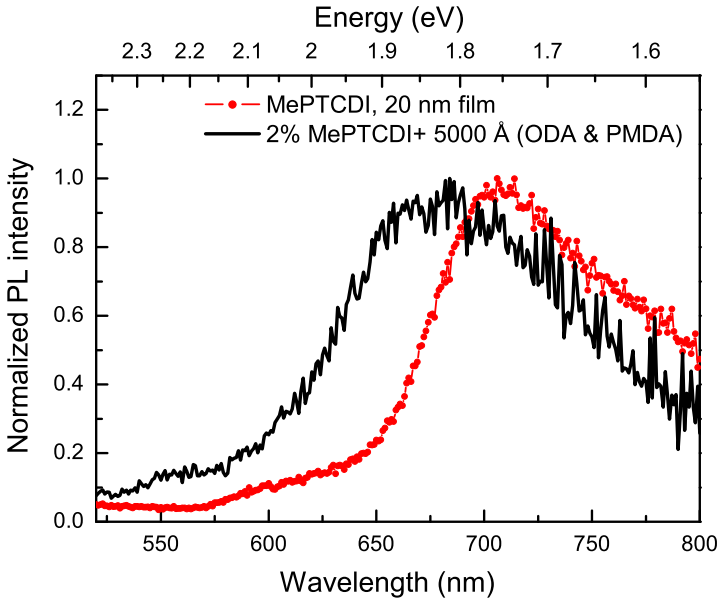

Figure 4.49: Normalized PL emission spectra of as-grown 2 vol% MePTCDI/PI and neat 10 nm MePTCDI films; excitation wavelength 500 nm.

1.18 (detection at 600 nm), ending up at 0.96 (detection at 650 nm). Additionally, the peak at 504 nm slightly broadens when the detection emission peak is 650 nm. Thus, the direct contribution of molecular aggregates in the overall luminescence can be retraced. Also, the observed alterations imply that upon excitation, the monomers are enabled to transfer their energy to neighboring molecular aggregates, hence pure monomer emission is practically not observed. On the other hand, since the luminescence intensity increases with increasing curing temperature, the imidization degree (i.e. the number of reacted precursors) and, related to it, the matrix morphology are significant for obtaining molecular distributions and possibly molecular orientations that favor a luminescence enhancement. Similar results are reported for polyimide films, grown also by vapor deposition polymerization, containing perylene units [128]. The formation of polyimide reduces the intermolecular interactions and luminescence quenching is avoided. Hence, by controlling the co-deposition conditions in a way that enhances the imidization reaction, we can improve the luminescence efficiency of the films. However, for a more detailed discussion on the subject, systematic structural studies in dependence on the thermal treatment conditions have to be carried out.

Figure 4.51 presents emission spectra of mixed films, thermally treated for 1h at 200°C, at different MePTCDI concentrations in the PI matrix. The luminescence centers at low dye contents (0.2 and 0.55 vol%) are single molecules. This is evident from the strong monomer emission with a peak at $\sim$ 547 nm, and is in

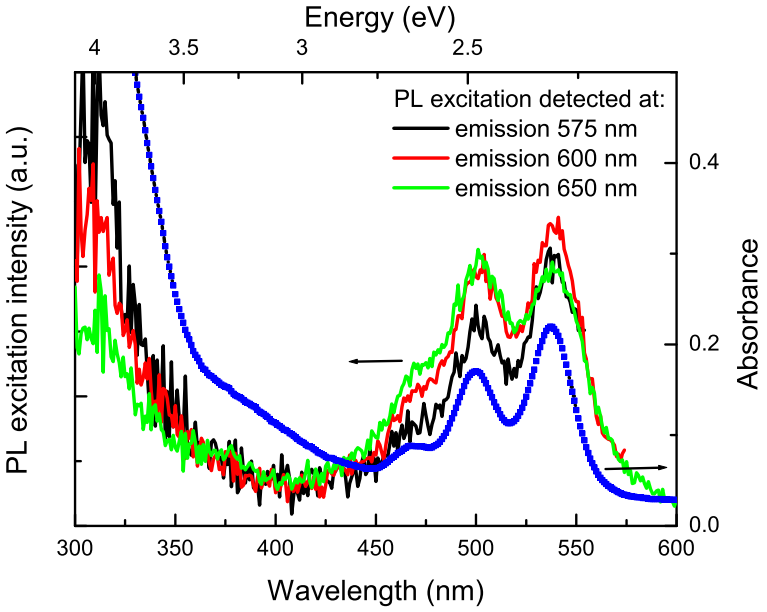

Figure 4.50: PL excitation spectra of 2 vol% MePTCDI/PI film cured at 250°C. Spectra are recorded at different emission wavelengths for detection.

agreement with the recorded monomer absorption spectra. The luminescence of the most diluted sample at 0.2 vol% is quite intense, while in comparison the emission of the most concentrated solid solution is nearly quenched. Although in general the recorded signals are quite noisy, in the emission spectrum of the 3 vol% sample, a weak feature around 685 nm can be distinguished. The spectral shape is excimer-type, indicating considerable intermolecular interactions. Therefore, the dramatic decrease in luminescence intensity could be attributed to self-quenching of MePTCDI at higher concentrations, as discussed in Section 4.1.

Since the intensity of the spectra in Fig. 4.51 is normalized to equal MePTCDI quantity, it further enables an evaluation of the luminescence efficiency of the samples. As expected, with increasing dye quantity the luminescence efficiency decreases. The 2 vol% film makes an exception to this tendency, showing the highest PL yield. We have to note, however, that this is quite a rough estimate. It is not related to absolute intensity values, since the baseline of the spectra is difficult to define. The complexity lies in (i) the scattering of the samples changes upon dye incorporation (ii) in general, we have to consider a three-component system comprising MePTCDI, ODA and PMDA. As already presented and confirmed from additional experiments, the conditions of thermal treatment are significant not only for the transformation of the initial monomers to polyimide, but also for the formation of a certain film structure. Therefore, the contribution of polyimide to the PL signal of the mixed samples depends also on the thin film structure. We

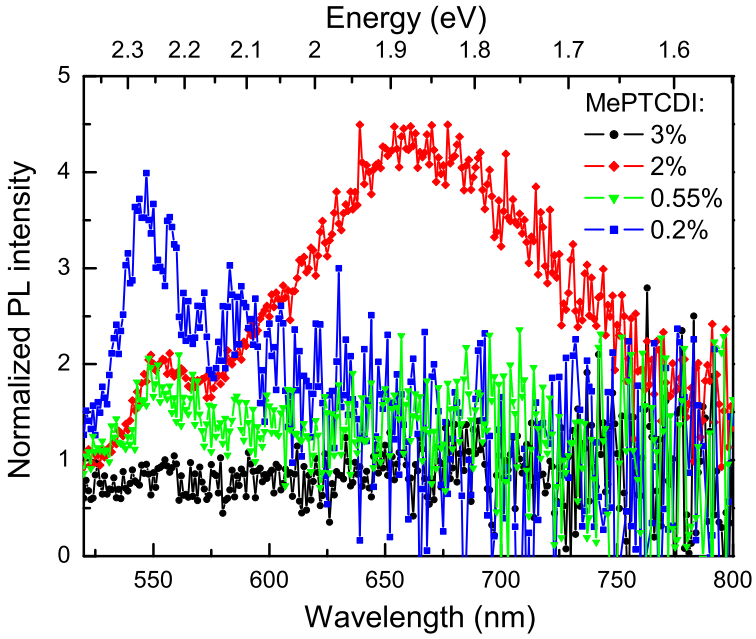

Figure 4.51: PL emission spectra of MePTCDI/PI films cured at 200°C. Spectra are recorded at 470 nm of excitation. PL intensity is normalized to equal dye quantity in the mixed layers.

can thus conclude that both the concentration of dye molecules and the number of obtained polymer chains affect the spectral response of the molecules within the organic host.

4.2.3 Alq_3 in PI matrix

As discussed earlier in this Chapter, we established a significant blue shift of the emission peak position for mixed Alq_3/SiO_2 layers, when Alq_3 is diluted in the inorganic matrix at low concentrations. Therefore, we carried out the following experiments with the objective to compare the spectral response of Alq_3 molecules, embedded in the PI matrix, with that in the SiO_2 matrix.

For the neat PI films, we determined that the transformation of the monomers to polyimide starts around 150°C, and is more efficient at higher curing temperatures. In case of Alq_3, however, the temperature at which the dye is evaporated (200°C - 250°C) is close to the usually applied thermal treatment conditions (170°C - 200°C). On the other hand, a study on molecularly doped electroluminescent (EL) polymer thin films, using Alq_3 as an active EL dye [53] shows that curing for 1.5 hours at a temperature of 150°C does not lead to thermal destruction of the co-deposited dye. Additionally, FTIR measurements confirm that the annealing at this "low" temperature facilitates to some extent the transformation of the as-grown film from polyamic acid to polyimide.

Aiming at higher imidization degree, we chose a two-step thermal treatment in order to avoid undesired effects, for instance sublimation of the dye from the substrate or thermal degradation. The latter includes one hour curing at 150°C as a starting step, followed by one hour at 200°C.

Figure 4.52 presents the obtained absorption and luminescence spectra of a 3 vol% Alq_3/PI film, thermally treated according to this scheme. The absorption band is broader and without defined maximum with respect to that of the pure Alq_3 film. Yet, comparison with the corresponding absorption spectrum of the as-grown sample indicates increased absorption in the region around 370 nm. Simulation of the mixed layer absorption with Film Wizard, using an EMA Bruggeman model and the optical constants of PI and Alq_3, agrees quite the well with the measured spectrum. We thus infer that the polymerization reaction is not disturbed by the co-deposited dye. The emission spectrum is characterized by a broad band with maximum centered at 514 nm. The luminescence intensity increases slightly upon curing, i.e. upon imidization. Contrary to MePTCDI, no dimer emission is observed in thin films of Alq_3 as well as in the crystalline forms of the dye [27]. Hence, the PL enhancement is due to a minor contribution of the matrix itself, rather than to dilution of the Alq_3 molecules.

Figure 4.53 depicts the normalized luminescence spectra of 3 vol% diluted Alq_3 molecules in both types of matrices, PI and SiO_2 (effective matrix evaporation rate 0.4 Å/s), along with a neat Alq_3 thin film. The thickness of the neat film (70 Å) is close to the total dye thickness in the mixed samples.

The emission spectra clearly point out that the spectral position of the luminescence depends significantly on the surrounding matrix. The position of the PL maximum in PI is almost identical with that of the pure Alq_3 film (blue shift of

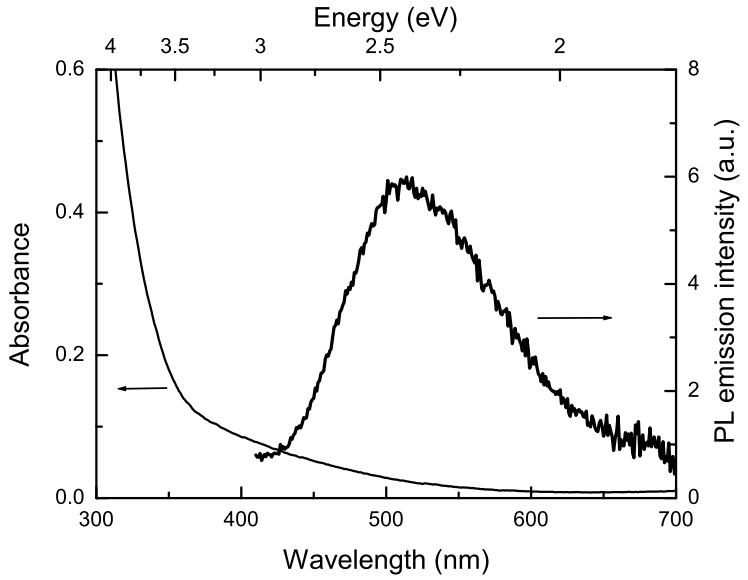

Figure 4.52: Absorption and PL emission spectra of 3 vol% Alq_3 embedded in PI matrix, total film thickness 2000 Å. The sample is cured for 1 hour at 150°C, followed by one hour at 200°C. Emission is recorded for 370 nm excitation.

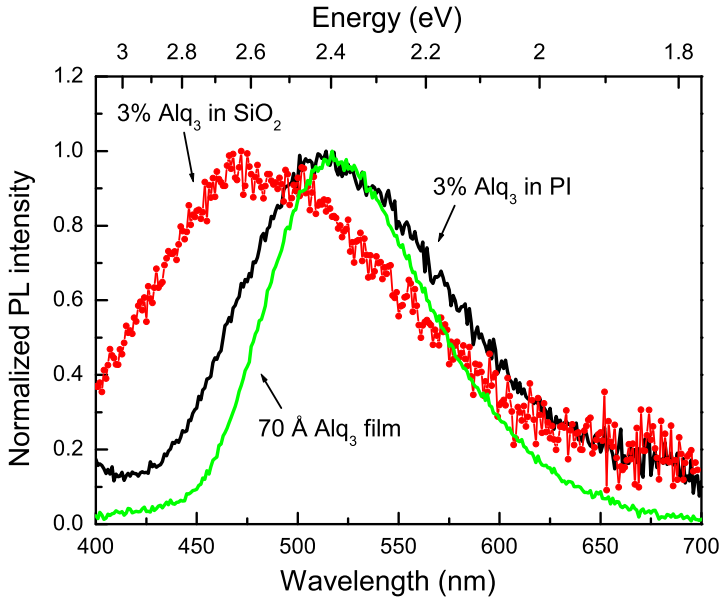

Figure 4.53: Normalized luminescence spectra of mixed Alq_3/PI and Alq_3/SiO_2 film, and a pure Alq_3 film. The total film thickness of the mixed layers is 2000 Å. Emission is recorded for 370 nm excitation.

only 14 meV). However, the emission line is broadened which could be attributed to the inhomogeneous matrix environment (i.e. PI, as well as unreacted monomers). In contrast, a significant blue shift of the emission peak appears when Alq_3 is distributed in the inorganic SiO_2 matrix (about 0.24 eV with respect to the pure dye film). This blueshifted luminescence is an expected effect. The Alq_3/SiO_2 sample is grown at low effective matrix evaporation rate, which accordingly to the results presented in Section 4.1, corresponds to beneficial conditions for the preservation of facial Alq_3 molecules. At the same time, a comparison between the as-recorded luminescence spectra show that the Alq_3/PI sample is characterized by integral luminescence intensity which is by a factor of 1.4 higher than that of the Alq_3/SiO_2 sample. Since both films have equal dye quantity, the decreased PL intensity in SiO_2 is consistent with our assumption of thermal stress for the Alq_3 molecules during the co-deposition process.

4.2.4 Summary

To summarize, the results presented above unambiguously show that in the case of mixed dye/PI films, it is generally important to study the behavior of dye molecules along with the change in surrounding environment in the dye/polyimide reaction system. Therefore, the problem about the PL quantum efficiency has to be considered in relation to the particular experimental parameters, defining

the matrix formation - deposition rates of the precursors ODA and PMDA (a stoichiometric ratio is required in order to achieve high degree of polymerization [140]), film thickness, and especially curing procedure.

In comparison to the rigid SiO_2 matrix, the PI matrix allows a limited motion of the dye molecules. Thus, the distribution of the molecules in the SiO_2 matrix is much more defined, respectively the luminescence properties are easier to predict. On the other hand, it is possible to obtain monomer emission in the polyimide matrix as well, however at much lower dye concentrations than in the SiO_2 matrix (≤ 0.5 vol%).

In contrast to the Alq_3/SiO_2 system, the spectral behavior of Alq_3 embedded in PI is similar to that in the solid state and in solution. Since there is no blue shift of the luminescence peak position and PI as organic material is rather flexible compared to SiO_2, we can conclude that the rigidity of the SiO_2 matrix is determinant for the conservation of the *fac*-Alq_3 molecules. That is, the distribution and hence the optical response of Alq_3 molecules are nearly independent of the morphological changes of the matrix in the course of the curing procedure, provided that the curing temperature does not exceed the sublimation temperature of the dye.

In addition, we have shown that by keeping the curing temperatures for the imidization of the PI matrix below the sublimation temperature of Alq_3, it is possible to (i) obtain mixed layers with the characteristic for Alq_3 green emission and (ii) reach a reasonable degree of polymerization, and hence a matrix with satisfactory optical and mechanical properties. Consequently, the major advantage of the PI host is that it offers the feasibility to choose the thermal treatment conditions with respect to the particular dye which has to be embedded in it.

5 Organic guests in an active Alq_3 matrix

In this Chapter, we first briefly address the luminescence response of the dye molecules DCM and rubrene embedded in the optically active Alq_3 matrix. We study samples at various concentrations of the guest molecules and present results about the efficiency of doping. The mechanism of resonant energy transfer is discussed.

In the second part of the Chapter, we present examples for application of the doped Alq_3 films as luminescence conversion layers in combination with blue LEDs as excitation light sources. We first consider some theoretical points. Next, we determine the optimal thickness and doping ratios of the composite films in order to obtain white light. The corresponding CIE coordinates of the PL converters and results from measurements of the angular dependence of the emission are presented. Finally, we discuss the stability of the samples.

5.1 Rubrene/Alq_3 and DCM/Alq_3 thin films

5.1.1 Introduction

The dilution of organic dyes in an optically inactive matrix, discussed in the previous Chapter, is only one approach to solve the problem of concentration quenching and to achieve an increase of the photoluminescence quantum efficiency. Another efficient method to obtain this goal, as discussed in Section 2.8, is selective doping of neat host organic layers with highly fluorescent guest organic molecules. In this case, the molecules of the matrix participate actively in the process of optical excitation. By absorption of photons, they are promoted to an excited state and before relaxation transfer their energy to the guest molecules via Förster mechanism [36, 141].

In the present study, we use Alq_3 as an optically active host material, profiting from its favorable qualities for optoelectronic applications, such as relatively high quantum yield in thin film. As molecular dopants, we selected 4-dicyanomethylene-2-methyl-6-(p-dimethylamino-styryl)-4H-pyran (DCM) and tetramethylnapthacene (rubrene). Both dopants absorb in the emitting range of the host and fluoresce in the yellow to orange-red range. In dilute solutions, they both are known to have high luminescence quantum efficiencies of 0.5 - 1 [64, 65]. In contrast, pure vapor deposited films of these dyes show a strongly reduced luminescence. The Förster transfer process is promoted by the well-aligned energy levels of the Alq_3 - rubrene or Alq_3 - DCM molecules, presented in Fig. 5.1.

Alq_3 films doped with DCM or rubrene are widely applied as emitting layers in OLED fabrication. However, the system DCM/Alq_3 attracted additional research interest after the demonstration of lasing from optically pumped evaporated thin films by Kozlov et al [172]. Since then, organic semiconductor lasers, based on

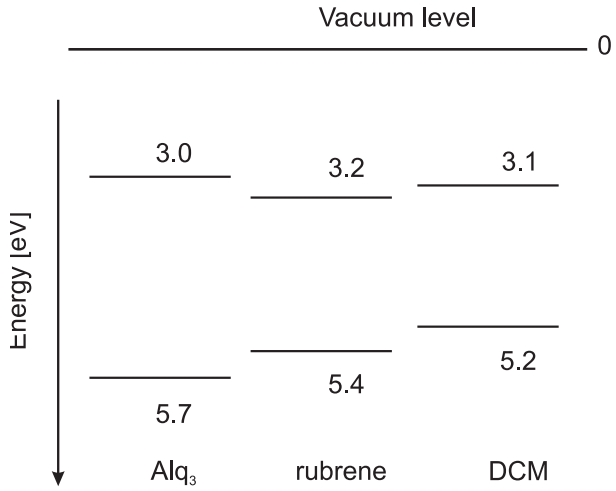

Figure 5.1: Energy levels of Alq_3, rubrene, and DCM. Data are taken from Refs. [141, 142].

DCM doped Alq_3, with various geometries such as microcavities [62, 173] or different planar waveguide structures [144, 174] were realized. Significant advantages of a gain medium with Förster transfer are established to be (i) high absorption at the pump wavelength and low optical loss at the emission wavelength due to the large shift between host absorption and guest emission (ii) the low concentration of emitting molecules results in reduced bimolecular annihilation or excimer formation and thus in low lasing threshold (1 - 20 μJ/cm^2, cf. Refs. [144, 173]).

5.1.2 Luminescence and efficiency of the doped films

Experimentally recorded absorption and emission spectra of pure VD film of the host Alq_3 along with the absorption spectra (presented are the extinction coefficients) of the guests DCM and rubrene, both diluted in DMSO at a concentration 2.10^{-5} mol/l, are depicted in Fig. 5.2. The Alq_3 film absorbs in the wavelength region below 450 nm, with a broad band centered at 400 nm. In contrast, guest dyes have absorption which extends to the green spectral region and thus covers almost half of the emission spectral region of Alq_3. The extinction coefficient of rubrene is about 4 times lower than that of DCM.

As discussed earlier, a crucial criterion for the occurrence of Förster transfer is the value of the energy overlap integral $J(\lambda)$ over the whole spectrum. The spectral dependence of the overlap functions for both guests is compared in Fig. 5.3. Integration over the full spectrum shows that the value of the overlap integral for DCM in Alq_3 is larger than for rubrene by factor 4 (1.96 x 10^{-14} for rubrene vs. 7.97 x 10^{-14} for DCM). Applying the expressions in Section 2.4, with $\phi_D = 0.25$ [65] and $n = 1.7$ for undoped Alq_3 film, and the corresponding values of the overlap integral $J(\lambda)$, we can calculate the Förster radii for energy transfer from Alq_3 to the dopants. For DCM R_0 amounts to 33 Å, which is indicative of an effective energy transfer process, while for rubrene $R_0 = 26$ Å. The shorter Förster radius

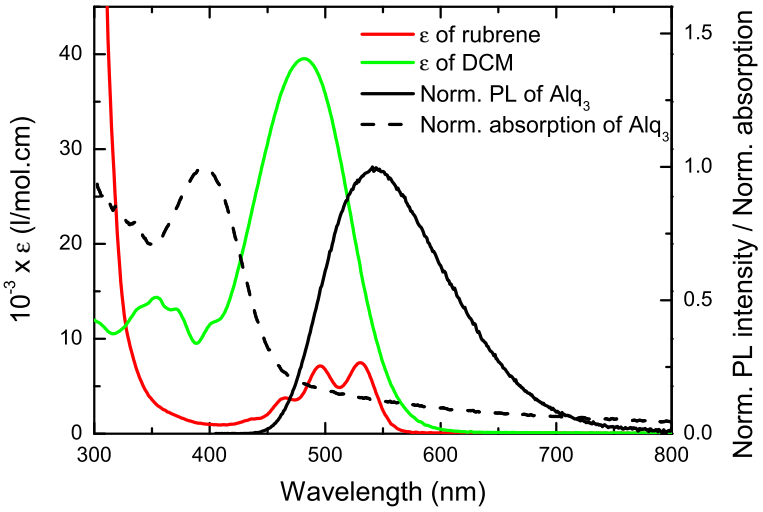

Figure 5.2: Normalized absorption and PL emission spectra of pure film of the host Alq_3 (thickness 300 Å) and exctinction coefficients ε of the guests DCM and rubrene, diluted in DMSO ($c = 2.10^{-5}$ mol/l).

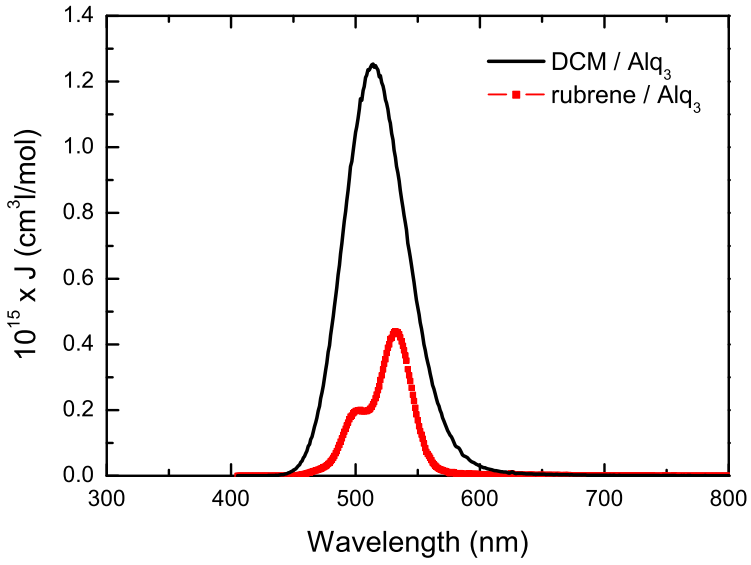

Figure 5.3: Overlap integral J for Alq_3 with DCM and rubrene.

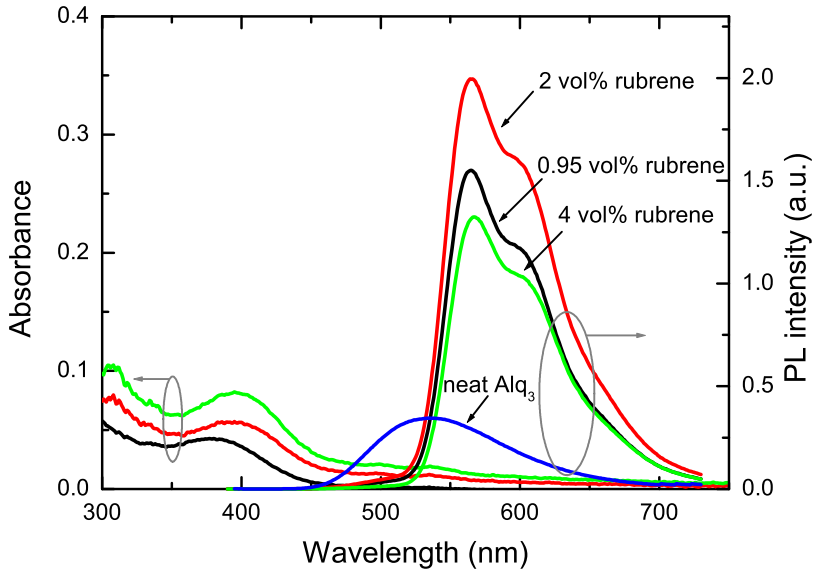

Figure 5.4: Absorption and luminescence spectra of rubrene doped in Alq_3. PL spectra are recorded using 370 nm as excitation wavelength and are normalized to equal film thickness.

for rubrene indicates that, in addition to considerable spectral overlap, effective energy transfer requires an acceptor with high extinction coefficient.

We followed the optical response of the molecules embedded in the active matrix investigating Alq_3 films doped with rubrene and DCM molecules at concentrations in the region 0.6 to 4 vol%. Figures 5.4 and 5.5 present the absorption (measured) and luminescence (normalized to equal film thickness) spectra of composite films of rubrene dispersed in Alq_3 (150 - 300 Å total film thickness) and of Alq_3 films doped with DCM (2200 - 3000 Å thickness), respectively. The PL spectrum of a pure Alq_3 film is given as a reference. All spectra are recorded by using 370 nm (rubrene/Alq_3) or 380 nm (DCM/Alq_3) as excitation wavelength.

The data reveal, first, that emission intensity and peak position strongly depend on the doping concentration of the guest used. A comparison between the absorption of the composite films (Figs. 5.4 and 5.5) and that of the pure Alq_3 film (cf. Fig. 5.2) suggests that absorption at the excitation wavelength in the mixed films is mostly due to the host material. Distributed DCM or rubrene molecules contribute to the absorption only at higher doping concentrations, i.e. $\sim$ 4 vol%. On the other hand, the luminescence of the composite films stems mainly from the guest molecules. Emission is tuned from green, centered at 540 nm (undoped Alq_3 film), to yellow, centered at $\sim$ 565 nm for rubrene, and to red $\sim$ 611 nm for DCM, respectively (doped films). Thus, the incident photons excite predominantly the host Alq_3 molecules. They further transfer their energy to the dispersed guest

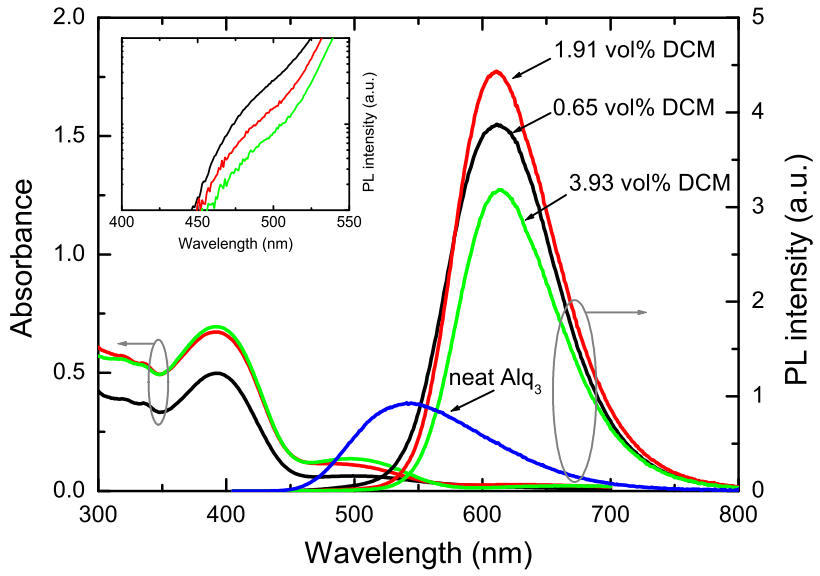

Figure 5.5: Absorption and PL spectra of DCM doped in Alq_3 at different concentrations. Luminescence is normalized to equal film thickness; spectra are recorded using 380 nm for excitation. The inset shows a logarithmic scale plot of the luminescence in the spectral region 450 - 550 nm, where a weak host contribution is present.

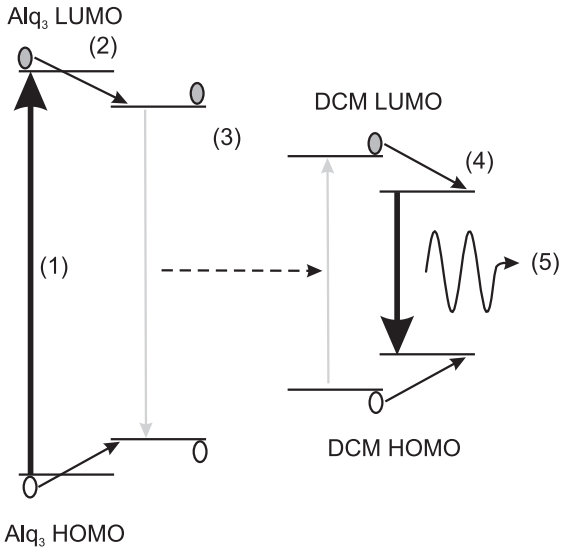

Figure 5.6: Energy level diagram of DCM/Alq_3 illustrating the excitation of DCM molecules by means of resonant Förster energy transfer from Alq_3 (dashed arrow (3)), and the Franck-Condon shift (solid thin black arrows (2,4)) in Alq_3 and DCM molecules (adapted from [144]).

molecules, which subsequently emit at lower energies. However, in a logarithmic scale plot of the luminescence (inset in Fig. 5.5), a weak contribution of the host Alq_3 is observed, with a shoulder at $\sim$ 510 nm. This residual Alq_3 emission is due to incomplete energy transfer, and decreases with increasing doping concentration.

As inferred, the relaxation of the doped films clearly depends on the doping level. Time-resolved relaxation studies on doped DCM/Alq_3 samples [143] confirm the dopant-concentration dependence of the excitation decay. The de-excitation follows a five step process presented in Fig. 5.6 [144]. The intermolecular resonant transfer from host to guest molecules occurs on a subpico- to nanosecond time scale and is more efficient than other competing processes, such as direct radiative or nonradiative decay of the host excitons [144, 145].

Another effect concerns the luminescence intensity. As the number of guest molecules increases, the PL intensity at first increases fast and then decreases. The PL integral intensities of the composite films in dependence on doping concentration are presented in Fig. 5.7. The highest PL efficiency is achieved at $\sim$ 2 vol% dye quantity for both guest molecules. As evident, at the optimal doping level, doped films give luminescence rise of 3 to 4.5 times compared to the undoped Alq_3 film. A further increase of the doping level leads to decrease of the PL efficiency. In addition, the increase of doping level up to 4 % is accompanied by a slight but gradual shift of the PL maximum to longer wavelengths. Thus, the number of dispersed guest molecules available in the transfer process is significant for the luminescence spectral position and intensity of the composite films. When the doping level is too low, the guest emission could be weak due to lack of molecules which could capture the generated excitons before they relax [58].

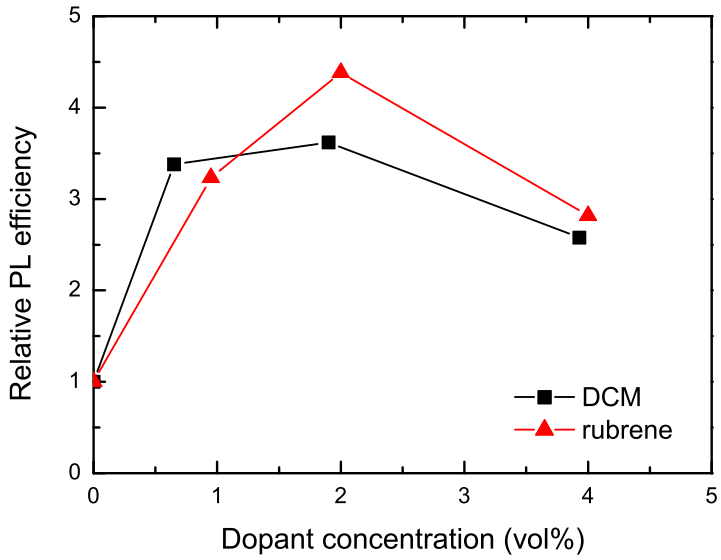

Figure 5.7: Relative PL efficiency of the doped films as a function of dopant concentration.

As seen from Figs. 5.4 and 5.5, pure emission from the guest is obtained at a doping level of around 1 %. If one assumes a homogeneous guest distribution, this concentration corresponds to one dopant molecule, surrounded by a sphere of 100 Alq_3 molecules, i.e. the radius of the sphere should be approximately three host molecules. As the diameter of Alq_3 is ~ 9 Å , the Alq_3 exciton has to be separated from a dopant molecule at a maximum distance of ≈ 30 Å [36]. The latter value is around the calculated Förster radii for rubrene and DCM. The exciton diffusion is another effect that further increases the probability for energy transfer [36]. The exciton diffusion length in Alq_3 is found to be 200 Å [64] which is much larger than the Förster radius. Hence, it is possible for excitons further away to migrate to a position within the Förster radius and to transfer energy to a guest molecule prior to relaxation.

At too high doping concentrations, the possibility for two or more of the guest molecules to come close to each other and form a dimer or higher-order molecule complex increases. This could lead to concentration quenching and is revealed in a drop of the quantum yield and a redshifted emission peak. Such concentration quenching via nearest neighbor excimer formation is known to be predominant in solid DCM, since the planar geometry of the dye molecules permits them to aggregate densely enough to allow efficient excimer formation [64, 143]. The latter effect could also explain the lower conversion efficiency obtained for the doped DCM/Alq_3 films with respect to the doped rubrene/Alq_3 films.

We measured the PL quantum efficiency for composite DCM/Alq_3 and rubrene/Alq_3 samples with concentrations corresponding to the most efficient doping de-

rived from the PL emission spectra, i.e. around 2 vol% (in molar proportions: 1.8 mol% for rubrene, 3 mol% for DCM). The efficiency of pure $\sim$ 700 Å thick Alq_3 film was measured for comparison. The samples were excited with the 325 nm line of a cw - HeCd laser. The determined values of the PL quantum yield, ϕ_{ext}, are as follows: 0.24 for the host Alq_3 film, 0.83 for 4900 Å DCM/Alq_3 film at concentration 2 vol%, and 0.94 for 3700 Å rubrene/Alq_3 at 1.8 vol%.

Our results for the PL quantum efficiency of pure and doped rubrene/Alq_3 films are in good agreement with those determined by Mattoussi et al., who applied the same measuring method [65]. The authors report values of 0.25 for pure Alq_3 and about 0.92 for a doping level of 2 mol%. Zhong et al. [58] estimated quantum efficiencies of Alq_3 doped with DCM, using the PL spectra of the samples and taking 0.25 as the PL efficiency of a pure Alq_3 film. The highest value thus derived lies at 0.61 and corresponds to 2.6 mol% DCM concentration in the doped film. Applying the same approach as in [58], with $\phi_{PL} \cong 0.24$ for pure Alq_3 film and the PL emission spectrum in Fig. 5.5, we estimated a value of $\cong 0.81$ for the 2 vol% DCM/Alq_3 sample. We can only speculate about the origin of the above difference. It is well known, however, that the preparation conditions, such as type of the substrate, substrate surface, dynamic state of the substrate during deposition, deposition rate, etc., play an important role for the film structure and for the dye distribution in the films, and hence for the decay dynamics.

We further studied the luminescence decay of the dye-doped Alq_3 films upon continuous irradiation. The corresponding results and detailed discussion on the photostability will be presented in the following Section, where we address the application of these organic/organic systems in luminescence conversion devices.

5.2 An application example: Luminescence conversion

5.2.1 Principle, requirements and color

The underlying physical principle, on which this application is based, is that of luminescence down-conversion as a consequence of the Stokes shift between light absorbed and reemitted by an inorganic phosphor or organic dye. The LUCO principle in connection with additive color mixing provided the basis for the first single chip white LED developed independently at Fraunhofer IAF and at Nichia (Japan) in 1996. This first generation white LED was based on a blue LED pump chip and the phosphor YAG:Ce^{3+} as converter material. A year later, Schlotter et al. [8] demonstrated luminescence conversion of blue LEDs using organic dyes as LUCO layers. Now, LUCO-LEDs based on phosphors are widely used particularly as lighting applications in advertising, for display purposes, and for illumination systems in cars and aircraft. Additionally, LUCO layers can be used for spectral aligning of detectors in order to increase their efficiency, or light outcoupling from waveguides.

A schematic presentation of the principle is given in Fig. 5.8. The radiation of the LED (primary light) excites the organic molecules in the LUCO layer to subsequent emission of secondary photons (secondary light), whereas the emitted light is shifted to the red with respect to the pump one. This way, the luminescence

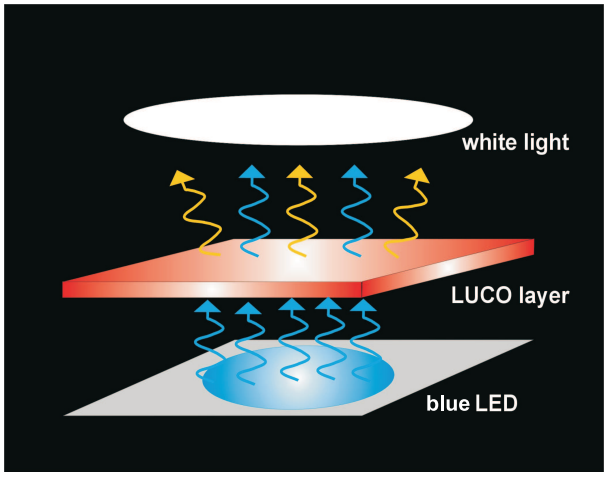

Figure 5.8: Schematic representation of the luminescence conversion principle.

from the converter layer and the remaining primary light are mixed additionally. Optimization of LUCO parameters, i.e. film thickness, doping ratio, or type of LUCO materials, can lead to proper color mixing of the blue from the LED with the secondary emitted light from the LUCO film, thus resulting in visible or in white emitting LUCO-LED.

Several essential requirements have to be fulfilled in order to realize luminescence conversion. There has to be a strong overlap between the electroluminescence (EL) spectrum of the LED and the absorption of the LUCO film. Next, for reasonable thickness of the LUCO layer, the organic materials should have relatively high absorption coefficients in the emission spectral range of the LED. Another important parameter is the internal quantum efficiency of the LUCO materials.

Figure 5.9 presents schematically the emission from a LUCO-LED device towards the exterior. Light produced in the LUCO layer approaches the film/air interface at an angle of incidence θ which can be greater or less than the critical angle θ_c which is defined by the relation

$$n \sin \theta_c = n_{air}, \tag{5.1}$$

where n is the refractive index of the organic material. When $\theta < \theta_c$, light is transmitted to the exterior. However, when $\theta > \theta_c$, light will be totally internally reflected within the device without reaching the exterior.

So, at the LUCO interior, emission going toward the frontal surface occurs in a half space, i.e. $\Omega_1 = 2\pi$. Thus, the portion of light which can leave the device is emitted within a solid angle limited to

$$\Omega_2 = 2\pi \int_0^{\theta_c} \sin \theta d\theta = 2\pi(1 - \cos \theta_c). \tag{5.2}$$

Given that $\sin\theta_c = 1/n$, the term (1 - $\cos\theta_c$) can be approximated as equal to

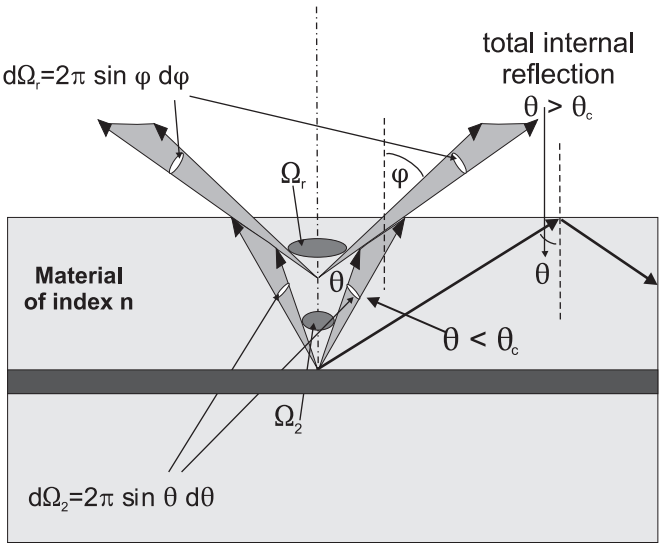

Figure 5.9: Internal and external emission of a LUCO-LED (adapted from [148]).

$1/2n^2$. Thus, $\Omega_2 = \pi/n^2$, and respectively

$$\Omega_2 = \frac{\Omega_1}{2n^2}. \tag{5.3}$$

From equations (5.2) and (5.3) follows that the solid angle at the exterior (Ω_2) is only a fraction of the total emission angle (Ω_1) and the external yields are considerably influenced [148].

If one considers a ray incident to the material/air interface with $\theta < \theta_c$, the refraction laws modify the geometry of the solid angle cones of the emission as presented in Fig. 5.9. The elementary solid angles $d\Omega_2$ and $d\Omega_r$ are such, that

$$\frac{d\Omega_2}{d\Omega_r} = \frac{\cos\varphi}{n(\sqrt{n^2 - \sin^2\varphi})}. \tag{5.4}$$

For organic materials, $n \approx 2$ and $\sin^2\varphi$ is well below 1. Therefore, $\sin^2\varphi \ll \mathrm{n}^2$, and respectively:

$$\frac{d\Omega_2}{d\Omega_r} \approx \frac{\cos\varphi}{n^2}. \tag{5.5}$$

Equation (5.5) indicates that the distribution of rays emitted directly toward the exterior, at a solid angle Ω_2, is Lambertian [149].

The internal quantum efficiency of the device can be related to I_0, the flux per unit solid angle of light leaving the device directly in the forward direction. The total flux Φ_{total} produced within the emissive layer, with $\varphi = 0$ ($\mathrm{d}\Omega_2/\mathrm{d}\Omega_r = 1/\mathrm{n}^2$), is

$$\Phi_{total} = 2\pi n^2 I_0. \tag{5.6}$$

Φ_{total} is used for calculation of the internal quantum efficiency [149]. On the other hand, the flux Φ_{ext} leaving the device directly can be calculated taking the

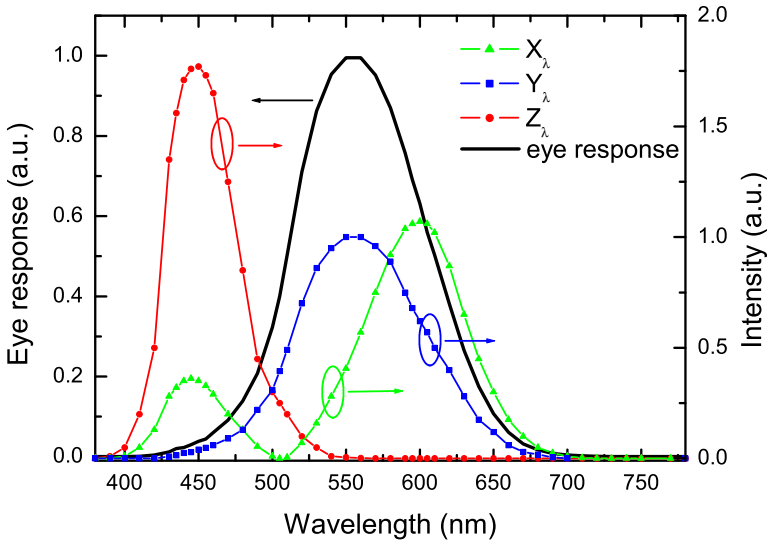

Figure 5.10: Normalized eye response curve and CIE 1931 tristimulus curves.

emission to be exactly Lambertian:

$$\Phi_{ext} = \int_0^{\pi/2} 2\pi I_0 \cos\varphi \sin\varphi d\varphi = \pi I_0. \tag{5.7}$$

In contrast, Φ_{ext} is used to define the external quantum efficiency of the device for directly emitted light. Thus, internal quantum efficiencies are a factor $2n^2$ larger than the external quantum efficiencies.

The color of light emitted from LUCO devices is determined on the basis of the measured emission spectra. The corresponding chromaticity coordinates x' and y', which are used to compare devices with different spectra are defined by the Commission International de l'Eclairage (CIE) as:

$$x' = \frac{X}{X+Y+Z},\ y' = \frac{Y}{X+Y+Z}. \tag{5.8}$$

The corresponding XYZ tristimulus values for a color with a spectral power distribution I(λ) is given by:

$$X = \int_{380}^{780} I(\lambda) X_\lambda d\lambda,\ Y = \int_{380}^{780} I(\lambda) Y_\lambda d\lambda,\ Z = \int_{380}^{780} I(\lambda) Z_\lambda d\lambda, \tag{5.9}$$

X_λ, Y_λ and Z_λ are the color matching functions (Fig. 5.10).

5.2.2 Systems

In the previous Section, we have shown that by doping of Alq_3, a substantial increase of the photoluminescence quantum efficiency can be reached. Moreover, depending on the type of dopant, the primary green emission of Alq_3 can be tuned to yellow (rubrene) or red (DCM). Both these effects are beneficial for the use of doped Alq_3 films as converter layers in luminescence conversion devices. In addition, Alq_3 has a relatively large absorption coefficient in the blue spectral range ($\alpha \approx 0.5$ x 10^5 cm^{-1}). Thus, optical density of the order of unity can be obtained by preparation of films of merely submicron thickness.

Successful white light generation based on organic materials as luminescence converters is already reported in literature. Schlotter et al. [8] fabricated whitish emitting LUCO-LEDs by mixing green and red emitting perylene-based dyes. Another approach developed by Hide et al. [164] and further improved by Zhang and Heeger [165] included conjugated polymers or copolymers, derivatives of poly(*p*-phenylene vinylene) (PPV). The luminescence converters were prepared either by dissolving the dyes in epoxy resin by standard LED technology or by spin casting from polymer solution. In contrast, in the present study we apply simple dry technology: the LUCO layers were grown by co-evaporation of host (Alq_3) and guest (DCM, rubrene) molecules as composite film, directly on top of the LED in HV. As an excitation source in the LUCO devices, we used light-emitting diodes with a maximum of the electroluminescence at $\sim$ 450 nm. The LEDs were delivered by OSRAM Opto Semiconductors, Germany. The aim of our investigations were to study the possibilities for converting the blue light of the LED into light of longer wavelengths and to find the optimal film parameters - thickness and doping ratio - for obtaining white-emitting LUCO-LEDs.

Figure 5.11 shows results from *in-situ* measurements of the overall luminescence in the vacuum chamber of a LUCO-LED with 1.8 vol% DCM/Alq_3 film on top. The *in-situ* spectra were recorded using a homemade spectrometer, designed by R. Gehlhaar within the framework of his doctoral thesis. All presented spectra are corrected with regard to inevitable current fluctuations by normalization to the total integrated area.

The EL of the blue LED is recorded as a starting reference. After that, the diode is switched on after every 800 Å Alq_3 layer thickness deposited in order to record the corresponding luminescence spectrum. The results clearly show that up to 3900 Å, the spectrum of the emitted light changes substantially. With increasing LUCO thickness, more of the primary light is absorbed, thus the EL intensity of the LED peak around 450 nm drops, while the PL from the doped Alq_3 film at $\sim$ 620 nm increases. This behavior confirms the emission mechanism discussed in the previous Section. The blue light of the LED is absorbed from the Alq_3 molecules; the excitation is further transferred to the DCM molecules, which relax to the ground state by radiation of low energy photons (red emission). The peak of the pure Alq_3 centered on 520 nm is not observable, which demonstrates the efficiency of the transfer with increasing film thickness and contribution of the DCM molecules.

However, a further increase of the LUCO layer thickness above 5500 Å does

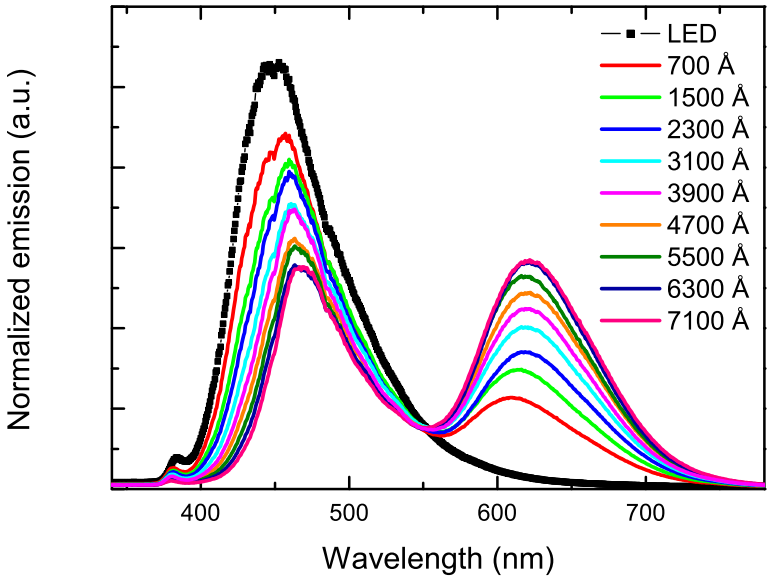

Figure 5.11: *In-situ* luminescence of LUCO-LED with 1.8 vol% doped DCM/Alq_3 film as LUCO layer in dependence on the LUCO thickness.

not change the LUCO-LED spectrum anymore. Additionally, in the final LUCO-LED spectrum, there is a slight shoulder at around 517 nm present, indicating that there is a contribution from the Alq_3 molecules as well. At the noted film thickness, Alq_3 absorbs around 80 % in the high energy region (340 - 400 nm), but only $\sim$ 30 % at the maximum LED emission. In fact, close examination of the absorbed part of the initial EL spectrum confirms that at this film thickness, part of the DCM molecules participate directly in the absorption of the initial light (Fig. 5.12). Such a behavior is attributed to the relatively wide EL spectrum of the pumping diode. Thus, the intensity of the reemitted light at 620 nm does not increase further, presumably due to direct nonradiative recombination of DCM.

At a final thickness of the converter layer of 7100 Å, this sample has chromaticity coordinates $x' = 0.37$, $y' = 0.30$ (see Fig. 5.13), which are close to the equal energy point $x' = y' = 0.33$. The ratio between the intensities of the peaks of the primary (at 470 nm) and the secondary (at 620 nm) light at this optimal LUCO thickness corresponds to $\sim$ 1. The conversion efficiency amounts to 0.74. In comparison, the employment of high PL efficiency polymers as luminescence converters results in white light with comparable coordinates (0.34, 0.29) and conversion efficiencies of up to 0.6 [164]. Hence, the DCM/Alq_3 system we study shows somewhat better performance. Further increase of the LUCO film thickness above 7100 Å for DCM/Alq_3 leads to strong absorption of the primary blue light (leading to a shift of the primary peak to the green) and pronounced red emission. The result is in this case an orange-emitting LUCO-LED.

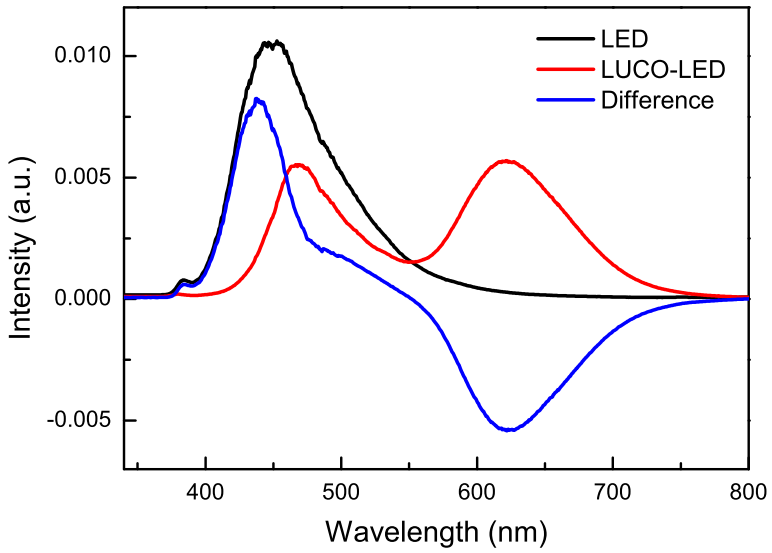

Figure 5.12: Initial EL spectrum, final LUCO-LED PL spectrum, and their difference (LUCO layer: 1.8 vol% DCM/Alq_3 film, 7100 Å thickness).

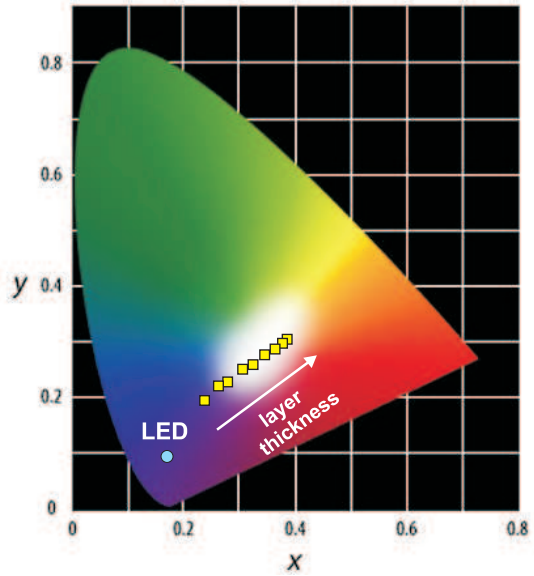

Figure 5.13: CIE diagram with the corresponding coordinates of LUCO-LED, based on 1.8 vol% doped DCM/Alq_3 as a LUCO layer upon increasing layer thickness. The color position of the primary blue LED is presented as a reference.

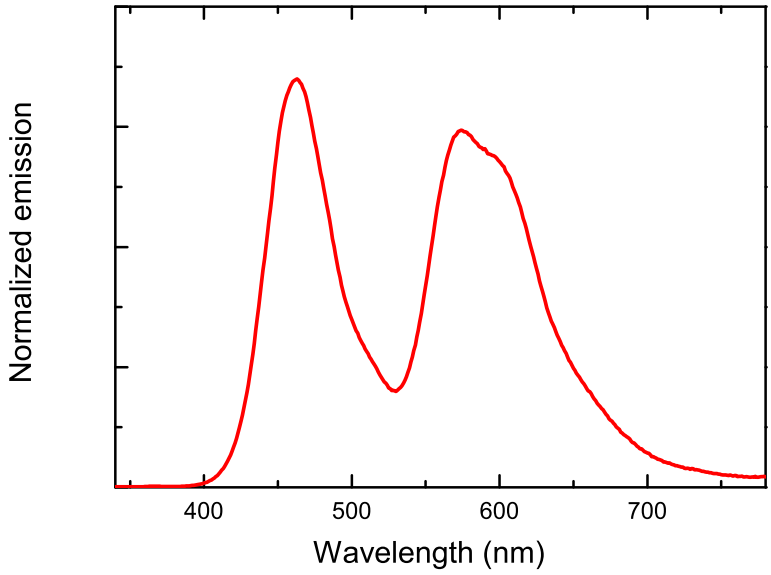

Figure 5.14: Luminescence of LUCO-LED with doped rubrene/Alq_3 film as a LUCO layer. The total LUCO layer thickness is 7000 Å at 4.4 vol% dopant concentration.

The emission spectra of LUCO-LED devices based on rubrene-doped Alq_3 films indicate that the doping concentration of around 2 vol% rubrene, optimal for highest quantum efficiency, is insufficient for obtaining white light. Up to 4000 Å LUCO film thickness, the remaining (not absorbed) primary blue light from the LED is still very intense in comparison to the yellow luminescence from the conversion layer, resulting in bluish or bluish-greenish LUCO-LED emission. The corresponding chromaticity coordinates for a 3700 Å thick LUCO film are $x' = 0.21$, $y' = 0.19$. Due to the low absorption of rubrene in the EL region of the LED, a further increase of the LUCO layer thickness at the above doping level (up to 8000 Å thickness) does not show a substantial change of the overall luminescence. The LED emission dominates the spectrum, thus the obtained LUCO-LED color is still in the blue region. However, the experiments have shown that an effective luminescence conversion to white light is obtained at 6500 - 7500 Å thick rubrene/Alq_3 films and 4 - 4.4 vol% rubrene concentration on top of the pumping diode. For example, the sample in Fig. 5.14 is characterized by CIE coordinates $x' = 0.35$, $y' = 0.31$ (see Fig. 5.15) and conversion efficiency of 0.65.

The color rendering index (CRI) of the rubrene/Alq_3 LUCO-LED is 74, which is quite good for a two-color-based converter device. For comparison, commercial blue LED/one-color phosphor white LEDs have a CRI of 70 - 80, while white LEDs comprising a blue LED and two(three)-color phosphor blend or organic white LEDs produce light with color rendering index in the region 75 - 91 [175, 176].

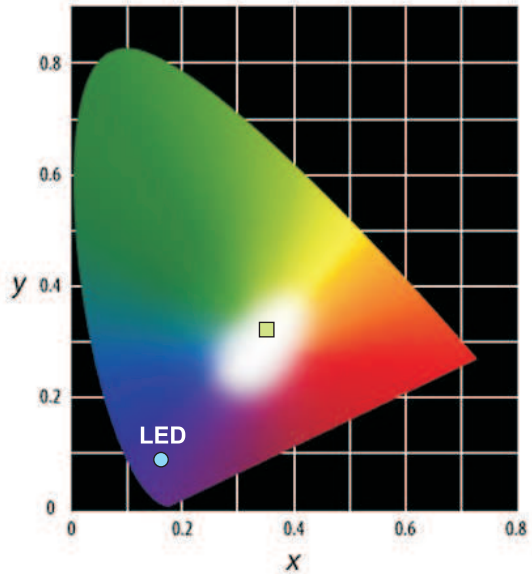

Figure 5.15: CIE diagram with the corresponding coordinates of LUCO-LED, based on 4.4 vol% doped rubrene/Alq_3 film as a LUCO layer. The color position of the primary blue LED is presented as a reference.

In contrast, the DCM-based LUCO-LED has a rather low CRI of 51. This is due to the relatively large gap in the yellowish-green region of the emission spectrum. The deposition of pure Alq_3 material in succession to the doped layer, when a saturation of the LUCO-peak intensity is reached, can be used in order to shift the LUCO-LED emission to higher energies. Thus, the color rendering index can be improved significantly.

The angular dependence of the light emitted from the converters was measured by using the emission spectrometer and the photomultiplier of the FluoroMax. The samples were mounted on a rotating holder. In the 0° rotation position, the axis joining the LUCO-LED and the entrance slit of the spectrophotometer was normal to the plane of the converter layer on top of the light-emitting diode. The distance between the sample and the entrance slit was 135 mm. The signal from the converter was measured as a function of the rotating angle φ. The latter was varied from - 90° to + 90°, with an experimental error of ± 2°. According to the obtained results (Fig. 5.16), the experimentally measured distribution of the directly emitted light from the introduced luminescence conversion devices is approximately Lambertian. The alterations in emission are negligible, thus barely any color changes can be perceived over a large viewing angle (Δx' = 0.01 - 0.07; Δy' = 0.02 - 0.05). This is an attractive quality of the introduced LUCO-LEDs, since no additional re-distribution of the emitted light is required. The viewing angle (defined as the angle at 50 % luminous intensity according to the definition in the data sheet of commercial LEDs) of about 120° is comparable to that of the commercially available white LEDs, combining blue InGaN LEDs and phosphors (typically 2φ = 110° - 120°).

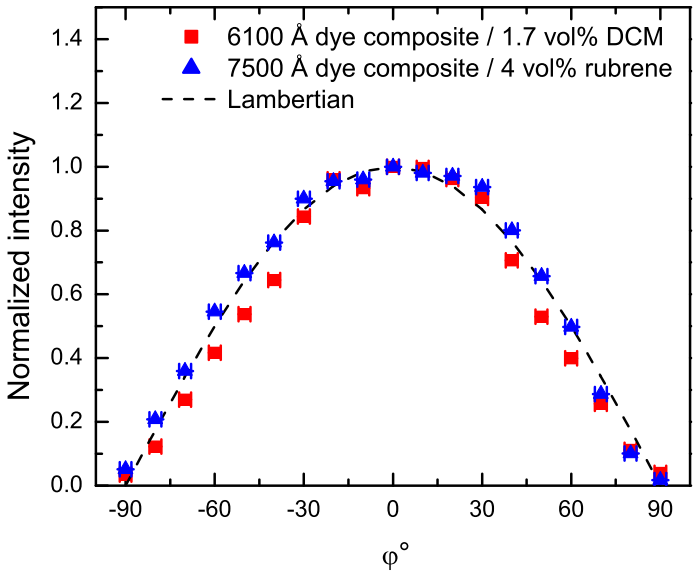

Figure 5.16: Measured angular dependence of the emission from LUCO-LEDs with doped DCM/Alq_3 and rubrene/Alq_3 films as LUCO layers. The dotted line shows the predicted angular dependence for Lambertian emission.

5.2.3 Stability

Concerning practical applications, the stability of the device performance in time is of great importance. When operated for a prolonged time, the dyes in the LUCO layer undergo thermal destruction, photochemical degradation by oxidation, or even volatilization. All these processes would lead to shift of the LUCO-LED color in direction to the initial color of the pumping LED. To check this, we recorded luminescence spectra of the devices during 20 to 40 minutes operational time in vacuum and air. Results from such measurements are presented in Figs. 5.17 and 5.18, respectively. The time evolution of the luminescence intensity of the DCM (620 nm) or rubrene (566 nm) peak and the evaluated time constants in both media are used as an indication for the photostability of the samples. The intensities of the dopant peaks are normalized to that of the irradiation source.

The luminescence intensity decreases due to degradation of dye molecules. As commented in Chapter 4, the decay behavior of the luminescence intensity in air, as well as in vacuum, is characterized by two regions: a fast drop of PL in the beginning, followed by long term decay. Here, the experimental curves are fitted using an exponential decay in the region after the fast initial decrease. Thus, mean time constants, τ_m, were determined. In vacuum, τ_m is in the range 2 - 2.5 x 10^4 s, while in air, the luminescence drops with 5 - 6.5 x 10^3 s. There is no significant difference in the time constants for rubrene and DCM.

Figure 5.19 shows an example for the time evolution of the PL spectrum of a

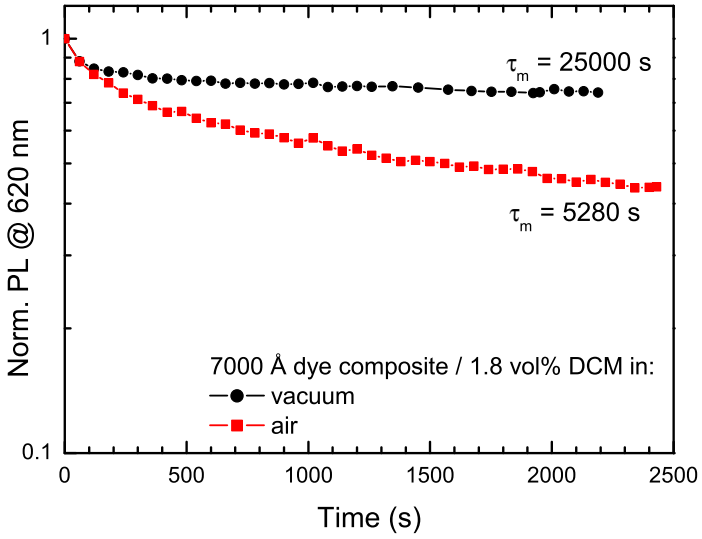

Figure 5.17: Time-dependence of the DCM luminescence peak intensity, measured in vacuum and in air, of DCM-doped Alq_3 films. The peak incidence irradiation intensity amounts to 995 mW/cm^2.

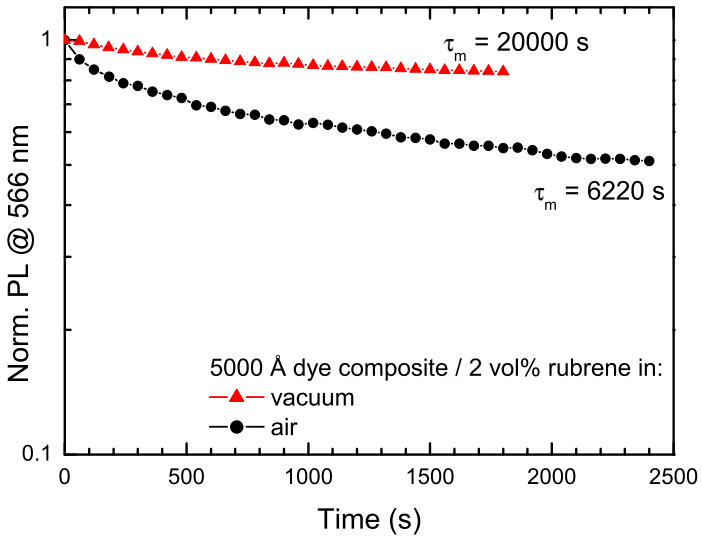

Figure 5.18: Time-dependence of the rubrene luminescence peak intensity of rubrene-doped Alq_3 films in vacuum and air. The peak excitation irradiance is 995 mW/cm^2.

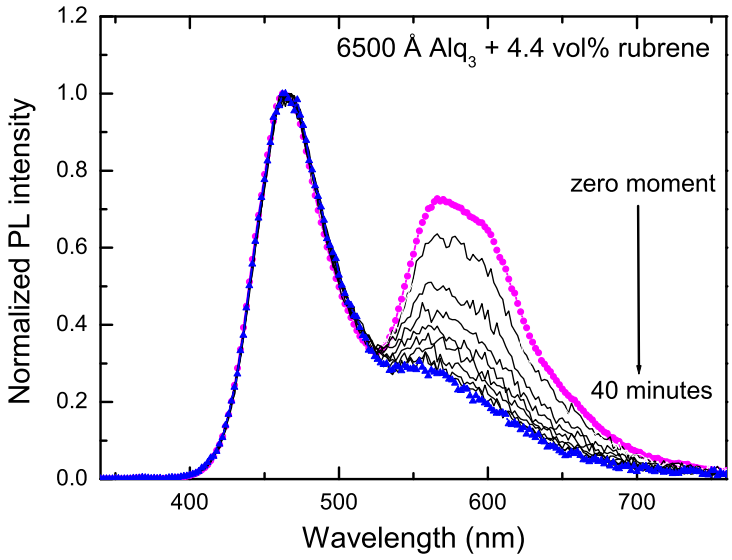

Figure 5.19: Time evolution of the luminescence intensity of LUCO-LED device with rubrene/Alq_3 films as converter layer, measured in air. In order to compensate for the power supply instabilities, the spectra are normalized to the peak intensity of the LED. The peak incident irradiance amounts to 995 mW/cm^2.

LUCO-LED device, based on rubrene/Alq_3 converter layer operating in air. An analysis of the individual luminescence spectra shows that the LUCO spectral peak position shifts to lower wavelengths. This is an implication for a reduced number of guest molecules contributing to the luminescence signal. Because of their predominant quantity in the converter layer, the Alq_3 molecules degrade slowly in comparison to the DCM or rubrene molecules. Additionally, due to the transfer of energy from the donors (Alq_3) to the acceptors (DCM, rubrene), the excited state in which the molecules are sensitive to bleaching is depopulated more quickly, thus making photodegradation a less probable process for the Alq_3 molecules [116]. Yet, the efficiency of the resonant transfer depends on the concentration of guest molecules. When there are not sufficient red emitters, the overall emission shifts to the green in direction of Alq_3 peak and the intensity decreases. Thereby, the ratio between the emission intensities of the exciting diode and the converter layer changes, revealing itself in change of the color position of the LUCO-LED.

We now present a simplified model, developed in cooperation with Markas Sudzius, IAPP, which enables the description of the experimentally observed bleaching curves and the determination of the lifetime τ for different excitation conditions. We consider the case of low irradiation intensities (below 10^5 W/cm^2) and "intrinsic" photobleaching, i.e. the contribution of a reaction partner (e.g. oxygen,

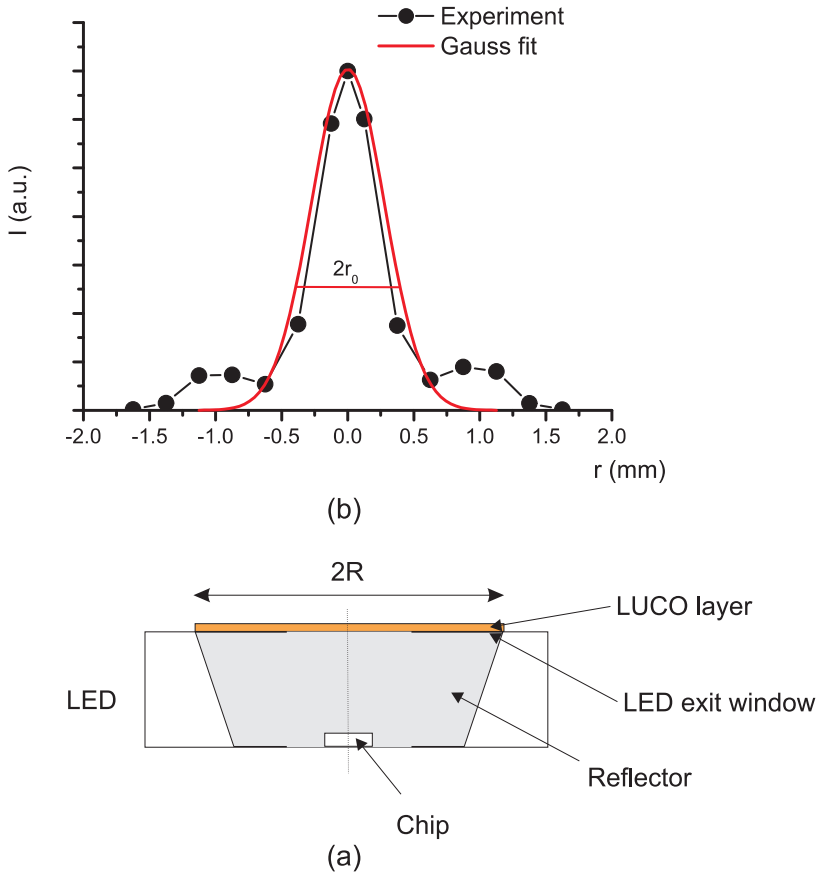

Figure 5.20: Scheme of (a) the LED with the LUCO layer on the top of its active surface and (b) the measured spatial profile of the LED intensity in the LUCO layer plane and the corresponding Gaussian fit.

impurities) to the rate of the photodegradation process is neglected. Accordingly, we assume that the product of the local excitation intensity I_{exc} and the corresponding local decay time τ of the luminescence signal from the layer is a constant

$$I_{exc} \times \tau = K. \tag{5.10}$$

Analysis of the spatial intensity distribution of the LED in the LUCO layer plane (see Fig. 5.20) has shown that it is characterized by a radial symmetry. The excitation signal I_{exc} in the film plane can be reliably described by a Gaussian profile (Fig. 5.20b):

$$I_{exc}(r) = I_{max} e^{-(r/r_0)^2}, \tag{5.11}$$

where I_{max} is the peak excitation intensity and r_0 is the radius of the Gaussian at 1/e. If the integral signal of the LED is I, then

$$I_{max} = \frac{\left(1 + \frac{1}{-1+e^{(S_{tot}/S_{eff})}}\right) I}{S_{eff}}, \tag{5.12}$$

with $S_{tot} = \pi R^2$ and $S_{eff} = \pi r_0^2$; R is the radius of the LED exit window.

We further assume an exponential decrease of the luminescence intensity. Hence, the local intensity of the PL signal is

$$I_F(r,t) = CI_{exc}(r)e^{-t/\tau(r)}, \tag{5.13}$$

with C, a constant proportional to the fluorescence quantum yield and the detection efficiency of the detection system. Using Eq. (5.10), the last equation can be re-written as

$$I_F(r,t) = CI_{exc}(r)\exp(-tI_{exc}(r)/K), \tag{5.14}$$

Consequently, the substitution of I_{exc}(r) and integration of Eq. (5.14) over the whole excitation profile leads to the solution

$$I_F(t) = \int_0^R \int_0^{2\pi} I_F(r,t)drd\theta = \frac{C\left(e^{-\frac{BtI_{max}}{K}} - e^{-\frac{tI_{max}}{K}}\right)KS_{eff}}{t}, \tag{5.15}$$

$$B = e^{-(S_{tot}/S_{eff})}. \tag{5.16}$$

If we define $\tau_{min} = K/I_{max}$ as the decay time corresponding to the peak excitation intensity, for the time-dependence of the PL signal the following expression is obtained

$$I_F(t) = \frac{C\left(e^{-\frac{Bt}{\tau_{min}}} - e^{-\frac{t}{\tau_{min}}}\right)S_{eff}I_{max}\tau_{min}}{t}. \tag{5.17}$$

A fit of the experimental PL decay signal using the $I_F(t)$ function thus derived gives the fastest decay time τ_{min} and accordingly, the constant K can be evaluated.

As introduced in Eq. (2.43), the quantum yield of photobleaching ϕ_b is

$$\phi_b = \frac{N_{bl}}{Q_{abs}}, \tag{5.18}$$

where N_{bl} is the number of degraded molecules and $Q_{abs} = AQ_0\tau$ is the number of absorbed photons during the same time interval τ. A denotes the absorption of the Alq_3 molecules in the active layer and Q_0 is the number of incident photons per unit time. However, since the LED has a certain spectral distribution, the LED spectrum is first normalized to its integral power (4.8 ± 0.3 mW). Thereby, the absolute number of incident photons is determined. Afterwards, the total number of absorbed photons is obtained by integration over the whole LED spectral range. Taking into account a probability for Förster transfer of $\simeq 1$ (for 3.5 vol% DCM distributed in Alq_3) and a fluorescence quantum yield of roughly 1, we further consider the fluorescence signal as a contribution of DCM molecules only. Thus, the integral signal I introduced in Eq. (5.12) is equivalent to the number of absorbed photons AQ_0. If we now assume that the excitation signal AQ_0 is distributed homogeneous over the area of the LED exit window πR^2, the corresponding decay time will be $\tau = K\pi R^2/AQ_0$. Hence,

$$\phi_b = \frac{0.63d\rho N_A}{Km_M} \tag{5.19}$$

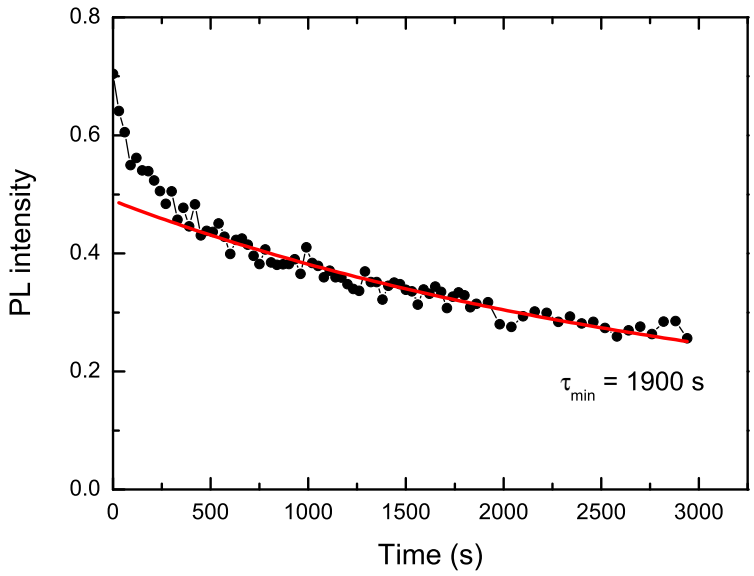

Figure 5.21: Experimental decay curve of LUCO-LED device with 3.5 vol% DCM/Alq_3 as active layer and its fit according to Eq. (5.17). The total film thickness of the LUCO layer is 4500 Å. The peak incident irradiance is 995 mW/cm^2.

with d - thickness of the DCM "layer", ρ - density of DCM, N_A - Avogadro constant, and m_M - molar mass of DCM.

The Gaussian fit of the excitation profile (Fig. 5.20b) gives a value of 0.04 cm for r_0. With R = 0.12 cm, the peak intensity of the LED is $I_{max} = 8.6 \times 10^{17}$ phot/s-cm^2. In Fig. 5.21, the experimental decay curve of a converter device with 3.5 vol% DCM/Alq_3 LUCO layer and the fit according to Eq. (5.17) are presented. The decay time τ_{min} thus obtained is 1900 s. Correspondingly, K = 1.6×10^{21} phot/cm^2. With m_M = 303 g/mol and $\rho \simeq 1.4$ g/cm^3, the quantum yield of photobleaching ϕ_b amounts to 1.7×10^{-6}. Consequently, for these excitation conditions, the number of excitation/emission cycles per molecule μ has a value of 5.9×10^5. Similar value of 6×10^5 was reported for DCM molecules incorporated by the sol-gel technique in a solid xerogel matrix [46]. There, however, the DCM molecules have been directly excited by a laser light at 532 nm and 2 kW/cm^2 irradiation intensity. We have to note here that the number of cycles is quite dependent on the chemical character of the emitting molecules, the nature of the molecular environment (i.e. organic or inorganic), the excitation conditions, etc. For instance, in the solid xerogel matrix, perylene orange has almost two orders of magnitude higher photostability than that of rhodamine 6G ($\mu = 1 \times 10^9$ and $\mu = 2 \times 10^7$, respectively) [46], whereas cycles of the order of 10^{11} were obtained

for red OLED using $Ir(piq)_3$[1] as emitter and α-NPD[2] as a host [177] as well as for co-deposited PTCDA/SiO_2 films [14].

In OLEDs, studies on device performance with Alq_3 as a host and DCM or rubrene as dopants generally discuss the emission mechanism and efficiency. Stability investigations consider mostly rubrene and its stabilizing role as a dopant or an assist-dopant in Alq_3 emitter layers [167, 168, 169]. For instance, lifetimes of 1300 to 3000 h at an initial luminance of about 500 cd/m^2 are reported for encapsulated devices [167, 169]. The improved stability is attributed to be due to the stabilizing effect of rubrene on the amorphous state of Alq_3 [167, 168]. Also, the different mechanism of light emission in the presence of rubrene is suggested to reduce further the device degradation. Since the HOMO and LUMO of rubrene are located within the energy gap of Alq_3, rubrene acts as a trap for both electrons and holes, thus recombination occurs on the dopant molecules [167, 169].

For the samples studied, due to the Förster transfer, the photostability of the guest molecules is defining for the luminescence decay. However, amorphous rubrene is known to be prone to oxidation [170]. Similarly, photooxidation is established to be the degradation mechanism for DCM upon light excitation [171]. Since the vacuum chamber assures a more controllable chemical environment compared to an air atmosphere, the higher stability of the samples in vacuum is reasonable to anticipate. In air, interactions with impurities and in particular with the oxygen can not be avoided, thereby leading to acceleration of the degradation process. Suitable encapsulation, preventing from water and oxygen exposure, can thus increase the lifetime.

In order to improve the device photostability, we further examined the effect of polyimide as protective layer, grown directly on top of the LUCO-LED. PI was selected due to its high mechanical, thermal, and photostability. The optimal PI film thickness was defined with respect to (i) relatively low curing temperature in accordance with the low sublimation temperatures of the LUCO dyes in order to avoid thermal destruction of the dyes and transformation of the initial LED and (ii) effective polymerization (high level of transformation of the monomers to PI) at these low curing temperatures. Hence, the grown PMDA-ODA films are 2000 Å thick. At this thickness, the PI layer has negligible absorption in the emission range of the exciting light-emitting diode.

The first samples were treated for 1 hour at 200°C. However, the resulting LUCO-LED spectra showed a strong shift of the LUCO peak to the high energy spectral range (about 56 nm) in addition to decreased LUCO intensity with respect to the uncured samples. Moreover, the intensity of the remaining primary LED light was increased, suggesting a reduced number of absorbing molecules. These effects could be due to sublimation or thermal degradation of host as well as guest DCM molecules since, as discussed, above 5000 Å LUCO layer thickness the guest molecules also contribute to the overall absorption. Therefore, the curing temperature was lowered to 150°C. Additionally, in order to compensate for

[1] tris(1-phenylisoquinoline) iridium (III)
[2] N,N'-di(naphthalene-2-yl)-N,N'-diphenyl-benzidine

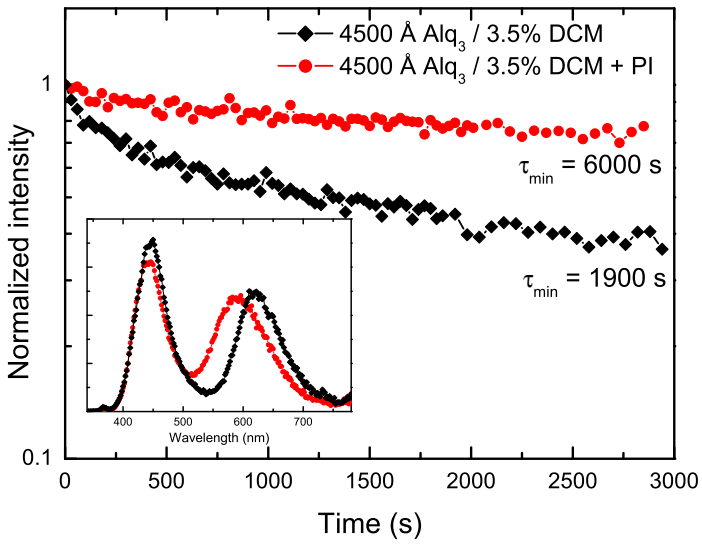

Figure 5.22: Time-dependence of the luminescence peak intensity of LUCO-LED DCM/Alq_3 devices with and without PI as protective layer. PI is treated for 1h at 150°C. In the inset, the initial emission spectra are presented. The peak LED intensity is 995 mW/cm^2.

the LUCO-LED color changes after the thermal treatment of the polyimide top layer, the concentration of DCM was increased above the optimal 2 vol%. Figure 5.22 presents the corresponding initial PL spectra of the LUCO-LED devices, along with the time dependence of the LUCO peak intensities. Comparison of the emission spectra indicates that this curing procedure is more friendly toward the organic molecules. The chromaticity coordinates change only slightly: x' = 0.34, y' = 0.27 after the curing with respect to x' = 0.35, y' = 0.21 without PI. The time evolution of the LUCO emission points at an increased photostability for the device with the PI protective layer by a factor of 3. Thus, the PI film has a positive influence on the photostability of the LUCO layers, reducing the impact of the reactive atmosphere on the photobleaching.

5.3 Summary

In this Chapter, we first studied the optical response of doped with DCM and rubrene Alq_3 films. In the context of dye/optically active matrix interactions, we emphasize the following dependencies: (i) Efficient Förster energy transfer from the optically active host Alq_3 to the guest molecules results in enhanced luminescence efficiency (ii) Aggregation of guest molecules leads to shift of PL maximum and decrease of luminescence (iii) PL intensity and peak position are concentration dependent. The highest PL efficiency is reached at $\sim$ 2 vol% guest dye quantity

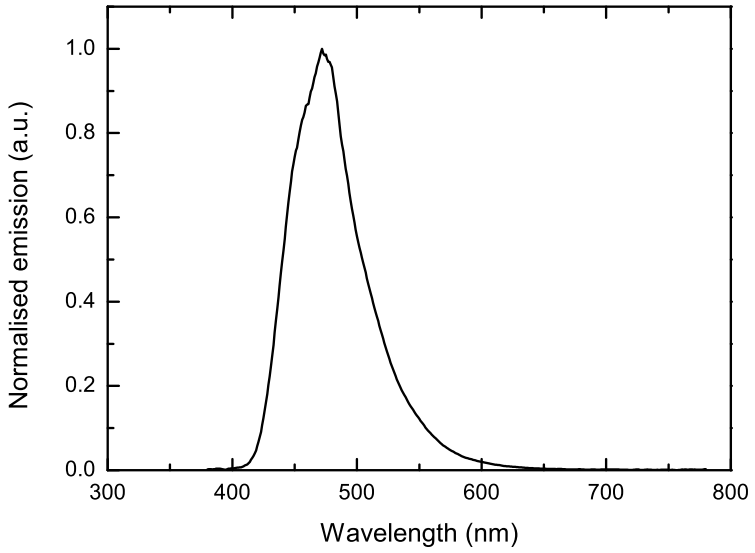

Figure 5.23: Normalized emission spectrum of a blue OLED with Spiro-DPVBi emission layer

which is in a good agreement with the determined Förster radius (iv) Doped Alq_3 films degrade relatively fast in both vacuum and air. Consequently, the results suggest that the optical behavior and photostability of a dye/active matrix system follow the general dependencies established in the previous Chapter: The distribution of dye molecules in the matrix influences their emission independent of the matrix character, active or inert. In contrast, the photobleaching is affected by both molecular distribution and matrix nature, rigid or flexible.

Next, we presented examples for an application of the molecularly doped Alq_3 thin films as effective luminescence conversion layers in combination with blue LEDs as primary light sources. We demonstrated that, depending on the LUCO film thickness and doping ratio, the primary blue light can be converted into white light. The introduced LUCO-LED devices are compact and easy to fabricate. They are characterized by high conversion efficiency, nearly Lambertian emission and relatively high colour rendering index. Thus, selective doping of one of the most promising emitters is an attractive way not only for increasing the PL quantum yield, but can also be applied for fabrication of white-emitting hybrid LEDs. Yet, the low values of the decay time constants, along with the relatively fast change of emission color, demonstrate the insufficient stability.

Until now, we discussed the stability of the LUCO layers when excited with an inorganic LED, i.e. an inhomogeneous, small-area, high-luminance source. Let us now make a transition to a homogeneous, large-area, low-luminance excitation source and consider the case of luminescence conversion device based on a doped Alq_3 film and organic blue LED with a luminous intensity I_v of 100 cd/m^2. A

typical spectrum of a blue OLED using Spiro-DPVBi[3] as emitter material is presented in Fig. 5.23 (the spectrum is provided by Thomas Rosenow, IAPP). Then, using the relation between the radiant flux P and the luminous flux Φ_v of the OLED

$$\Phi_v = 683\ lm/W \int_{380}^{780} P(\lambda)V(\lambda)d\lambda, \tag{5.20}$$

with V(λ) the eye sensitivity function, we can calculate the decay time of the LUCO layer. For that purpose, we apply Eq. (5.10) in which I_{exc} now corresponds to the number of absorbed photons per square meter at an incident illuminance of 100 cd/m^2 and K is the constant determined from the model presented above. Thus, for the doped 3.5 vol% DCM/Alq_3 LUCO layer without encapsulation[4] (cf. Fig 5.22) we find a lifetime of 10880 h. For the device with PI protective layer, using a linear extrapolation

$$I_v \times \tau = const, \tag{5.21}$$

the decay time increases to values higher than those referred for OLEDs with doped rubrene/Alq_3 emitter films (about 6530 h for illuminance of 500 cd/m^2, cf. p. 141 above). In order to further improve the LUCO-LED performance lifetime, the development of an adequate encapsulation technique is required. PI is not optimal as encapsulation layer, since the thermal stability of the used organic dyes puts restraints on the PI curing temperature.

[3] 2,2',7,7'-tetrakis-(diphenylvinyl)spiro-9,9'-bifluorene

[4] For the purpose of comparison, we used exactly the same LUCO layer parameters as in the case of the inorganic LUCO-LED device. However, since the spectrum of the OLED is shifted to higher wavelengths with respect to that of the inorganic LED, an optimization of the LUCO layer might be necessary, for example, in order to generate white light.

6 Conclusions and outlook

6.1 Conclusions

In this thesis, we investigated solid solutions of organic dye molecules in various types of hosts - organic and inorganic, optically active and inert. The dyes under study, perylene, 2,2-difluoro-1,3,2-dioxaborine derivatives, and Alq_3, were chosen with respect to their particular structural properties. For all dyes, we have shown that the preparation of stable and reproducible luminescent solid systems using physical vapor deposition is feasible. However, extensive experimental experience indicates that the high temperature required for evaporation of the inorganic SiO_2 matrix could in some cases spoil the luminescent properties of the systems, due to lack of thermal stability of the organic compounds.

The results obtained reveal that the optical response of the studied solid solutions depends on dye distribution and thin film structure. In the matrix, it is possible to achieve enhanced photoluminescence quantum efficiency with respect to the pure dye film. Determinant for the PL efficiency is the Förster transfer since, due to migration of excitation, the energy transfer to dye aggregates or destructed (inactive) molecules, leads to decrease of the luminescence efficiency. Therefore, the effective isolation and separation of dye molecules in the matrix (predominant monomer distribution) results in increased PL efficiency.

We have demonstrated that the microscopic structure of the mixed films can be affected by the preparation technology. Alterations in preparation scheme, dynamic state of the substrate, etc., result in diverse properties at the same macroscopic dye concentration. We introduced a layer-by-layer growth mode which allows to control the molecular distribution in two directions - in plane and in depth of the film. With respect to the classical co-deposition approach, for all investigated dyes incorporated in SiO_2, layer-by-layer growth assures more homogeneous dye distribution. Moreover, the spectroscopic studies show that, since dye and matrix condense successively in time, luminescence losses due to thermal degradation of molecules are reduced. Hence, the film structure can be optimized with regard to high absorption and luminescence quantum efficiency.

Further, we have shown that, similar to liquid solutions, the luminescent properties of the embedded dyes are influenced by the nature of the host environment as well. In the rigid SiO_2 matrix, it is possible to observe isolated *fac*-Alq_3 molecules with distinctive blue luminescence. In contrast, in the "soft" organic PI matrix Alq_3 exhibits the ordinary green luminescence. Thus, the structural properties of the SiO_2 host, rigidity and density, are found to be crucial for the preservation of the *fac*-Alq_3 molecules. Similarly, due to the rigidity of the SiO_2 environment, the formation of free rotamers is impeded. Hence, the incorporation of unbridged 2,2-difluoro-1,3,2-dioxaborine derivatives in SiO_2 results in increased PL efficiency.

The photostability studies carried out indicate that the structure of the host

affects also the photobleaching behavior of the solid dye solution. Molecules incorporated in the inorganic SiO_2 matrix show higher stability against irradiation. Although oxygen is able to penetrate through SiO_2 and reach the dye, increasing the host density and homogeneity results in more efficient trapping of the molecules. In general, the rigid matrix environment restricts considerably molecular motions, and thus the probability for participation in photobleaching reactions decreases.

In PI matrix, according to the absorption and luminescence spectra, the behavior of the dye molecules is governed by the morphological changes of the host. These changes are defined by the curing procedure, needed for imidization, and give rise to a certain film structure. Consequently, the photophysical properties of the mixed dye/PI layers have to be discussed in dependence on the particular experimental parameters. In contrast to the stiff SiO_2 matrix, PI allows a limited dye motion. Thus, in PI the separation and isolation of molecules at higher dye concentrations is less effective compared to SiO_2.

Finally, our studies confirmed that the incorporation of DCM and rubrene molecules in the optically active Alq_3 host leads to efficient Förster transfer of the excitation energy from Alq_3 to the guest molecules. The luminescence and photobleaching behavior follow the general tendencies established for dye molecules in the optically inert hosts SiO_2 and PI. Emission is affected by the guest distribution in the matrix: PL intensity and peak position are concentration dependent. At optimal dopant concentration of around 2 vol%, the luminescence efficiency achieved is close to unity. Photostability depends on matrix nature: In the plastic Alq_3 host, molecules degrade faster than in the rigid SiO_2. It is also affected by molecular distribution: Molecular aggregates are less stable than isolated molecules.

On the basis of doped Alq_3 films, we realized luminescence conversion devices using commercial blue LEDs as primary light sources. Optimization of the LUCO layer parameters resulted in effective white light generation. The LUCO devices have high conversion efficiency, nearly Lambertian emission and color rendering index comparable to that of commercial two-color LUCO-LEDs. However, they show the disadvantage of low photostability and thus are rather ineligible for applications without an adequate encapsulation.

6.2 Outlook

In the present thesis, several issues require some further experimental and theoretical considerations. The first one concerns the photobleaching mechanism in the studied solid systems. According to the obtained results, it is necessary to consider two different types of mechanisms: one for the isolated molecules and another including dye-dye interactions. For that purpose, it is necessary to identify the products of the photodegradation reaction. This can be done using for example mass spectrometric methods. First experiments in this direction on irradiated dye/SiO_2 films were carried out, however without satisfactory results. The difficulties lie mainly in the low dye quantities in the layers, and correspondingly low detection sensitivity. Additionally, since oxygen is found to play double role

in the photobleaching reactions, i.e. participating in formation of non-fluorescing complexes or deactivating long living dark states, as discussed in [151], in order to clarify its influence on the studied systems irradiation, experiments should be performed in high vacuum as well. Because the porosity of the SiO_2 host is found to be significant for the photostability, detailed studies of the film morphology in dependence on the matrix evaporation rate, combined with photobleaching measurements have to be carried out. The specific surface area and pore volumes can be determined using the standard BET (Brunauer-Emmett-Teller) method.

Second, as commented in Section 4.1.3, due to the low molecular concentration, it was not possible to prove the presence of facial Alq_3 molecules in the SiO_2 matrix by an independent method. The problem can be solved by assuring experimental conditions at which the facial molecules can be extracted from the matrix and at the same time conserved in the facial state. This can be done using a suitable solvent while keeping the samples at low temperature (e.g. in dry ice). For identification of the *fac*-Alq_3 molecules simply luminescence spectroscopy can be used. Besides, preparation of mixed layers of Alq_3 in thermally evaporable matrices, for example LiF, and study of their luminescent properties, can verify the assumption for thermal interactions between the dye and the matrix causing isomer transformation. It is known that, similar to Alq_3, $Ir(ppy)_3$ exists in two isomer forms and the meridional isomer converts to the facial one during high-temperature synthesis [160]. Therefore, as complimentary study the luminescence behavior of incorporated in the SiO_2 host $Ir(ppy)_3$ molecules should be followed.

Third, systematic structural studies on dye/PI layers in dependence on thermal treatment conditions can help to resolve the effect of the matrix morphology on the optical response of the embedded dyes. For that purpose, microscopic techniques such as SEM or transmission electron microscopy (TEM) can be applied. For a deeper understanding of the relaxation processes in the dye-polymer system, these experiments should be carried out in combination with low-temperature and transient PL measurements.

Finally, both high luminescence efficiency and stability can be achieved if the improved resistivity against photobleaching in SiO_2 is combined with efficient Förster energy transfer, as in the case of doped Alq_3 films. A feasible solution represents the selective doping of a host dye within the matrix. The results in this direction obtained so far have not been satisfactory. However, this could be due to several reasons: low thermal stability of the embedded dopant dyes, alteration of the spectral properties of the donor and thus following violation of the requirements for resonant transfer, etc. Therefore, it is reasonable to carry out further experiments, including new combinations of donor - acceptor pairs, extensive analysis of the individual spectral response of donor and acceptor embedded in SiO_2, examination of various doping ratios within the inorganic matrix, and so on.

Bibliography

[1] C. W. Tang, *Appl. Phys. Lett.* 48 (1986) 183

[2] C. W. Tang and S. A. VanSlyke, *Appl. Phys. Lett.* 51 (1987) 913

[3] J. K. Mahon and M.-H. M. Lu, *Solid State Technology Online* January 04 (2005), http://www.solid-state.com

[4] C. D. Dimitrakopoulos and D. J. Mascaro, *IBM J. Res. & Dev.* 45 (2001) 11

[5] P. Peumans, V. Bulovic, and S. R. Forrest, *Appl. Phys. Lett.* 76 (2000) 2650

[6] S. E. Shaheen, C. J. Brabec, N. S. Sariciftci, F. Padinger, T. Fromherz, and J. C. Hummelen, *Appl. Phys. Lett.* 78 (2001) 841

[7] W. Ma, C. Yang, X. Gong, K. Lee, and A. J. Heeger, *Adv. Funct. Mater.* 15 (2005) 1617

[8] P. Schlotter, R. Schmidt, and J. Schneider, *Appl. Phys. A* 64 (1997) 417

[9] A. Costela, I. Garcia-Moreno, J. Barroso, and R. Sastre, *J. Appl. Phys.* 83 (1998) 650

[10] A. Costela, I. Garcia-Moreno, J. M. Figuera, F. Amat-Guerri, R. Mallavia, M. D. Santa-Maria, and R. Sastre, *J. Appl. Phys.* 80 (1996) 3167

[11] D. Avnir, D. Levy, and R. Reisfeld, *J. Phys. Chem.* 88 (1984) 5956

[12] B. M. Krasovitskii and B. M. Bolotin, *Organic Luminescent Materials*, VCH, Weinheim (1988)

[13] S. V. Gaponenko, I. N. Germanenko, A. P. Stupak, M. Eyal, D. Brusilovsky, R. Reisfeld, S. Graham, and C. Klingshirn, *Appl. Phys. B* 58 (1994) 283

[14] H. Fröb, M. Kurpiers and K. Leo, *MRS Spring Meeting '99*, 103; publ. by Material Research Society, San Francisco/CA (USA), 1999

[15] K. Yagi, S. Shibata, T. Yano, A. Yasumori, M. Yamane, and B. Dunn, *J. Sol-Gel Sci. Technol.* 4 (1995) 67

[16] J. G. Calvert and J. N. Pitts, *Photochemistry*, Wiley, New York (1966)

[17] T. Suratwala, Z. Gardlund, K. Davidson, D. R. Uhlmann, J. Watson, and N. Peyghambarian, *Chem. Mater.* 10 (1998) 190

[18] D. Avnir, V. R. Kaufman, and R. Reisfeld, *J. Non-Cryst. Sol.* 74 (1985) 395

[19] R. E. Hermes, T. H. Allik, S. Chandra, and J. A. Hutchinson, *Appl. Phys. Lett.* 63 (1993) 877

[20] M. V. Bondar, O. V. Przhonska, and Y. A. Tikhonov, *J. Phys. Chem.* 96 (1992) 10831

[21] S. Jäger and H. Böttcher, *Adv. Mater.* 8 (1996) 93

[22] S. Jäger, *Surf. Coat. Techn.* 93 (1997) 58

[23] S. Jäger, *Thin Solid Films* 286 (1996) 154

[24] H. Böttcher, O. Hertz, and M. A. Fox, *Chem. Phys. Lett.* 158 (1989) 453

[25] H. Böttcher, T. Fritz, and B. Vaupel, *Z. Chem.* 29 (1989) 368

[26] E. Spassova, *Vacuum* 70 (2003) 551

[27] M. Brinkmann, G. Gadret, M. Muccini, C. Taliani, N. Masciocchi, and A. Sironi, *J. Am. Chem. Soc.* 122 (2000) 5147

[28] A. Curioni, W. Andreoni, R. Treusch, F. J. Himpsel, E. Haskal, P. Seidler, C. Heske, S. Kakar, T.van Buuren, and L. J. Terminello, *Appl. Phys. Lett.* 72 (1998) 1575

[29] A. Curioni, M. Boreo, and W. Andreoni, *Chem. Phys. Lett.* 294 (1998) 263

[30] V. Bulovic, M. A. Baldo, and S. R. Forrest (Chapter 11) in: *Organic Electronic Materials, Conjugated Polymers and Low Molecular Weight Organic Solids*, R. Farchioni and G. Grosso (Eds.), Springer-Verlag, Berlin Heidelberg (2001)

[31] M. Pope and C. E. Swenberg (Eds.), *Electronic processes in organic crystals*, Oxford University Press, New York (1982)

[32] M. Klessinger and J. Michl, *Excited States and Photochemistry of Organic Molecules*, VCH, New York (1995)

[33] K. Puech, H. Fröb, M. Hoffman, and K. Leo, *Optics Lett.* 21 (1996) 1606

[34] A. Gilbert and J. Baggot, *Essentials of Molecular Photochemistry*, Blackwell Scientific Publications, Oxford (1991)

[35] Z. Shen and S. R. Forrest, *Phys. Rev. B* 55 (1997) 10578

[36] A. A. Shoustikov, Y. You, and M. Thompson, *IEEE Journal of Selected Topics of Quantum Electronics* 4 (1998) 3

[37] Christian Reichardt, *Solvents and Solvent Effects in Organic Chemistry*, Wiley-VCH Publishers, Weinheim (1988)

[38] A. Sharma and S. G. Schulman, *Introduction to Fluorescence Spectroscopy*, Wiley-Interscience Publication, New York (1999)

[39] V. Bulovic, S. Coe, C. Madigan, and D. Mascaro, *Research Laboratory of Electronics Progress Report*, Massachusetts Institute of Technology, 143 (2000) 13

[40] V. Bulovic, R. Deshpande, M. E. Thompson, and S. R. Forrest, *Chem. Phys. Lett.* 308 (1999) 317

[41] C. Eggeling, J. Widengren, R. Rigler, and C. A. M. Seidel (Chapter 10) in: W. Retting, B. Strehmel, S. Schrader, and H. Seifert (Eds.), *Applied Fluorescence in Chemistry, Biology and Medicine*, Springer-Verlag, Berlin Heidelberg (1999)

[42] A. Reuther, D. N. Nikogosyan, and A. Laubereau, *J. Phys. Chem.* 100 (1996) 5570

[43] T. Suratwala, K. Davidson, Z. Gardlund, and D. R. Uhlmann, *SPIE* 2986 (1997) 141

[44] H. Piwonski, R. Kolos, A. Meixner, and J. Sepiol, *Chem. Phys. Lett.* 405 (2005) 352

[45] T. Suratwala, Z. Gardlund, K. Davidson, D. R. Uhlmann, J. Watson, S. Bonilla, and N. Peyghambarian, *Chem. Mater.* 10 (1998) 199

[46] A. Dubois, M. Canva, A. Brun, F. Chaput, and J.-P. Boilot, *Synth. Met.* 81 (1996) 305

[47] M. Talhavini, W. Corradini, and T. D. Z. Atvars, *J. Photochem. Photobiol. A* 139 (2001) 187

[48] R. Zondervan, F. Kulzer, M. A. Kol'chenko, and M. Orrit, *J. Phys. Chem. A* 108 (2004) 1657

[49] M. Talhavini and T. D. Z. Atvars, *J. Photochem. Photobiol. A* 114 (1998) 65

[50] T. Suratwala, Z. Gardlund, K. Davidson, D. R. Uhlmann, S. Bonilla, and N. Peyghambarian, *J. Sol-Gel Sci. Tech.* 8 (1997) 953

[51] R. L. Fork and Z. Kaplan, *Appl. Phys. Lett.* 20 (1972) 472

[52] M. Kurpiers, Diploma Thesis, *Untersuchungen an Farbstoff-Einzelmolekül-/Clusterschichten*, Technische Universität Dresden (1997)

[53] W.-K. Wen, J.-H. Jou, H.-S. Wu, and C.-Li Cheng, *Macromolecules* 31 (1998) 6515

[54] A. Quaranta, S. Carturan, G. Maggioni, G. Della Mea, M. Ischia, and R. Campostrini, *Appl. Phys. A* 72 (2001) 671

[55] Z. Zhi-Iin, J. Xue-yin, X. Shao-hong, T. Nagamoto, and O. Omoto, *J. Phys. D* 31 (1998) 32

[56] C.-Ti Chen, *Chem. Mater.* 16 (2004) 4389

[57] Y. W. Ko, C.-H. Chung, J. H. Lee, Y.-H. Kim, Ch.-Y. Sohn, B.-C. Kim, C.-S. Hwang, Y.-H. Song, J. Lim, Y.-J. Ahn, G.-W. Kang, N. Lee, and C. Lee, *Thin Solid Films* 426 (2003) 246

[58] G. Y. Zhong, J. He, S. T. Zhang, Z. Xu, Z. H. Xiong, H. Z. Shi, X. M. Ding, W. Huang, and X. Y. Hou, *Appl. Phys. Lett.* 80 (2002) 4846

[59] H. Murata, C. D. Merritt, and Z. H. Kafafi, *IEEE Journal of Selected Topics in Quantum Electronics* 4 (1998) 119

[60] T.-H. Liu, C.-Y. Iou, S.-W. Wen, and C. H. Chen, *Thin Solid Films* 441 (2003) 223

[61] N.-H. Lee, M.-J. Lee, J.-Ho Song, C. Lee, and D.-H. Hwang, *Mat. Sci. Eng. C* 24 (2004) 233

[62] V. Bulovic, A. Shoustikov, M. A. Baldo, E. Bose, V. G. Kozlov, M. E. Thompson, and S. R. Forrest, *Chem. Phys. Lett.* 287 (1998) 455

[63] T. Mori, K. Obata, and T. Mizutani, *J. Phys. D* 32 (1999) 1198

[64] C. W. Tang, S. A. VanSlyke, and C. H. Chen, *J. Appl. Phys.* 65 (1989) 3610

[65] H. Mattoussi, H. Murata, C. Merritt, Y. Iizumi, J. Kido, and Z. H. Kafafi, *J. Appl. Phys.* 86 (1999) 2642

[66] R. S. Deshpande, V. Bulovic, and S. R. Forrest, *Appl. Phys. Lett.* 75 (1999) 888

[67] G.Klebe, F. Graser, E. Hädicke, and J. Berndt, *Acta Cryst. B* 45 (1989) 69

[68] F. Graser and E. Haedicke, *Liebigs Ann. Chem.* (1984) 483

[69] M. Hoffmann, PhD thesis, *Frenkel and Charge-Transfer Exsitons in Quasi-One-Dimensional Molecular Crystals with strong Intermolecular Orbital overlap*, Technische Universität Dresden (2000)

[70] Y. Hamada, T. Sano, M. Fujita, T. Fujii, Y. Nishio, and K. Shibata, *Jpn. J. Appl. Phys.* 32 (1993) L514

[71] P. E. Burrows and S. R. Forrest, *Appl. Phys. Lett.* 64 (1994) 2285

[72] T. Mori, H. Fujikawa, S. Tokito, and Y. Taga, *Appl. Phys. Lett.* 73 (1998) 2763

[73] D. S. Qin, D. C. Li, Y. Wang, J. D. Zhang, Z. Y. Xie, G. Wang, and L. X. Wang, *Appl. Phys. Lett.* 78 (2001) 437

[74] W. Brütting, S. Berleb, and A. G. Mückl., *Org. Electr.* 2 (2001) 1

[75] W. Brütting, H. Riel, T. Beielein, and W. Riess., *J. Appl. Phys.* 89 (2001) 1704

[76] G. M. Credo, D. L. Winn, and S. K. Buratto, *Chem. Mater.* 13 (2001) 1258

[77] L. F. Cheng, L. S. Liao, W. Y. Lai, X. H. Sun, N. B. Wong, C. S. Lee, and S. T. Lee, *Chem. Phys. Lett.* 319 (2000) 418

[78] R. L. Martin, J. D. Kress, I. H. Campbell, and D. L. Smith, *Phys. Rev. B* 61 (2000) 15804

[79] P. E. Burrows, Z. Shen, V. Bulovic, D. M. McCarty, S. R. Forrest, J. A. Cronin, and M. E. Thompson, *J. Appl. Phys.* 79 (1996) 7991

[80] P. E. Burrows, L. S. Sapochak, D. M. Mackarty, S. R. Forrest, and M. E. Thompson, *Appl. Phys. Lett.* 64 (1994) 2718

[81] M. Braun, J. Gmeiner, M. Tzolov, M. Coelle, F. D. Meyer, W. Milius, H. Hillebrecht, O. Wendland, J. U. von Schütz, and W. Brütting, *J. Chem. Phys.* 114 (2001) 9625

[82] M. Cölle, R. E. Dinnebier, and W. Brütting, *Chem. Commun.* 23 (2002) 2908

[83] M. Cölle, J. Gmeiner, W. Milius, H. Hillebrecht, and W. Brütting, *Adv. Funct. Mater.* 13 (2003) 108

[84] M. Brinkmann, B. Fite, S. Pratontep, and C. Chaumont, *Chem. Mater.* 16 (2004) 4627

[85] K. A. Higginson, X.-M. Zhang, and F. Papadimitrakopoulos, *Chem. Mater.* 10 (1998) 1017

[86] G. Görlitz, H. Hartmann, J. Kossanyi, P. Valat, and V. Wintgens, *Ber. Bunsenges. Phys. Chem.* 102 (1998) 1449

[87] Y. Dromzee, J. Kossanyi, V. Wintgens, P. Valat, H. Hartmann, and G.Görlitz, *Z. Kristallogr.* 212 (1997) 372

[88] A. G. Mirochnik, B. V. Bukvetskii, E. V. Fedorenko, and V. E. Karasaev, *Russ. Chem. Bull., Int. Ed.* 53 (2004) 291

[89] M. Halik, Ph.D.-thesis, *2,2-Difluor-1,3,2-(2H)-dioxaborine als Bausteine zur Darstellung von langwellig absorbierenden Methinfarbstoffen*, Martin-Luther-Universität Halle-Wittenberg (1998)

[90] P. Czerney, C. Igney, G. Haucke, and H. Hartmann, *Z. Chem.* 28 (1988) 23

[91] G. Haucke, P. Czerney, H.-D. Ilge, D. Steen, and H. Hartmann, *J. Mol. Struct.* 219 (1990) 411

[92] K. Hübner, *Isolatorphysik des SiO_2*, Akademie Verlag, Berlin (1984)

[93] S.-C. Hsu, W.-T. Whang, and S.-C. Chen, *J. Polym. Res.* 10 (2003) 7

[94] S. S. Hardaker and R. J. Samuels, *J. Polym. Sci. B* 35 (1997) 777

[95] J. E. Mahan, *Physical Vapor Deposition of Thin Films*, Wiley Interscience Publication, New York (2000)

[96] O. S. Heavens, *Optical Properties of Thin Films*, Butterworths Scientific Publications, London (1955)

[97] A. B. Djurisic, T. Fritz, and K. Leo, *Opt. Comm.* 183 (2000) 123

[98] T.Fritz, J. Hahn, and H. Böttcher, *Thin Solid Films* 170 (1989) 249

[99] D. L. Andrews, *Perspectives in Modern Chemical Spectroscopy*, Springer Verlag, Berlin Heidelberg (1990)

[100] N. C. Greenham, I. D. W. Samuel, G. R. Hayes, R. T. Phillips, Y. A. R. R. Kessener, S. C. Moratti, A. B. Holmes, and R. H. Friend, *Chem. Phys. Lett.* 241 (1995) 89

[101] CERAC *Coating Materials News* 15 (2005) 2, http://www.cerac.com

[102] C. A. Parker, *Photoluminescence of Solutions*, Elsevier, Amsterdam (1968)

[103] M. Hoffmann, K. Schmidt, T. Fritz, T. Hasche, V. M. Agranovich, and K. Leo, *Chem. Phys.* 258 (2000) 73

[104] M. Hoffmann and Z. G. Soos, *Phys. Rev. B* 66 (2002) 024305

[105] M. Hoffmann, Z. G. Soos, and K. Leo, *Nonlin. Optics* 29 (2002) 227

[106] T. W. Canzler, PhD thesis, *Ultrafast Dynamics in Quasi-One-Dimensional Organic Molecular Crystals. Self-Assembled Monolayers of Photochromic Molecules*, Technische Universität Dresden (2002)

[107] E. Engel, K. Schmidt, D. Beljonne, J.-L. Brédas, J. Assa, H. Fröb, K. Leo, and M. Hoffmann, *Phys. Rev. B* 73 (2006) 245216

[108] H. Langhals, J. Karolin, and L. B.-Å. Johansson, *J. Chem. Soc., Faraday Trans.* 94 (1998) 2919

[109] Y. Takahashi, M. Iijima, K. Inagawa, and A. Itoh, *J. Vac. Sci. Technol.* A 5 (1987) 2253

[110] J. R. Lakowicz, *Topics in Fluorescence spectroscopy*, Plenum press, New York London (1991)

[111] A. Nollau, M. Hoffmann, K. Floreck, T. Fritz, and K. Leo, *J. Appl. Phys.* 87 (2000) 7802

[112] R. Gehlhaar, Diploma thesis, *Untersuchungen an Festkörperlösungen organischer Farbstoff-Moleküle*, Technische Universität Dresden (2002)

[113] V. Bulovic, P. E. Burrows, S. R. Forrest, J. A. Cronin, and M. E. Thompson, *Chem. Phys.* 210 (1996) 1

[114] H. Proehl, T. Dienel, R. Nitsche, and T. Fritz, *Phys. Rev. Lett.* 93 (2004) 097403

[115] M. Talhavini and T. D. Z. Atvars, *J. Photochem. Photobiol. A* 120 (1999) 141

[116] A. Imhof, M. Megens, J. J. Engelberts, D. T. N. de Lang, R. Sprik, and W. L. Vos, *J. Phys. Chem. B* 103 (1999) 1408

[117] M. Amati and F. Lelj, *J. Phys. Chem.* 107 (2003) 2560

[118] A. Curioni and W. Andreoni, *IBM J. Res. & Dev.* 45 (2001) 101

[119] M. Amati and F. Lelj, *Chem. Phys. Lett.* 358, (2002) 144

[120] J. Assa, H. Froeb, R. Gelhaar, K. Leo, M. Levichkova, V. Lyssenko, *MRS Spring Meeting 2003*, Book of Abstracts, 243, San Francisco (USA), 2003

[121] http://www.trimen.pl/witek/ciecze/liquids.html

[122] M. Cölle, S. Ferero-Lenger, J. Gmeiner, and W. Brütting, *Phys. Chem. Chem. Phys.* 5, 2958 (2003)

[123] H.-D. Ilge, E. Birckner, D. Fassler, M. V. Kozmenko, M. G. Kuzmin, and H. Hartmann, *J. Photochem.* 32 (1986) 177

[124] A. G. Mirochnik, E. V. Fedorenko, B. V. Bukvetskii, and V. E. Karasaev, *Russ. Chem. Bull., Int. Ed.* 54 (2005) 1060

[125] A. G. Mirochnik, B. V. Bukvetskii, E. V. Gukhman, P. A. Zhikhareva, and V. E. Karasev, *Russ. Chem. Bull, Int. Ed.* 50 (2001) 1612

[126] H. Li, F. Zhang, and D. Zheng, *Semicond. Sci. Technol.* 18 (2003) 278

[127] W. Lu, G. P. Gao, Z. Y. Wang, Y. Qi, G. G. Sacripante, J. D. Duff, and P. R. Sundararajan, *Macromolecules* 32 (1999) 8880

[128] H. Usui, M. Watanabe, C. Arai, K. Hibi, and K. Tanaka, *Jpn. J. Appl. Phys.* 44 (2005) 2810

[129] H. Icil and S. Icli, *Polym. Chem.* 35 (1997) 2137

[130] Y. Sakakibara and T. Tani, *J. Vac. Sci. Technol. B* 17 (1999) 1361

[131] J. R. Salem, F. O. Sequela, J. Duran, W. Y. Lee, and R. M. Yang, *J. Vac. Sci. Technol. A* 4 (1986) 369

[132] R. Pethe, C. Carlin, H. Patterson, and W. Unert, *J. Mater. Res.* 8 (1993) 3218

[133] M. Zuo, T. Takeichi, A. Matsumoto, and K. Tsutsumi, *Colloid Polym. Sci.* 276 (1998) 555

[134] H. J. Kook and D. Kim, *J. Mater. Sci.* 35 (2000) 2949

[135] G. Danev, E. Spassova, J. Assa, I. Karamancheva, A. Paskaleva, K. Popova, and J. Ihlemann, *Vacuum* 70 (2003) 37

[136] M. Bessonov, M. Koton, V. Kudryavtsev and L. Laius, *Polyimides: thermally stable polymers*, New York: Consultants Bureau (1992)

[137] I. Karamancheva, V. Stefov, B. Soptrajanov, G. Danev, E. Spasova, and J. Assa, *Vib. Spectrosc.* 19 (1999) 369

[138] Y. Sakakibara, H. Matsuhata, and T. Tani, *Jpn. J. Appl. Phys.* 32 (1993) L 1688

[139] S. Xu, M. Yang, and F. Bai, *J. Mater. Sci. Lett.* 21 (2002) 1903

[140] M. Iijima and Y. Takahashi, *Macromolecules* 22 (1989) 2944

[141] Y. Hamada, H. Kanno, T. Tsujioka, H. Takahashi, and T. Usuki, *Appl. Phys. Lett.* 75 (1999) 1682

[142] T. Dantas de Morais, F. Chaput, K. Lahlil, and J.-P. Boilot, *Adv. Mater.* 11 (1999) 107

[143] K. Read, H. S. Karlsson, M. M. Murnane, H. C. Kapteyn, and R. Haight, *J. Appl. Phys.* 90 (2001) 294

[144] V. G. Kozlov, V. Bulovic, P. E. Burrows, M. Baldo, V. B. Khalfin, G. Parthasarathy, S. R. Forrest, Y. You, and M. E. Thompson, *J. Appl. Phys.* 84 (1998) 4096

[145] Z. H. Kafafi, H. Murata, L. C. Picciolo, H. Mattoussi, C. D. Merritt, Y. Iizumi, and J. Kido, *Pure Appl. Chem.* 71 (1999) 2085

[146] S. S. Khohlova, N. G. Lebedev, S. L. Bondarev, V. N. Knyukshto, A. A. Turban, V. A. Mikhailova, and A. I. Ivanov, *Int. J. Quant. Chem.* 104 (2005) 189

[147] E. Hädicke and F. Graser, *Acta Cryst. C* 42 (1986) 189

[148] D. Troadec, A. Moliton, B. Ratier, R. Antony, and R. C. Hiorns, *J. Appl. Phys.* 97 (2005) 043103

[149] N. C. Greenham, R. H. Friend, and D. D. C. Bradley, *Adv. Mater.* 6 (1994) 491

[150] H. Fröb, M. Kurpiers, and K. Leo, *Patent: Photolumineszenzschicht im optischen und angrenzenden Spektralbereichen*, PCT/DE 00/00498, Internat. Anmeldedatum 23.02.2000

[151] A. Renn, J. Seelig, and V. Sandoghdar, *Mol. Phys.* 104 (2006) 409

[152] M. D. Halls and H. B. Schlegel, *Chem. Mater.* 13 (2001) 2632

[153] R. F. Saraf, *Polym. Eng. Sci.* 37 (1997) 1195

[154] H. Haken and H. C. Wolf, *Molecular Physics and Elements of Quantum Chemistry*, Springer, Berlin Heidelberg (2004)

[155] H. Fröb, IAPP, Technische Universität Dresden, in collaboration with the group of V. Sandoghdar, ETH, Zürich, private communication (2003)

[156] M. Adachi, Y. Murata, and S. Nakamura, *J. Phys. Chem.* 99 (1995) 14240

[157] K. Akers, R. Aroca, A. M. Hor, and R. O. Loutfy, *Spectrochim. Acta A* 44 (1988) 1129

[158] K. Gustav, M. Leonhardt, and H. Port, *Monatsh. Chem.* 61 (1997) 13659

[159] R. Scholz, A. Yu. Kobitski, T. U. Kampen, M. Schreiber, D. R. T. Zahn, G. Jungnickel, M. Elstner, M. Sternberg, and Th. Frauenheim, *Phys. Rev. B* 61 (2000) 13659

[160] A. B. Tamayo, B. D. Alleyne, P. I. Djurovich, S. Lamansky, I. Tsyba, N. N. Ho, R. Bau, and M. E. Thompson, *J. Am. Chem. Soc.* 125 (2003) 7377

[161] B. Walker, H. Port, and H. C. Wolf, *Chem. Phys.* 92 (1985) 177

[162] M. Berggren, A. Dodabalapur, R. E. Slusher, and Z. Bao, *Nature* 389 (1997) 466

[163] I. Vragovic, R. Scholz, and M. Schreiber, *Europhys. Lett.* 57 (2002) 288

[164] F. Hide, P. Kozodoy, S. P. DenBaars, and A. J. Heeger, *Appl. Phys. Lett.* 70 (1997) 2664

[165] C. Zhang and A. J. Heeger, *J. Appl. Phys.* 84 (1998) 1579

[166] H. Hoppe and N. S. Sariciftci, *J. Mater. Chem.* 16 (2006) 45

[167] Y. Sato, S. Ichinosawa, and H. Kanai, *IEEE J. Sel. Top. Quant. Electr.* 4 (1998) 40

[168] S.-Y. Cheng, J.-S. Wang, and Gu Xu, *Phys. Rew. B* 62 (2000) 11405

[169] H. Kanno, Y. Hamada, and H. Takahashi, *IEEE J. Sel. Top. Quant. Electr.* 10 (2004) 30

[170] D. Käfer and G. Witte, *Phys. Chem. Chem. Phys.* 7 (2005) 2850

[171] Y. Ren and G. H. Cross, *J. Nonlin. Opt. Phys. Mater.* 11 (2002) 131

[172] V. G. Kozlov, V. Bulovic, P. E. Burrows, and S. R. Forrest, *Nature* 389 (1997) 362

[173] M. Koschorreck, R. Gehlhaar, V. G. Lyssenko, M. Swoboda, M. Hoffmann, and K. Leo, *Appl. Phys. Lett.* 87 (2005) 1

[174] S. Riechel, U. Lemmer, J. Feldmann, T. Benstem, W. Kowalsky, U. Scherf, A. Gombert, and V. Wittwer, *Appl. Phys. B* 71 (2000) 897

[175] U. Kaufmann, M. Kunzer, K. Köler, H. Obloch, W. Pletschen, P. Schlotter, J. Wagner, A. Ellens, W. Rossner, and M. Kobusch, *Phys. Stat. Sol. A* 192 (2002) 246

[176] G. Schwartz, K. Walzer, M. Pfeiffer, and K. Leo, *Proc. of SPIE* 6192 (2006) 61920Q-1

[177] R. Meerheim, K. Walzer, M. Pfeiffer, and K. Leo, *Appl. Phys. Let.* 89 (2006) 061111

Publications

Articles

1. M. Levichkova, J. Assa, H. Fröb, and K. Leo, Blue luminescent Alq_3 molecules in a solid state matrix, *Appl. Phys. Lett.* 88 (2006) 201912

2. M. Levichkova, J. Assa, H. Fröb, and K. Leo, Photoluminescence properties of vacuum deposited organic molecule-oxide (MePTCDI - SiO2) mixed layers, *J. Lum.*, submitted

Conference reports

1. J. Assa, H. Froeb, R. Gelhaar, K. Leo, M. Levichkova, V. Lyssenko, Evaporated organic - inorganic mixed layers: luminescence conversion devices of high variety in optical properties, Materials Research Society (MRS) Spring Meeting, San Francisco (USA), 2003, In: Book of Abstracts, 243

2. M.Levichkova, J. Assa, H. Fröb, and K. Leo, Optical properties of organic - inorganic mixed layers in dependence on preparation conditions, AKF-Frühjahrstagung der Deutschen Physikalischen Gesellschaft, Regensburg (Germany), 2004, In: Verhandl. DPG 2 (2004) 189

3. M. Levichkova, J. Assa, H. Fröb, and K. Leo, Blue luminescent Alq_3 single molecules, European Materials Research Society (E-MRS) Spring Meeting, Strasbourg (France), 2004

4. M. Levichkova, J. Assa, H. Fröb, R. Gehlhaar, and K. Leo, Vacuum deposited composite films for luminescence conversion, 69. Jahrestagung der Deutschen Physikalischen Gesellschaft, Berlin (Germany), 2005, In: Verhandl. DPG 2 (2005) 642

5. M. Levichkova, J. Assa, H. Fröb, R. Gehlhaar, and K. Leo, Doping of vacuum deposited Alq_3 films - a trend for higher quantum efficiency, 3rd International Symposium on Irradiation Phenomena in Chalcogenide, Oxide and Organic Thin Films, Tryavna (Bulgaria), 2005, In: Book of Abstracts, 43

6. M. Levichkova, J. Assa, H. Fröb, and K. Leo, The luminescent shift in Alq_3 - SiO_2 system - phase transformation of Alq_3, 3rd International Symposium on Irradiation Phenomena in Chalcogenide, Oxide and Organic Thin Films, Tryavna (Bulgaria), 2005, In: Book of Abstracts, 60

List of Symbols and Abbreviations

1D	one-dimensional
ABMBF	4-methyl-6-phenyl-2,2-difluoro-1,3,2-dioxaborine
AFM	atomic force microscopy
Alq_3	tris(8-hydroxyquinoline) aluminium
c	concentration
CT	Charge-transfer exciton
CuPc	Cu-phtalocyanine
cw	continuous wave
d	film thickness
DBMBF	4,6-diphenyl-2,2-difluoro-1,3,2-dioxaborine
DCM	4-dicyanomethylene-2-methyl-6-(p-dimethylaminostyril)-4H-pyran
DMF	dimethylformamid
DMSO	dimethyl sulfoxide
ε	extinction coefficient
EL	electroluminescence
EMA	effective medium approximation
fac-Alq_3	facial Alq_3
ϕ_{ext}	external PL quantum efficiency
ϕ_{int}	internal PL quantum efficiency
FTIR	Fourier transform infrared spectroscopy
FWHM	full width at half maximum
HOMO	highest occupied molecular orbital
HV	high vacuum
$Ir(ppy)_3$	tris(2-phenylpyridine) iridium (III)
J	overlap integral
k	absorption index
k_i	photobleaching rate constant
LED	light-emitting diode
LOM	Lorentz oscillator model
LUCO	luminescence conversion
LUMO	lowest unoccupied molecular orbital
MC1	merocyanin dye
MePTCDI	N,N'-dimethylperylene-3,4,9,10-bis-dicarboximide
mer-Alq_3	meridional Alq_3
n	refractive index
OD	optical density
ODA	oxydianilline
OLEDs	organic light-emitting diodes

PI	polyimide
PL	photoluminescence
PMDA	pyromellitic dianhydride
PTCDA	3,4,9,10-perylenetetracarboxylic-dianhydride
PVD	physical vapor deposition
R	reflectance
R_0	Förster radius
RT	room temperature
SEM	scanning electron microscopy
τ_i	decay time constant of photobleaching
T	transmittance
VD	vacuum deposited
VDP	vacuum deposition polymerization
WM	Wannier-Mott exciton

Acknowledgements

At this point I would like to thank the many people without whom this work would not have been possible.

First of all, I would like to thank my professor, Karl Leo, for giving me the opportunity to research at the IAPP, for his supervision of this work, and for the competent correcting of the manuscript.

Next, I would like to thank the members of the Organic - Inorganic Mixed Layers Group for the close collaboration and their friendship. I am especially grateful to the leader of the group, Dr. Hartmut Fröb, for his guidance and constant support. It is him who taught me the essentials of luminescence spectroscopy measurements. Dr. Jacky Assa I would like to thank for the sample preparation, for sharing his experience in vacuum technology and thin film growth, and for the encouragement during my research years. Robert Gehlhaar I thank for designing the set-up for in-situ PL measurements and for his help and useful suggestions in various questions. Prof. Vadim Lyssenko I thank for all the motivating discussions and his infectious sense of humor.

To Prof. Horst Hartmann and his co-workers I am much obliged for their responsiveness to provide us with novel dyes for our studies, thus giving me the opportunity to accumulate spectroscopic experience.

Dr. Markas Sudzius I want to thank for considerable help in theoretical modeling and fruitful discussions.

I thank also Dr. Andreas Schwab for the AFM measurements.

Further, I like to mention the friendly and open atmosphere at IAPP. It was a pleasure to share the company of my roommates Rico Schüppel, Marco Koschorreck, Marco Swoboda, and Philip Schneeweiss, the witty conversations and scientific discussions over a cup of tea.

A warm word of thanks also goes to:
Dr. Michael Hoffmann for the absorption and luminescence spectra of dissolved MePTCDI and valuable comments.

Dr. Torsten Fritz and Dr. Robert Nitsche for useful advice concerning optics questions.

Gregor Schwartz for evaluation of the CRIs.

Thomas Rosenow for the blue OLED spectrum.

Kai Schmidt for patient help with computers and printers.

Sylke Furkert and Maik Koch for assistance in the chemistry lab.

To our secretary Eva Schmidt I am obliged for her kindness and help in all

administrative problems.

Annette Petrich, Dr. Martin Pfeiffer and Dr. Bert Männig I want to thank for their lasting friendship and the support, professional and personal. The warm reception I was met with made my stay in Dresden an enjoyable one.

I thank also all my colleagues in Sofia, Bulgaria, for their professional cooperation. I am particularly obliged to Dr. Pirov, Central Laboratory of Photoprocesses, for providing the SEM images, and Dr. Erinche Spassova, Central Laboratory of Photoprocesses, and Dr. Ilyana Karamancheva, University of Chemical Technology and Metallurgy, for the FTIR measurements.

Finally, I want to thank my parents and family for their unfailing confidence, encouragement and love along all these years.

Versicherung

Hiermit versichere ich, dass ich die vorliegende Arbeit ohne unzulässige Hilfe Dritter und ohne Benutzung anderer als der angegebenen Hilfsmittel angefertigt habe; die aus fremden Quellen direkt oder indirekt übernommenen Gedanken sind als solche kenntlich gemacht. Die Arbeit wurde bisher weder im Inland noch im Ausland in gleicher oder ähnlicher Form einer anderen Prüfungsbehörde vorgelegt.

Diese Arbeit wurde am Institut für Angewandte Physik/Photophysik der Technischen Universität Dresden unter der wissenschaftlichen Betreuung von Prof. Dr. Karl Leo angefertigt.

Ich erkenne die Promotionsordnung der Fakultät Mathematik und Naturwissenschaften der Technischen Universität Dresden an.

Dresden, den 10.09.2007